INVESTIGATION OF CRYSTALLIZATION OF DIBLOCK COPOLYMER BY DYNAMIC MONTE CARLO SIMULATION

Submitted in Partial Fulfillment of the Requirements for the Degree of

DOCTOR OF PHILOSOPHY

by

CHITRITA KUNDU

(Roll Number: 11610720)

Supervisor:

Dr. Ashok Kumar Dasmahapatra

DEPARTMENT OF CHEMICAL ENGINEERING

INDIAN INSTITUTE OF TECHNOLOGY GUWAHATI

April, 2017

Preface

The present report is the result of Ph.D. work, which was started in December 2011 at Department of Chemical Engineering, Indian Institute of Technology Guwahati, under the supervision of Dr. Ashok Kumar Dasmahapatra. I declare that this written submission emphasizes my ideas in my own words. If other ideas or words have been incorporated, I adequately cite the original sources.

Certificate

It is certified that the work enclosed in the thesis entitled “Investigation of crystallization of diblock copolymer by Dynamic Monte Carlo Simulation”, by Chitrita Kundu, has been carried out under my supervision and that this work has not been submitted elsewhere for a degree.

Date:

……

(Dr. Ashok Kumar Dasmahapatra)

Associate Professor

Chemical Engineering Department

IIT Guwahati

This dissertation is dedicated to my parents

MR. TAPAN KUMAR KUNDU

&

MRS. INDRANI KUNDU

Acknowledgements

First of all, I wish to thank my supervisor Dr. Ashok Kumar Dasmahapatra, Associate Professor of Department of Chemical Engineering for believing me and giving me an opportunity to pursue research under his guidance. Since familiar with the world of research, I learn a lot about the new possibility of science and I have a continuous association with it. I never had a tough time. It was entirely because of the kind patience and commendable understanding of my supervisor. I have evolved a lot during these years working with him. His excellent guidance, valuable insights, fruitful discussions and continuous support have made this dissertation possible.

I thank Dr. Dipankar Bandyopadhyay, Associate Professor of Department of Chemical Engineering and Chairperson of Ph.D. doctoral committee, for his continuous encouragement, enormous help and thought provoking advices.

I wish to express my sincere thanks to doctoral committee members Dr. Amit Kumar, Associate Professor of Department of Chemical Engineering and Dr. S. Kanagaraj, Professor of Department of Mechanical Engineering for their valuable suggestions which helped me a lot in taking research forward.

My special thanks to Jayanta Kumar Mout and Md. Ariful Hoque for providing immense technical support during my tenure. They were always cordial to offer help.

I cannot thank enough the present and past group members Pradeep Kumar Ramteke, Sidharth Thakur, Pankaj Vardhe, Pritam Sardar, Nikhil Joshi and Shatrudhan Palsaniya, who were with me during my good and bad times.

I wish to acknowledge Department of Chemical Engineering and Indian Institute of Technology Guwahati for contributing necessary infrastructures and academic resources throughout my research work. I am also grateful to Department of Science and Technology and Ministry of Human Resource Development, Government of India for their financial support.

Finally, I can never forget the support given by my family who have been eagerly waiting all these years for my achievement. It would have been impossible for me to finish this work without their encouragement.

Abstract

This research work focuses on the understanding of interplay between crystallization and microphase separation, and their influence on the final crystal morphology of diblock copolymer. The aim is to relate the crystallization mechanism with segregation strength and block asymmetry. In this view, crystallization mechanism under different types of confinement has been studied by Dynamic Monte Carlo simulation.

We investigate the crystallization of double crystalline symmetric A-B diblock copolymer, wherein the melting temperature of A-block is larger than B-block. As a result, crystallization of A-block is followed by the crystallization of B-block upon cooling from a homogeneous melt. The morphological evolution is dominated by the interplay between crystallization and microphase separation. With the increasing of segregation strength, we observe a gradual decrease in crystallinity accompanying with smaller and thinner crystals. During the process, A-block crystallizes first and offers confinement for the crystallization of B-block. Therefore, the crystallization of B-block is reduced significantly influencing the overall crystal morphology. At higher segregation strength, due to the repulsive interaction between two blocks, block junction is stretched out, which is exhibited by an increased value of mean square radius of gyration. As a result, large number of smaller size crystals generate with less crystallinity. The onset of microphase separation moves towards higher temperature with increasing segregation strength. Isothermal crystallization reveals that the transition kinetics is primarily governed by segregation strength. The value of Avrami index indicates the presence of two dimensional lamellar crystals. Two-step, compared to one-step isothermal crystallization, yields higher crystallinity in A-block whereas the crystallinity of B-block is almost similar in both cases.

To unfold the inherent relationship between block asymmetry and crystallization behaviour, we have investigated the crystallization of diblock copolymer by varying block compositions (viz., by varying the relative block length of A- and B-block) with weak and strong segregation strength between the blocks. In weak segregation limit, we observe that with increasing the composition of B-block, the crystallization temperature of B-block increases accompanying with higher crystallinity. In contrast, A-block crystallizes at a relatively low temperature along with the formation of thicker and larger crystallites with the increase in B-block composition. This non-intuitive crystallization trend relates with the

dilution effect imposed by B-block. When the composition of the B-block is large enough, it behaves like a “solvent” during the crystallization of A-block. Therefore, A-block segments are more mobile and hence less facile to crystallize, ensuing depression in crystallization temperature with the formation of thicker crystals. At strong segregation limit, crystallization and morphological development are driven by the confinement effect, rather than block asymmetry. Isothermal crystallization discloses that the crystallization follows a homogeneous nucleation mechanism with the formation of two-dimensional crystals. Two-step, compared to one-step isothermal crystallization promotes the formation of thicker crystals of A-block due to the dilution effect of the B-block.

In order to understand the effect of microphase separation, we have examined the crystallization behaviour of diblock copolymer instigated from microphase separated melt. During crystallization, the morphological evolution of microphase separated melt is comprehensively dictated by thermal history. Isothermal crystallization restricts crystallization in phase separated microdomains, whereas non-isothermal crystallization upholds morphological perturbation of melt microdomains. Annealing of microphase separated melt successfully reorients melt morphology where both type of crystallization preserves melt morphology intact due to the presence of hard confinement resulted during microphase separation. The rate of crystallization of microphase separated annealed melt is much faster than microphase separated melt without annealing due to less entanglement and more relaxed structure of microphase separated melt accomplished through the process of annealing.

We have studied the crystallization behaviour of diblock copolymer from thin film to understand the effect of additional confinement (viz., 1D confinement) on crystallization. Film thickness is one of the most influential parameters of thin film crystallization which successfully determine the process of crystallization and final crystal morphology. We study the non-isothermal crystallization of symmetric diblock copolymer for a series of film thickness (z) ranging from z = 4 to 20. With the increase of film thickness (z), the value of crystallinity remains similar with the formation of thinner crystal. Similarly the transition points of both the blocks get influenced by film thickness (z). The crystallization temperature of both blocks decreases with the increment of film thickness (z). Isothermal crystallization reveals that the transition kinetics follows different kinetic pathways with the variation of film thickness (z). The value of Avrami Index confirms the existence of homogeneous nucleation with two-dimensional crystal growth.

Contents

List of Figures

List of Tables

Chapter 1

Introduction

The discovery of the chain folded lamellar crystal structure [1] captivates scientists to explore polymer crystallization as a fascinating topic in the last few decades. The kinetics of polymer crystallization and crystal morphology are governed by several factors, such as molecular weight, chain flexibility, stereo-regularity, etc. The experimental conditions such as temperature, pressure, nucleating agents, flow-field also dictate the crystallization behavior [2, 3]. In this chapter, we will briefly review thermodynamics and kinetics of polymer crystallization and the development of crystal morphology. Subsequently, we will discuss diblock copolymer and their crystallization mechanism.

1.1 Thermodynamics of Polymer Crystallization

Crystallization of polymer is a liquid-solid phase transition which associates with the reorientation of polymer chains. If the temperature of liquid approach towards melting point, the liquid tends to solidify. From the viewpoint of thermodynamics, when the temperature is below melting point, a crystal is in lower free energy state than melt state. Figure 1.1 schematically represents the change in the free energy per unit volume of liquid and crystal as a function of temperature.

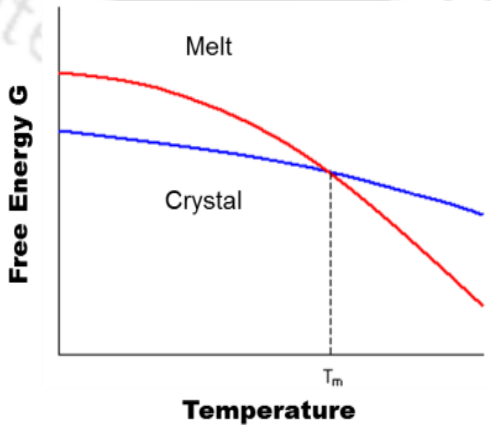

Figure 1.1 Change in Gibbs free energy per unit volume with temperature [4].

The crystallization of polymer follows a two-step mechanism - nucleation and growth. Nucleation offers the formation of tiny crystalline mass of polymer, which assists further growth. Crystal growth is facilitated by the addition of folded polymer chain segments into the nucleus, which involves the diffusion of chain segments to the crystal growth front. To understand the thermodynamics of homogeneous nucleation, an isothermal quiescent melt is considered whose temperature T is kept below the equilibrium melting temperature (T_m^∞). Nucleation can be accompanied by the reduction of Gibb's free energy (ΔG_v) per unit volume and the addition of surface energy γ per unit area created by the area bound within nucleus. Thus, a typical sphere of radius r is taken as a nucleus and the net change in energy due to formation of the sphere is

$$\Delta G = 4\pi r^2\gamma + \frac{4}{3}\pi r^3 \Delta G_v \qquad (1.1)$$

Where, ΔG_v is a negative number. Primarily ΔG_v increases with increasing r and goes through a maximum to become negative. This maximum value characterizes an energy barrier which must be overcome by the thermal motion of the molecules before a stable nucleus can be grown. At this point, the critical radius of the nucleus r^* is calculated from the derivative of ΔG^*.

$$r^* = -\frac{2\gamma}{\Delta G_v} \qquad (1.2)$$

$$\Delta G^* = \frac{16\pi\gamma^3}{3(\Delta G_v)^2} \qquad (1.3)$$

During crystallization, ΔG^* is considered as an energy barrier of the system and the probability of a group of molecules having energy ΔG^* greater than the average energy at temperature T, calculated from Boltzmann relation is

$$probability \propto \exp(-\frac{\Delta G^*}{KT}) \qquad (1.4)$$

Consider a system with N_0 number of solid particles at temperature T. Among those particles, N^* numbers of particle actually retain the activation energy ΔG^*.

$$N^* = N_0 \exp(-\frac{\Delta G^*}{KT}) \tag{1.5}$$

Nucleation is followed by the growth of the nuclei which involves the diffusion of polymer chain segments to the growth front. Nuclei basically grow with the addition of chain segments. The process of diffusion also plays major role in crystal formation. So, the probability of rate of diffusion is calculated by

$$rate \propto \exp(-\frac{E_D}{KT}) \tag{1.6}$$

Where, E_D is the activation energy for diffusion. So, the combination of previous equations indicate that the rate of nucleation N , nuclei per unit time is given by

$$N = N_0 \exp(-\frac{E_D}{KT}) \exp(-\frac{\Delta G^*}{KT}) \tag{1.7}$$

The overall linear growth rate G will also be proportional to N

$$G = G_0 \exp(-\frac{E_D}{KT}) \exp(-\frac{\Delta G^*}{KT}) \tag{1.8}$$

Now, if we plot linear growth rate as a function of temperature (Figure 1.2), a bell shaped curve is developed signifying the growth rate is zero in glass transition temperature (T_g) due to the small rate of diffusion and also tends to zero close to melting point (T_m) because of the less driving force (ΔT) for crystallization [4]. Therefore, the degree of super cooling is the major thermodynamic force which drives crystallization primarily.

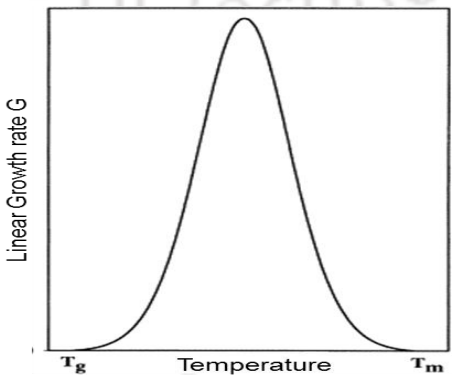

Figure 1.2 Temperature dependence of linear growth rate.

1.2 Kinetic Theory of Polymer Crystallization

During polymer crystallization, the morphological development and the spherulitic growth rate are effectively controlled by kinetic factors rather than thermodynamic one [5]. Therefore, a kinetic theory is also essential to describe the process of crystallization. Kinetically, the crystal growth rate is driven by the competition between the thermodynamic driving force, which associates with the degree of undercooling and a free energy barrier for crystallization. On top of that, the subsequent growth rate is a function of lamellar thickness. Therefore, for larger lamellar thickness, the free energy barrier is also larger which leads to larger driving force. On the other hand, in order to promote the crystallization process, a section of chain requires to be deposited on the crystal growth front. The localization of the stem on the crystal surface involves with the decrease in the entropy of the polymer chain. This leads to an entropic barrier that increases with crystal thickness. Kinetic theories assume that, the thickness, corresponding to the maximum growth rate on the lateral growth surfaces prefer to grow macroscopic lamellae.

The two most successful kinetic theories on polymer crystallization are the surface nucleation model formulated by Lauritzen and Hoffman (LH) [6, 7], and the entropic barrier model proposed by Gilmer and Sadler (GS) [8, 9]. Both are established on the consideration of kinetic processes on the lateral growth faces which leads to secondary nucleation theories (growth theories). It is the origin of the energy barrier that distinguishes these two models. In the LH model, an energy barrier is reflected and it must be overcome via random fluctuation as a molecule or a segment of a long chain assigns itself to the crystal growth front. In contrast, the GS model asserts that in addition of free energy terms, the retardation of attachment of a long segment onto a growth front is affected by discovering many possible configurations, only a few of which are favourable to grow further. Therefore, the barrier of GS model is fundamentally entropic in nature. Finally the LH model has been widely accepted theory and it has been extensively used to quantitatively fit experimental results. The recent progress in polymer crystallization originates from the study of early stages of crystallization [10]. It has been anticipated that crystallization is introduced by an ordered precursor, which is either prompted by a spinodal-assisted mechanism [11, 12] or involves a mesomorphic phase on the crystal growth front [13-15]. Therefore, several kinetic theories have been discussed hereby to follow crystallization process effectively along with thermodynamic factors.

1.3 Morphology of Semi-crystalline Polymers

According to the extent of molecular arrangement, polymers are broadly divided into two categories. Some polymers rearrange their chains upon freezing, but they are in lack of long range order characteristic of crystal. They are known as amorphous material. Some polymers able to align and fold their chains in long range order upon cooling. They are known as crystalline material. In general, most of the polymers are semi crystalline in nature. In early studies of polymer morphology, the "fringed-micelle" model was recommended in which the polymer chains crystallize through several crystallites via intermediate amorphous regions. This model is based on a two-phase system where the crystalline region consists of stacks of short length chains aligned parallel to each other, and the amorphous regions are in disordered states as shown in Figure 1.3 [16].

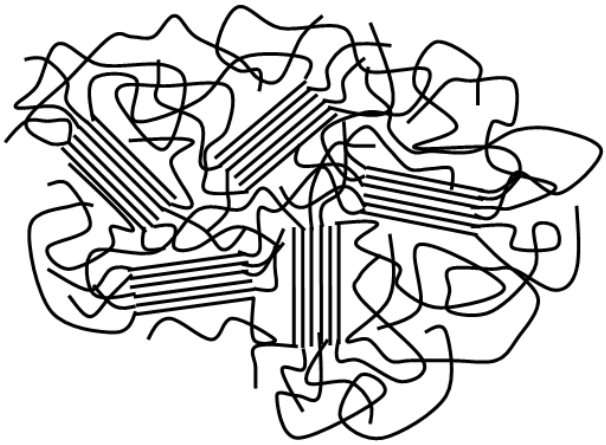

Figure 1.3 Schematic of fringed-micelle model for semi-crystalline polymers.

This model is quite suitable for explaining the changes of molecular rearrangement during crystallization. However, it is incapable to clarify the morphological features such as spherulite associated with melt crystallized polymers. These superstructures are later clarified by the chain-folding model. According to the chain-folding model, polymer single crystals are very thin platelets (~ 10 nm) and the chain axis is almost perpendicular to the crystal basal plane. In that model, a single polymer chain arranges parallel by folding regularly on the crystal basal surfaces through the same crystallites. Such thin platelets are called "chain-folded lamellar crystal" (see Figure 1.4) [1]. The existence of such type of structures in melt crystallized polymer was also discussed by Palmer et al. [17].

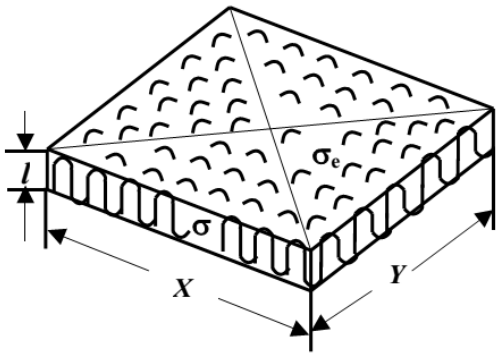

Figure 1.4 Schematic of chain-folded lamellar structure in semi-crystalline polymers with lateral dimensions X, Y and thickness *l*. σ and σ_e are the surface free energies associated with lateral and fold surfaces, respectively.

In the introduction, we mostly limit our discussion on the morphology of melt crystallizes polymers. The most common superstructures in melt-crystallized polymers are spherulites, which comprises of radiating arrays of periodic lamellar sub-structures. In most of the cases, the radius of spherulites increases linearly with time during growth before the spherulites interrupt each other. The typical size of spherulites ranges from several to hundreds of microns, depending on the nucleation density. The microbeam X-ray diffraction technique has revealed that the molecular chains are normal to the radial direction in spherulites [18-21]. Superstructures like spherulites are frequently absent when short chain branches or stereo defects are introduced in the chain backbone. The presence of defects also reduces the lateral dimension and thickness of lamellar crystals which inhibit the crystallization processes. The introduction of defects into the chain backbone mainly diminishes the frequency of adjacent re-entry folding, which leads to the formation of regularly and tightly chain folded lamellar crystals. As a result, there exists a distribution of loose fold, cilia and tie chain lengths in the amorphous phase, which generates small secondary crystals in the constrained amorphous region [22, 23]. The development of secondary crystals provides the continuous increase in degree of crystallinity, which has been detected after primary crystallization [22, 24]. Marand et al. suggested a model to describe how the characteristics of polymer chains and the crystallization conditions affect the mechanism of secondary crystallization [23, 24]. In that model, the formation of secondary crystals happens in a constrained environment below some critical temperature. At high undercooling, the formations of secondary crystals are most likely to be the fringed-micellar type [24]. Therefore, lots of diverse studies have been proposed to understand the development of morphology minutely.

1.4 Diblock Copolymer

Recently crystallization and spatially ordered structure formation in diblock copolymer have successfully drawn large attention due to its numerous applications in nanotechnology and biomedical applications [25]. Block copolymer consists of two different repeat units with different chemical nature and structure, which are in most of the cases incompatible with each other. This thermodynamic incompatibility between two units leads to phase separation in microscopic scale. The phase separated block copolymer produces a large variety of morphologies including spherical and cylindrical microstructures as well as lamellar morphology [26, 27]. In diblock copolymer where both blocks are amorphous in nature, polymer chains are evenly dispersed with increasing temperature or decreasing molecular weight. When the temperature is decreased or molecular weight is increased, both blocks try to segregate into their microdomain lowering the free energy of mixing. Microphase separation is driven by the chemical incompatibility between two blocks and the separations are counterbalanced by the entropic forces from the covalent linkages holding both blocks together. However due to excess free energy of the system which is unfavourable for mixing, copolymers must adopt extended chain conformation to keep apart two dissimilar blocks [27]. Crystallization of diblock copolymer has a unique property to control material properties via self-assembly into nano structures. By the advancement of the modern synthetic chemistry, it is possible to tailor block copolymer structures to tune material properties of both blocks and their ensemble. Microphase separation helps polymer chains to self-organize where the contacts between similar units are maximized and the contacts between dissimilar units are minimized. Different thermodynamically stable phases are observed in A-B diblock copolymer with increasing composition of A-block (f_A) including body centred cubic of A-spheres in B-matrix, hexagonally packed A-cylinders in B-matrix, bicontinuous gyroid phases & alternating lamellar phases. Figure 1.5 represents A-B diblock copolymer by a simple two colour chain where red one is A-block and Blue one is B-block followed by the self-organization of polymer chains to reduce block immiscibility and finally a long rang ordered structures which are primarily determined by the relative lengths of the polymer blocks. Therefore, the tunability of block copolymer size, shape and composition supports nanoscience to develop a large number of nanomaterials for advance technology [25].

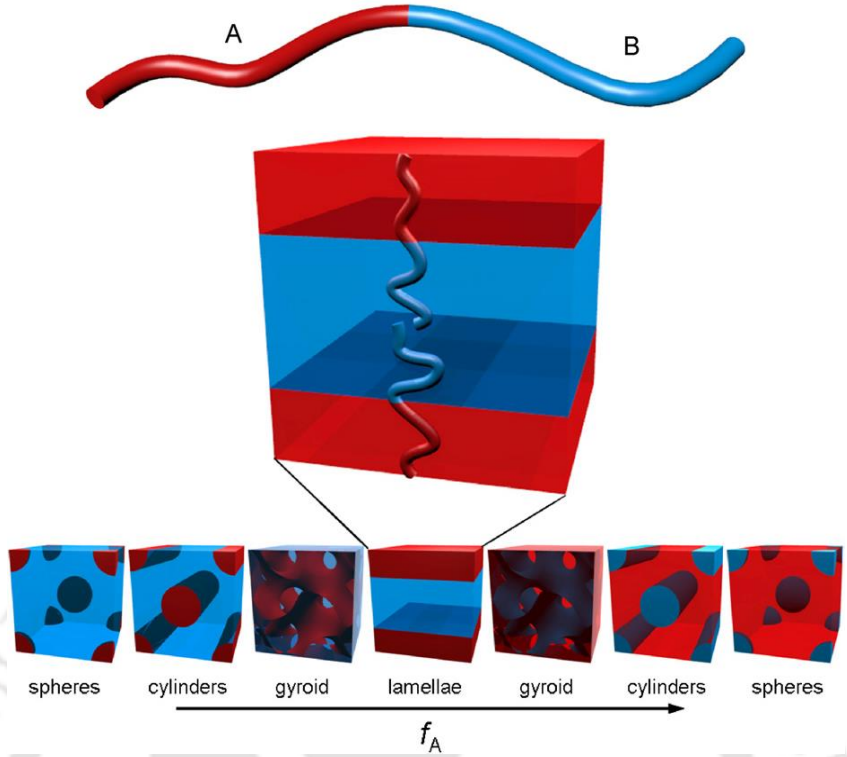

Figure 1.5 Schematics of different morphologies of diblock copolymer [25].

1.5 Crystallization of Semi-Crystalline Diblock Copolymer

In a diblock copolymer, the interplay between crystallization and microphase separation plays a crucial role to dictate final crystal morphology. The final morphology of a semi crystalline diblock copolymer containing ethylene and ethylene-alt-propylene (E-*b*-EP) has been investigated from homogeneous melt state over a wide range of composition of ethylene block. For all cases, diblock copolymer exhibits lamellar morphology with spherulitic super structure, and microphase separation is induced by crystallization [28]. The dynamics of crystallization in semi crystalline block copolymer has also been studied by rapid cooling of homogeneous melt resulting strongly segregated microdomain structures. Initially, the ordered structure simply grows without any internal arrangement of the domains but after a long interval, a small decrease in microdomain spacing is observed which reflects a contraction of both crystalline and amorphous domains due to the relaxation of amorphous chain from non-equilibrium extended conformation during crystallization [29]. Again, the structure development process of semi crystalline polyethylene and poly ethyl ethylene (PE-*b*-PEE) diblock copolymer has been studied from the ordered melt structure. In this diblock copolymer the ordered melt morphologies are completely destroyed due to chain folding of

crystalline PE block because of the free energy towards chain folding during crystallization completely overcomes the enthalpy associated with the microphase separated melt structure [30]. For a semi crystalline diblock copolymer, the process of crystallization competes with microphase separation. The symmetric diblock copolymer of PE and a glassy amorphous block having ordered structure in melt can also crystallize without changing initial melt morphology producing lamellar solid structures. The crystal morphology for semi crystalline block copolymer basically depends on whether the crystallization takes place from weak segregated melt or strong segregated melt. Weakly segregated melt morphologies are completely destroyed during crystallization but in case of phase separated melt, as the stability of micro domains increases with increasing immiscibility, the crystallization phenomenon is unable to disturb the previous melt morphologies [31].

The effect of copolymer composition on development of crystallinity and morphology formation of semi crystalline diblock copolymer of poly(ε-caprolactone)-*block*-polystyrene quenched from phase separated melt has been observed. When fraction of PCL (ϕ_{PCL}) is larger than 64%, crystallization of PCL block with distinct lamellar morphology is visible. When ϕ_{PCL} is less than 26%, no crystallization is observed while ϕ_{PCL} of 34% produces partial crystallization [32]. The other key factor to restrict crystallization is the location of glass transition temperature (T_g) of the amorphous block and melting temperature (T_m) of crystalline block. The crystallization behaviour of poly(ε-caprolactone) and polystyrene (PCL-*b*-PS) diblock copolymer quenched from melt has been followed. The evolution of crystallinity in PCL block is majorly determined by the glass transition temperature of the PS block ($T_{g,PS}$). When $T_{g,PS}$ is greater than the crystallization temperature of the system (T_c), the molecular motion of crystalline PCL block is extremely restricted by the vitrification of PS block, resulting no crystallization whereas PCL crystallizes partially, when $T_{g,PS}$ is lower than crystallization temperature. However the characteristics of lamellar morphology including long spacing and lamellar thickness are independent of T_g of the PS block [33].

The transition kinetics of a series of polyethylene (PE) containing diblock copolymers where polyethylene is minority block and rubbery hydrocarbon is majority block has been studied. When the inter-block segregation strength is extremely high, crystallization of PE block is confined within the spherical micro domains created by microphase separated melt indicating first order transition kinetics where Avrami index (n) is 1. But when the

segregation strength is low, crystallization can disrupt the micro structures in melt resulting sigmoidal kinetics, where Avrami index is greater than 1. The scenario is different in case of cylindrical microdomain generated by microphase separated melt. The crystallization in moderate segregation strength template with partial confinement retains its melt morphology during cooling producing conventional sigmoidal kinetics [34]. The relative location of order-disorder transition temperature (T_{ODT}), crystallization temperature (T_C) of crystalline block and glass transition temperature (T_g) of amorphous block also has an immense effect on the formation of final crystal structure in a semi crystalline block copolymer whether the diblock crystallized from microphase separated melt or homogeneous melt. If $T_{ODT} < T_C > T_g$, the diblock copolymer generating homogeneous melt, finally shape up in lamellar morphology after crystallization where the crystalline lamellar are sandwiched by the amorphous layers and microphase separation is followed by the crystallization [28, 29, 35-37]. In case of $T_{ODT} > T_C > T_g$ with soft confinement, the phase separated ordered melt structures are majorly destroyed by the crystallization to form new lamellar solid state structures [37-42]. Strongly segregated system with soft confinement by rubbery amorphous block where $T_{ODT} > T_C > T_g$, exhibits confined crystallization within spherical or cylindrical or lamellar micro domains [34, 36, 40, 43-46] whereas strongly segregated system with hard confinement having $T_{ODT} > T_g > T_C$ displays more confined crystallization within micro domains of glassy amorphous block [47-53]. A brief discussion on the crystallization of diblock copolymer and several influential parameters which instigate various morphological patterns have been summarized here.

In 1980, Dimarzio suggested that diblock copolymers display equilibrium chain folding when one of component is crystallisable and other one is amorphous with incompatibility between two blocks. In homopolymer, chain folding is in metastable state while infinite annealing produces extended chain crystal. In diblock copolymer where only one block is crystalline, crystallization generates an alternate layer of crystalline and amorphous regions. In such a system the value of lamellar thickness is strongly affected by the two opposing tendencies where the energetics of crystallization provokes the crystalline regions for extended chains with minimal folding but this tendency is hindered by the amorphous regions which favour random like chains resulting equilibrium amount of chain folding in crystalline regions [54]. This is one of the most well-known theoretical illustrations of chain folded lamellar crystal for diblock copolymer.

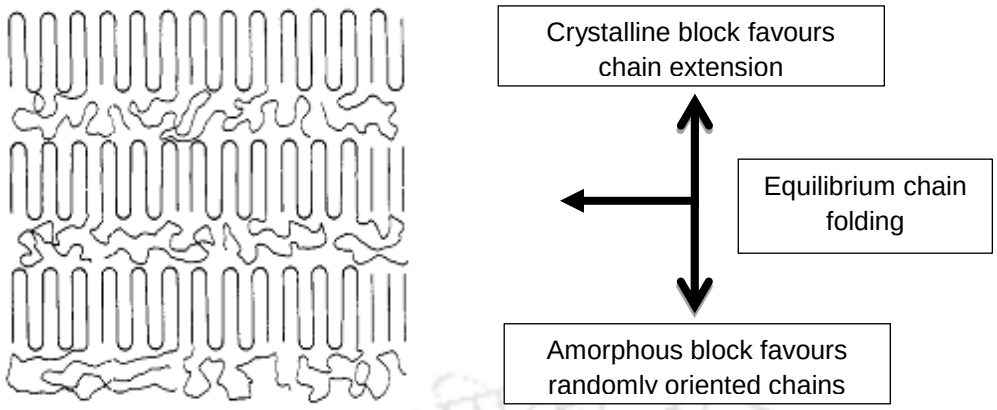

Figure 1.6 Equilibrium chain folding in semi crystalline diblock copolymer [54].

1.6 Organization of Thesis

The thesis is organized as follows: we narrate the main objectives in chapter 2 and modelling and simulation technique in chapter 3. We discuss our key results in chapter 4 to chapter 7. Chapter 4 and 5 represent the simulation results for symmetric and asymmetric diblock copolymer, respectively. Chapter 6 represents the crystallization from a microphase separated melt. Chapter 7 deals with the crystallization from thin film. Finally, we summarise our key findings and highlight the scope for future studies in Chapter 8.

References

1. Keller A. Phil. Mag. 1957;2(21):1171-1175.
2. Keller A and Goldbeck-Wood G. Comprehensive polymer science, 2nd Edition. Oxford: Elsevier, 1996.
3. Mandelkern L. Crystallization of Polymers. New York: McGraw-Hill, 1964.
4. Kumar A and Gupta RK. Fundamentals of Polymer Engineering. New York: Marcel Dekker, 2003.
5. Armitstead K, Goldbeck-Wood G, and Keller A. Polymer crystallization theories. Macromolecules: Synthesis, Order and Advanced Properties. Berlin, Heidelberg: Springer Berlin Heidelberg, 1992. pp. 219-312.
6. Hoffman JD and Miller RL. Polymer 1997;38(13):3151-3212.
7. Jr. JIL and Hoffman JD. J. Chem. Phys. 1959;31(6):1680-1681.
8. Sadler DM and Gilmer GH. Phys. Rev. Lett. 1986;56(25):2708-2711.
9. Sadler DM and Gilmer GH. Phys. Rev. B 1988;38(8):5684-5693.
10. Baert J and Van Puyvelde P. Macromol. Mater. Eng. 2008;293(4):255-273.
11. Olmsted PD, Poon WCK, McLeish TCB, Terrill NJ, and Ryan AJ. Phys. Rev. Lett. 1998;81(2):373-376.
12. Matsuba G, Kaji K, Nishida K, Kanaya T, and Imai M. Macromolecules 1999;32(26):8932-8937.
13. Strobl G. Prog. Polym. Sci. 2006;31(4):398-442.
14. Liu Y-X and Chen E-Q. Coord. Chem. Rev. 2010;254(9):1011-1037.
15. Prudhomme RE. Prog. Polym. Sci. 2016;54–55:214-231.
16. Flory PJ. Principles of Polymer Chemistry. Ithaca, New York: Cornell University Press, 1953.
17. Palmer RP and Cobbold AJ. Makromol. Chem. 1964;74(1):174-189.
18. Keller A. J. Polym. Sci. 1955;17(85):351-364.
19. Fujiwara Y. J. Appl. Polym. Sci 1960;4(10):10-15.
20. Mann J and Roldan-Gonzalez L. J. Polym. Sci. 1962;60(169):1-20.
21. Magill JH. J. Poly. Sci. A-2 1966;4(2):243-265.
22. Alizadeh A, Richardson L, Xu J, McCartney S, Marand H, Cheung YW, and Chum S. Macromolecules 1999;32(19):6221-6235.

23. Alizadeh A, Sohn S, Quinn J, Marand H, Shank LC, and Iler HD. Macromolecules 2001;34(12):4066-4078.
24. Marand H, Alizadeh A, Farmer R, Desai R, and Velikov V. Macromolecules 2000;33(9):3392-3403.
25. Darling SB. Prog. Polym. Sci. 2007;32:1152-1204.
26. Bates FS and Fredrickson GH. Annu. Rev. Phys. Chem. 1990; 41:525-557.
27. Bates FS and Fredrickson GH. Phys. Today 1999; 52(2):32-38.
28. Rangarajan P and Register RA. Macromolecules 1993;26(17):4640-4645.
29. Rangarajan P, Register RA, Adamson DH, Fetters LJ, Bras W, Naylor S, and Ryan AJ. Macromolecules 1995;28(5):1422-1428.
30. Ryan kJ, Hamley IW, Bras W, and Bates FS. Macromolecules 1995;28(11):3860-3868.
31. Hamley IW, Fairclough JPA, Terrill NJ, Ryan AJ, Lipic PM, and Bates FS. Macromolecules 1996;29(27):8835-8843.
32. Nojima S, Fujimoto M, Kakihira H, and Sasaki S. Polym. J. 1998;30(12):968-975.
33. Nojima S, Tanaka H, Rohadi A, and Sasaki S. Polymer 1998;39(8):1727-1734.
34. Loo Y-L, Register RA, and Ryan AJ. Macromolecules 2002;35(6):2365-2374.
35. Richardson PH, Richards RW, Blundell DJ, MacDonald WA, and Mills P. Polymer 1995;36(16):3059-3069.
36. Quiram DJ, Register RA, Marchand GR, and Ryan AJ. Macromolecules 1997;30(26):8338-8343.
37. Ryan AJ, Hamley IW, Bras W, and Bates FS. Macromolecules 1995;28(11):3860-3868.
38. Rangarajan P, Register RA, Fetters LJ, Bras W, Naylor S, and Ryan AJ. Macromolecules 1995;28(14):4932-4938.
39. Nojima S, Kato K, Yamamoto S, and Ashida T. Macromolecules 1992;25(8):2237-2242.
40. Quiram DJ, Register RA, and Marchand GR. Macromolecules 1997;30(16):4551-4558.
41. Ryan AJ, Fairclough JPA, Hamley IW, Mai S-M, and Booth C. Macromolecules 1997;30(6):1723-1727.
42. Douzinas KC, Cohen RE, and Halasa AF. Macromolecules 1991;24:4457-4459.
43. Reiter G, Castelein G, Sommer J-U, Röttele A, and Thurn-Albrecht T. Phys. Rev. Lett. 2001;87(22):226101.

44. Nojima S, Toei M, Hara S, Tanimoto S, and Sasaki S. Polymer 2002;43:4087-4090.
45. Ueda M, Sakurai K, Okamoto S, Lohse DJ, MacKnight WJ, Shinkai S, Sakurai S, and Nomura S. Polymer 2003;44:6995 - 7005.
46. Quiram DJ, Register RA, Marchand GR, and Adamson DH. Macromolecules 1998;31(15):4891-4898.
47. Muller AJ, Balsamo V, Arnal ML, Jakob T, Schmalz H, and Abetz V. Macromolecules 2002;35(8):3048-3058.
48. Zhu L, Cheng SZD, Calhoun BH, Q.Ge, Quirk RP, Thomas EL, Hsiao BS, Yeh F, and Lotz B. Polymer 2001;42:5829 - 5839.
49. Zhu L, Chen Y, Zhang A, Calhoun BH, Chun M, Quirk RP, Cheng SZD, Hsiao BS, Yeh F, and Hashimoto T. Phys. Rev. B 1999;60(14):10022-10031.
50. Arnal ML, Balsamo V, López-Carrasquero F, Contreras J, Carrillo M, Schmalz H, Abetz V, Laredo E, and Müller AJ. Macromolecules 2001;34(23):7973-7982.
51. Loo Y-L, Register RA, Ryan AJ, and Dee GT. Macromolecules 2001;34(26):8968-8977.
52. Floudas G and Tsitsilianis C. Macromolecules 1997;30(15):4381-4390.
53. Gervais M and Gallot B. Polymer 1981;22(8):1129-1133.
54. DiMarzio EA, Guttman CM, and Hoffman JD. Macromolecules 1980;13(5):1194-1198.

Chapter 2

Objectives

The main objective of the present study is to monitor the interplay between microphase separation and crystallization under different types of confinement of diblock copolymer. Monte Carlo Simulation is an efficient tool to investigate polymer crystallization. Therefore, the crystallization of diblock copolymer investigated by Monte Carlo Simulation is a challenging job to get various insights of polymer crystallization.

- **Crystallization of Double Crystalline Symmetric Diblock Copolymer:**

We implement non-isothermal crystallization and isothermal crystallization to follow the behavior of a symmetric double crystalline diblock copolymer. The effect of segregation strengths on crystallinity and crystal morphology will be discussed.

- **Effect of Block Asymmetry on Crystallization:**

Effect of block asymmetry on the crystallization of double crystalline diblock copolymer will be investigated – isothermal and non-isothermal. We fix two different types of segregation strengths (viz., weak and strong) between the blocks.

- **Crystallization from Microphase Separated Melt:**

Diblock copolymer exhibits several phase separated morphologies due to the immiscibility of two blocks. There is a reorientation of the phase separated microdomains due to annealing. A comparative analysis of crystallinity and other structural parameters of microphase separated melt with and without annealing are very much useful.

- **Crystallization on Thin Films:**

Attempt will be made to simulate diblock copolymer thin films to understand the effect of additional confinement on the crystallization of a diblock copolymer. Film thickness and the nature of the substrate are most influential parameters to determine the final crystal morphology and crystal orientation. In the present work, we vary film thickness to observe the crystallization behavior, while keeping the substrate inert (viz., no polymer-substrate interaction).

Chapter 3

Modelling and Simulation Method

Monte Carlo simulation has evolved as a powerful tool to investigate the phase behaviour of polymeric systems during the last few decades. Several Monte Carlo techniques such as Pruned Enriched Rosenbluth Method (PERM) [1], random end-switch-configuration biased Monte Carlo (RES-CBMC) [2] and wormhole algorithm [3] are successfully applied to simulate a single polymer chain with some limitations for dense systems. Lattice simulations of dense systems have successfully been implemented by Pakula et al. [4] with the cooperative motion algorithm (COM) [5] and by Hu et al. [6] with the single site bond fluctuation algorithm [7-9]. In cooperative motion algorithm (CMA), the occupation density of lattice polymer is 100%, however, the morphological evolution with time cannot be explicitly mapped with Monte Carlo steps; whereas by using bond fluctuation model, Hu et al. produced the experimentally observed nontrivial trend of copolymer crystallization [10]. Moreover, Hu et al. have studied the effect of sequence distribution of comonomer on crystallization of different statistical copolymers [10], Single site bond fluctuation algorithm have been successfully employed to investigate the effect of sticky additives in polymer crystallization [11] and the crystallization of double crystalline diblock copolymer where the crystallization of one block accelerates the crystallization of other block [12]. In the present work, we employ dynamic Monte Carlo simulation to study the crystallization of double crystalline diblock copolymer.

To simulate the crystallization of diblock copolymer, we implement dynamic Monte Carlo (DMC) method, which has been successfully applied to investigate phase transition of bulk polymers [6, 10, 11, 13]. A polymer chain is represented by joining the successive sites in a lattice with size 32 × 32 × 32. A total 480 polymer chains each having 64 repeat units are placed successively one by one ensuring that the connectivity of the chain is maintained. Thus, the lattice occupation is as high as 0.9375, representing a bulk polymer system [10]. The degree of polymerization of polymer is N (viz., 64) which includes N_A and N_B number of A-type and B-type repeat units respectively. A homogeneous and monodisperse melt is generated by applying a set of microrelaxation algorithms. The Monte Carlo schemes which are extremely useful to simulate polymer motion mostly depend on the

single site jumping models. Larsen et al. has initially developed a model based on kink generation and end to end sliding diffusion [14]. Later on, the kink generation scheme was modified to bond fluctuation model Deutsch and Binder [15]. The microrelaxation algorithm in our simulation consists of a set of Monte Carlo move such as bond fluctuation, end bond rotation and slithering diffusion [10, 11, 16-18]. Followings are the schematics to illustrate the different Monte Carlo moves.

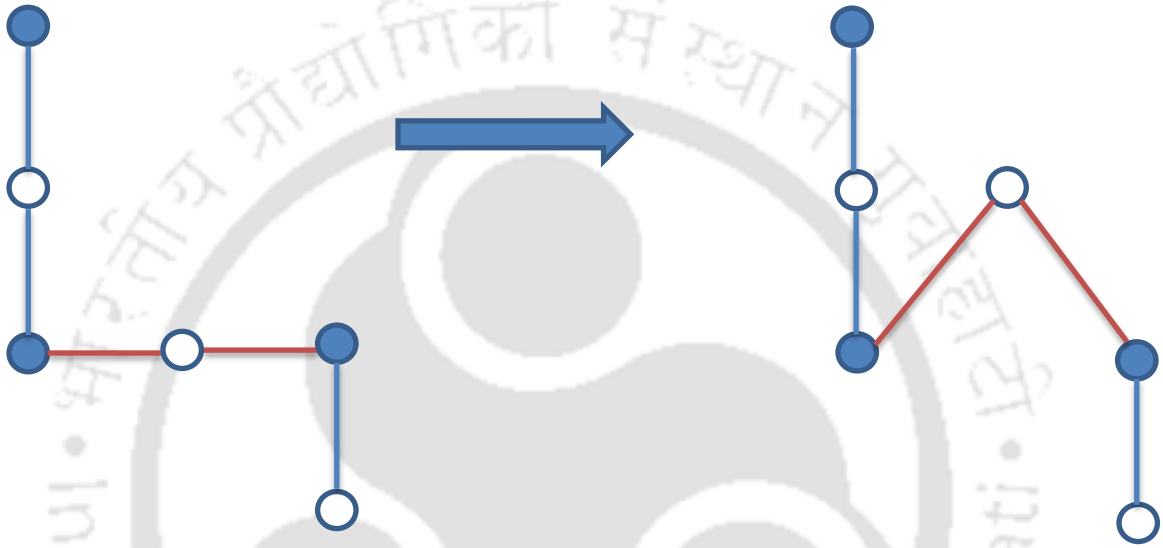

Figure 3.1 Schematic for bond fluctuation.

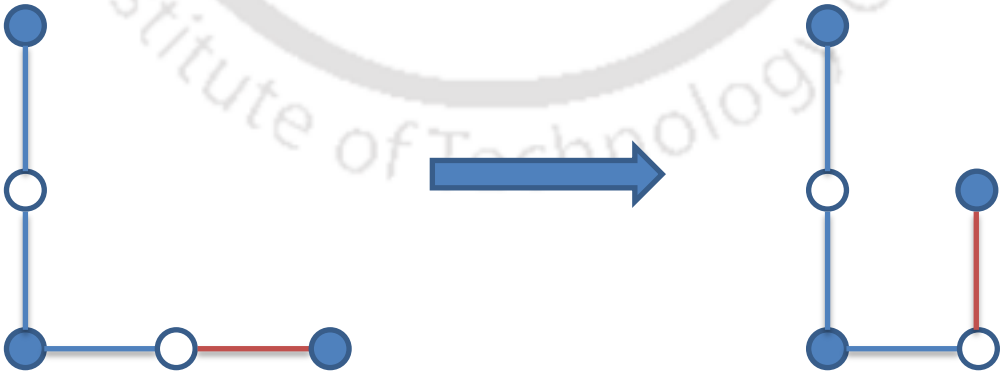

Figure 3.2 Schematic for end bond rotation.

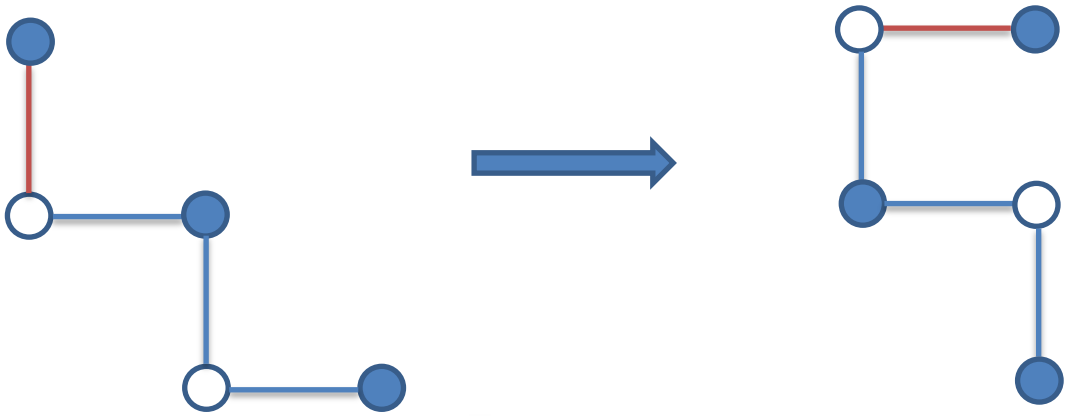

Figure 3.3 Schematic for slithering diffusion (reptation).

The coordination number of our lattice model is 26 (6 along the lattice axis, 12 along the face diagonals and 8 along the body diagonal). Thus, bond length can be 1 (along the axis), √2 (along the face diagonal) or √3 lattice units (along the body diagonal) [19, 20]. We start our simulation by selecting a vacant site randomly from the available vacant sites and then search for a nearest neighbour site occupied either by A-type or B-type monomer. Appropriate micro relaxation moves are selected in accordance with the position of monomers along the chain. To give further details, if the selected monomer is terminal one, end bond rotation and slithering diffusion is implemented with equal probability. On the other hand, if the unit is non-terminal, single site bond fluctuation move is implemented [11].

The interaction between A-type and B-type is modelled as the repulsive interaction to represent their mutual immiscibility. The energy penalty to create A-B contact is modelled by U_{AB} . The crystallization driving force is modelled as an attractive interaction between neighbouring parallel bonds and collinear bonds within A- or B- type units and given by U_p and U_c respectively. The change in energy per Monte Carlo move is then:

$$\Delta E = -\left(\Delta N_p U_p + \Delta N_c U_c\right)_A - \left(\Delta N_p U_p + \Delta N_c U_c\right)_B + \Delta N_{AB} U_{AB} \qquad (3.1)$$

Where, ΔN_A and ΔN_B represents the net change in the number of parallel and collinear bond respectively for the A and B block, and ΔN_{AB} represents the change in the number of contacts between A and B units.

As the block copolymer consists of two different crystallizable blocks, the melting temperatures of the two blocks are different. We model B-block as the low melting one and less facile to crystallize upon cooling from a high temperature melt. Therefore, the crystallization driving force of B-block is smaller than that of A-block. To implement this, we use $U_{pB} = \lambda_m U_{pA}$ and $U_{cB} = \lambda_m U_{cA}$ for the parallel and collinear bond respectively. We set $\lambda_m = 0.75$ (<1) to represent that B-block has less driving force for crystallization compared to A-block. Further, we assume that $U_p = U_c$, for the coarse grained interactions used in our simulation. U_{AB} is calculated as λU_p, where λ represents the segregation strength (viz., A-B demixing energy) relative to the parallel bond interaction energy, and equivalent to Flory's χ parameter. In our work $\lambda \geq 0$ and higher λ implies stronger segregation strength between the blocks. In terms of Flory's χ parameter, segregation strength is calculated as χN, which may be correlated to $(q-2)\times U_{AB} \times N$ in our system [16], where q is coordination number and N is the degree of polymerization. All the energies are normalized by $k_B T$, where, k_B is the Boltzmann constant and T is temperature in Kelvin; thus, $U_p \sim 1/T$. Now the change in energy per MC move is modified as follows:

$$\Delta E = \left[-\left(\Delta N_p + \Delta N_c\right)_A - \lambda_m \left(\Delta N_p + \Delta N_c\right)_B + \lambda \Delta N_{AB} \right] U_p \qquad (3.2)$$

We use the Metropolis sampling scheme with periodic boundary conditions to sample the conformations. We strictly implement excluded volume criteria and avoid bond crossing throughout the simulation [19, 20]. One lattice site is occupied by one unit (viz., either A-type, or B-type units) only or remains vacant throughout the simulation. In a given Monte Carlo (MC) move, during the formation of a new bond, if it crosses any of the existing bonds, then that move is rejected. We have checked the no-bond crossing criteria by calculating the midpoint of a bond. If any two bonds tend to cross each other, their mid-point should overlap on each other. We have calculated the midpoint coordinate of each bond and stored in an array. During each MC move we have checked the midpoint of newly form bond(s), whether it is occupied or not. If the point is occupied, the move is rejected and a new move has been initiated. This implementation technique is similar to the simulation technique followed by Dasmahapatra et al. [11].

The probability of an MC move is given by $\exp(-\Delta E)$. We accept new conformation if $\exp(-\Delta E) \geq r$, where r is the random number in the range (0, 1), generated by using

random number generator MT19937 [21]. We start our simulation at $U_p = 0$ (viz., at infinite temperature, athermal state) and cool the system by increasing U_p with a step size 0.02. To equilibrate the system we calculate mean square radius of gyration, $\langle R_g^2 \rangle$, as a function of Monte Carlo Steps (MCS). We did not observe appreciable change in the value of $\langle R_g^2 \rangle$ beyond 5000 MCS and it is considered as the equilibration time. We calculate thermodynamics and structural parameters averaged over subsequent 5000 MCS. A schematic is attached herewith which illustrates the sequence of simulation technique.

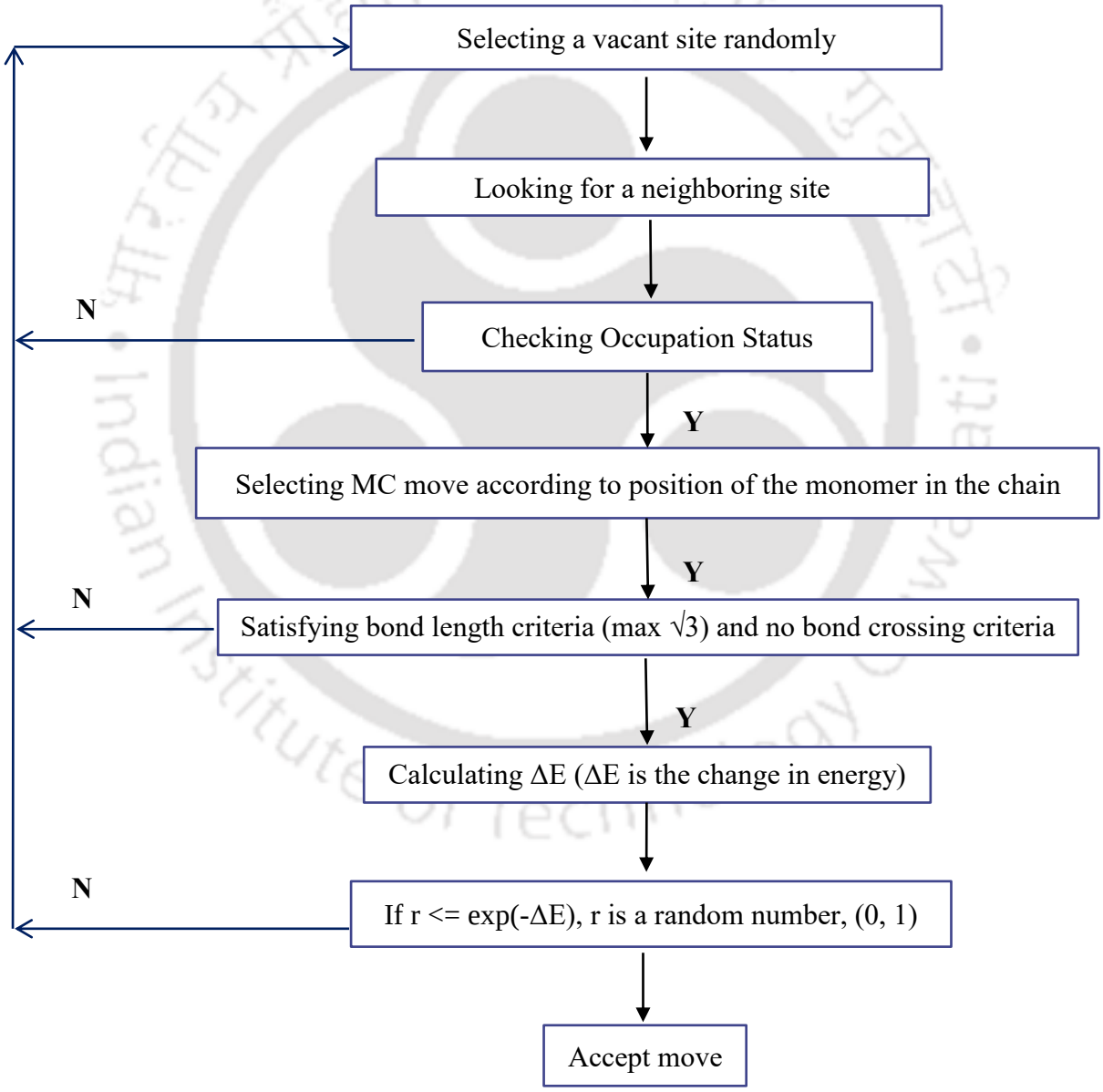

Figure 3.4 Schematic for the sequence of simulation algorithm.

To monitor transition from a disordered melt to an ordered crystalline phase, we calculate fractional crystallinity, X_c of A-block, B-block and overall, and specific heat (C_v) as a function of U_p. Specific heat is calculated as equilibrium specific heat from the total energy fluctuations (for all the monomer and comonomer units in simulation box) [11, 22]. We separately estimate C_v for A-B pair, based on the de-mixing energy between A and B-block, to locate the microphase separation point. During microphase separation, individual block forms respective domains, and the resultant transition is considered as disordered to ordered transition, which would give a peak in C_v at the transition point. We define crystallinity as the ratio of crystalline bonds to the total number of bonds present in the system. A bond is defined as crystalline if it is surrounded by more than 5 nearest non-bonded parallel bonds [10, 11, 23]. Therefore, the crystallinity of monomer is defined as the ratio of monomer bonds, which are surrounded by more than five parallel monomer bonds to the total number of monomer bonds [10]. This definition of crystallinity provides an idea about maximum achievable crystallinity. In contrast, experiments only report about relative crystallinity, which is, by definition, the fraction in the number of monomers rather than the number of monomer bonds [10]. We also calculate average crystallite size $\langle S \rangle$ and lamellar thickness $\langle l \rangle$. A crystallite is defined as a small microscopic aggregate having crystalline bonds in same orientation. The crystallite size is defined as the total number of crystalline bonds present in it. We compute the average crystallites size as a function of U_p. We express lamellar thickness as the average number of monomer units in the direction of crystal thickness in a given crystallite, and average thickness is calculated over all crystallites present in the system [11]. We also analyse the orientation of crystalline bonds by calculating bond order parameter (P) which is defined as:

$$P = \frac{3\langle \cos^2 \theta \rangle - 1}{2} \qquad (3.3)$$

Where, θ is the angle of a concerned bond with the reference of Z-axis and $\langle ..... \rangle$ represents an average over all the bonds containing more than 10 nearest parallel bonds. According to the definition, if all concerned bonds are in parallel with Z-axis, P is equal to 1 whereas if they are perpendicular with Z-axis, P is equal to -0.5. But if all concerned bonds are randomly oriented, P is close to zero [16]. We determine the change in mean square radius

of gyration $\left\langle R_g^2 \right\rangle$ with U_p for all compositions to understand morphological evolution. By definition, the square radius of gyration is the average squared distance of any point from its centre of mass which is expressed as:

$$\langle R_g^2 \rangle = \frac{\sum_{i=1}^{N} (r_i - r_{cm})^2}{N} \qquad (3.4)$$

Where, r_i is the distance from centre of mass and r_{cm} is the coordinate of centre of mass. N is the number of repeat units in a single polymer chain.

References

1. Grassberger P. Phys. Rev. E 1997;56(3):3682-3693.
2. Karaiskos E, deJoannis J, Anastasiadis SH, and Bitsanis IA. Macromol. Theory Simul. 2004;13:762-770.
3. Houdayer J. J. Chem. Phys. 2002;116(5):1783-1787.
4. Pakula T and Geyler S. Macromolecules 1987;20(11):2909-2914.
5. Pakula T. Macromolecules 1987;20(3):679-682.
6. Hu W. J. Chem. Phys. 2000;113(9):3901-3908.
7. Kremer K and Binder K. Comput. Phys. Rep. 1988;7(6):259-310.
8. Carmesin I and Kremer K. Macromolecules 1988;21(9):2819-2823.
9. Binder K and Paul W. Macromolecules 2008;41(13):4537-4550.
10. Hu W, Mathot VBF, and Frenkel D. Macromolecules 2003;36(6):2165-2175.
11. Dasmahapatra AK, Nanavati H, and Kumaraswamy G. J. Chem. Phys. 2009;131:074905-074901-074905-074910.
12. Li Y, Ma Y, Li J, Jiang X, and Hu W. J. Chem. Phys. 2012;136:104906-104901-104906-104907.
13. Hu W. J. Chem. Phys. 2001;115(9):4395-4401.
14. Larson RG, Scriven LE, and Davis HT. J. Chem. Phys. 1985;83(5):2411-2420.
15. Deutsch HP and Binder K. J. Chem. Phys. 1991;94(3):2294-2304.
16. Hu W. Macromolecules 2005;38(9):3977-3983.
17. Wang M, Hu W, Ma Y, and Ma Y-Q. J. Chem. Phys. 2006;124:244901-244901-244901-244906.
18. Dasmahapatra AK, Kumaraswamy G, and Nanavati H. Macromolecules 2006;39(26):9621-9629.
19. Shaffer JS. J. Chem. Phys. 1994;101(5):4205-4213.
20. Shaffer JS. J. Chem. Phys. 1995;103(2):761-772.
21. Nishimura T and Matsumoto M. 2002.
22. D.L.Goodstein. States of Matter: Dover, New York, 1985.
23. Li Y, Ma Y, Li J, Jiang X, and Hu W. J. Chem. Phys. 2012;136(10):104906.

Chapter 4

Crystallization of Symmetric Diblock Copolymer

We present here a study associated with the crystallization of double crystalline symmetric diblock copolymer to explore how the crystallization of one block influences the crystallization of other block. We implement non-isothermal crystallization as well as isothermal crystallization to understand crystallization behaviour and morphological evolution. We observe the effect of enhanced block immiscibility on crystallization. Observations are made on several diblock copolymers with variable segregation strength.

4.1 Literature Review

Diblock copolymers consist of two chemically distinct units, covalently bonded together. In majority of the cases, the two blocks are incompatible (viz. immiscible) with each other. The thermodynamic incompatibility between the blocks initiates self-organization (viz. self-assembly) via microphase separation, which maximizes the contacts between similar units and minimized the contacts between dissimilar units [1]. The Flory–Huggins interaction parameter (χ), block composition and chain length, (viz. degree of polymerization) determines the extent of separation and final morphology of polymer. The value of (χN) controls the strength of segregation. For a weakly segregated system the value of (χN) is around 10.5 whereas for strongly segregated system the value is more than 10.5 [2-4]. A diblock copolymer introduces a large variety of morphologies including lamellar structure, hexagonally packed cylinder or body centered cubic phases that are stable over a wide range of copolymer composition [2, 3].

In double crystalline diblock copolymer, phase behaviour is mostly governed by the interplay between crystallization and microphase separation. Usually, the block with higher melting point crystallizes first, followed by the second block with lower melting point [5-9]. During crystallization, first crystallizing block produces confinement for the crystallization of second block. As a result, the crystallization of second block slows down with lesser crystallinity [5, 6, 10-15]. A diblock copolymer of PE and PEO with 1:1 composition,

exhibits two sharp exothermic peak at 95.4 °C and 12.9 °C during DSC experiments, which triggers sequential crystallization of PE and PEO blocks [5]. In the diblock copolymer of linear polyethylene (LPE) and hydrogenated polynorbornene (hPN), although the melting points of hPN (156°C) and LPE (145.8°C) are marginally different, the final morphology of symmetric diblock copolymer was dictated by the hPN block while LPE block is forced to crystallize in between existing hPN lamellar morphology [8].

Polymer crystallization is not a truly thermodynamically equilibrium process. Therefore, the crystallization temperature (T_c) and cooling pathways (viz., isothermal and non-isothermal) play a crucial role to establish final semi-crystalline morphology. The crystalline-crystalline diblock copolymer, PCL-*b*-PE quenched from a microphase separated melt produces PE lamellar morphology. This lamellar morphology is preserved after crystallization of PCL block when T_c < 30 °C. But when the polymer is crystallized at T_c > 30 °C and T_c < 45 °C, PCL block completely destroys the previous morphology of PE, producing PCL lamellar morphology in which PE crystals are fragmentally dispersed [16]. Symmetric diblock copolymer PPL-*b*-PE, cooled from a microphase separated melt at a constant cooling rate (viz., non-isothermal crystallization), exhibit coincident crystallization; however, during isothermal crystallization both blocks crystallized separately (viz., sequential crystallization) [10].

Apart from the difference in melting points, the extent of mutual immiscibility, determined by the χ parameter influences the phase behaviour. The magnitude of χ changes with changing type of blocks present in the diblock copolymer. Subsequently, the extent of microphase separation and the crystal morphology changes which would enable to tune the properties of the final materials. For example, PEO in PLLA-*b*-PEO diblock copolymer lowers T_g of PLLA and makes it more flexible. However, the crystallization of PEO block is delimited by PLLA blocks [17]. On the other hand, the presence of PCL block in the PLLA-*b*-PCL diblock copolymer increases the molecular stability of the resulting block copolymer while keeping the biodegradability of PLLA intact [18]. The existence of PEG block reduces the crystallization of PLLA block and the degradation of PLLA-*b*-PEG diblock copolymer happen faster than pure PLLA [19]. During crystallization of strongly segregated symmetric diblock copolymer (PLLA-*b*-PE), the crystallization is confined by the respective melt microdomains producing thin lamellar micro domains without forming spherulites [14].

In most of the diblock copolymers, first crystallizing block suppresses the crystallization of second block. However, it has also been observed that during crystallization, both the block may crystallize together (viz., coincident crystallization) even if their melting points are widely different, or one block accelerates the crystallization of the other [20-24]. For example, the crystallization behaviour of PPDX-*b*-PCL diblock copolymer with a significant difference in the melting point of PPDX (100°C) and PCL block (57°C) exhibits coincident crystallization. This is attributed to the extremely slow crystallization rate of PPDX block [20, 21] compared to homopolymer. Recently, Monte Carlo simulation on lattice polymer reveals that the crystallization of one block accelerates the crystallization of other [22].

4.2 Results and Discussion

4.2.1 Non-Isothermal Crystallization

We consider symmetric diblock copolymer having 480 polymer chains with 64 repeat units, out of which 32 units are A-type and 32 are B-type units. In this section, we are going to discuss thoroughly the location of transition point, development of crystallinity and dimension of crystallite sizes during non-isothermal crystallization. We vary segregation strength (λ) from 0 to 5 and calculate crystallinity, lamellar thickness and crystallization temperature by implementing non-isothermal crystallization.

4.2.1.1 Monitoring Phase Transition

We cool the sample system from an equilibrated high temperature melt at U_p = 0 to U_p = 0.6 with a step size 0.02 to apply the cooling process of non-isothermal crystallization. During cooling, polymer chain segments are stiffened and aligned parallel with each other. This process is a realistic representation of the polymer crystallization. We start our simulation from a homogeneous melt at U_p = 0 where, A-type and B-type monomers are uniformly distributed (Figure 4.1).

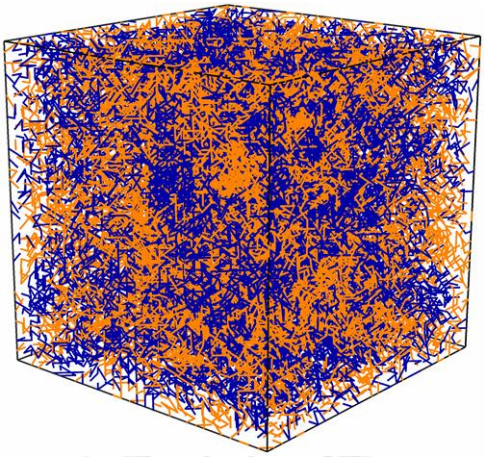

Figure 4.1 Snapshot of the simulation box at U_p = 0 representing homogeneous melt of diblock copolymer with comonomer composition (x_B = 0.5). Blue and orange line represents segments of A- and B-block respectively.

Increasing value of U_p signifies the gradual evolution of disordered molten state to ordered crystalline state. We observe crystallization of diblock copolymer by following the change in equilibrium specific heat [25], calculated from energy fluctuations as a function of U_p. At the transition point, C_v gives a peak as fluctuations in energy and the U_p value at which peak appears on cooling from the melt is considered as crystallization U_p in tune with experimental observation [25, 26]. We plot C_v vs. U_p (Figure 4.2) by varying segregation strength from λ = 0 to λ = 5 to obtain melt to crystal transition points in terms of U_p.

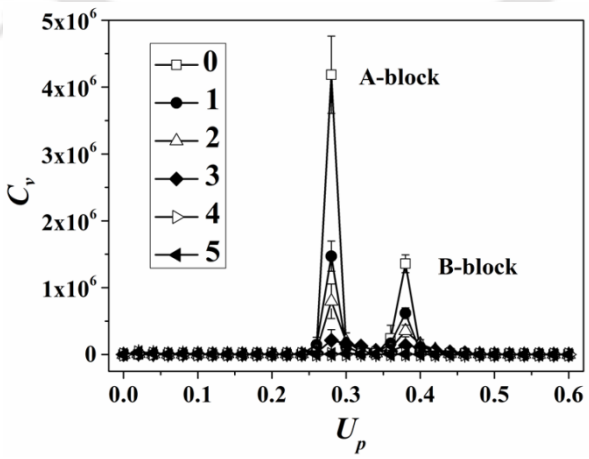

Figure 4.2 Change in specific heat (C_v) with U_p for λ = 0, 1, 2, 3, 4 and 5.

As diblock copolymer integrates two crystallizable blocks, Figure 4.2 gives two different peaks demonstrating the phase transition of A- and B-block at different values of U_p. The above observation is in accord with the experimental observation by Sun et al. [5] where the symmetric diblock copolymer PE-*b*-PEO reveals sequential crystallization behavior at 95.4 °C for PE block and 12.9 °C for PEO block. A-block crystallizes first due to its higher driving force towards crystallization, followed by B-block. The transition point of both the blocks remains similar for λ = 0, 1, 2, 3. But in case of λ = 4 and λ = 5, the transition points move towards higher value of U_p for A-block and lower value of U_p for B-block which is evident from Figure 4.3. High segregation fabricates large de-mixing energy between two blocks which influences the transitions of both blocks. The magnitude of the peak value of $C_v(C_v^*)$ decreases for both the blocks with increasing λ, representing the suppression of the phase transition at the higher segregation strength which is available in Figure 4.4.

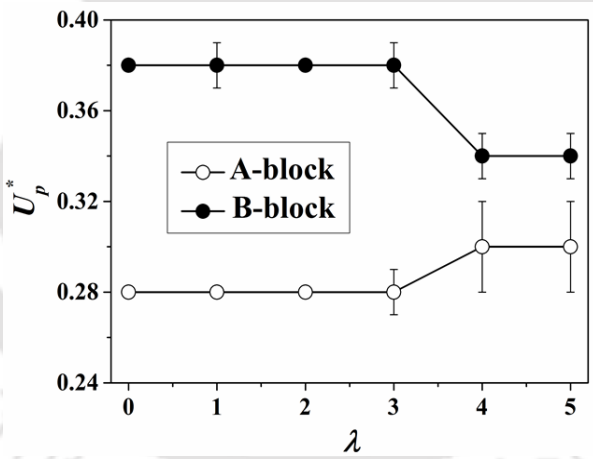

Figure 4.3 Change in transition point, U_p^* with λ for A- and B-block.

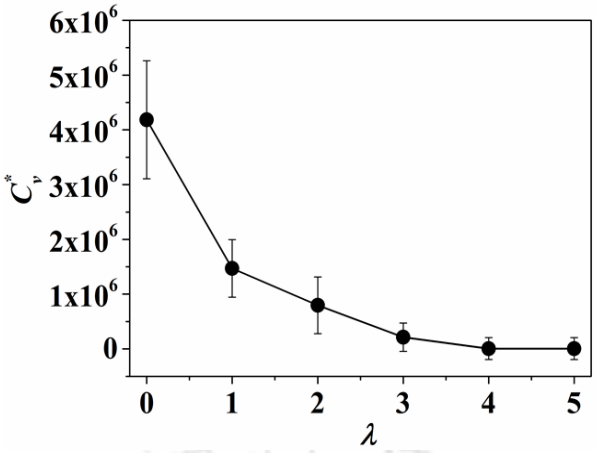

Figure 4.4 Change in specific heat at transition point, C_v^* with λ.

4.2.1.2 Locating Microphase Separation

In a diblock copolymer, due to block immiscibility, unlike contacts are minimized and similar contacts are maximized during microphase separation. Therefore, energy fluctuation based on the de-mixing energy of A and B units (viz., U_{AB}) also display a peak through microscopic phase segregation. We evaluate specific heat of A-B contact as a function of U_p. The plot of C_v of A-B contact (viz., C_{v-AB}) indicates a peak at an early stage of crystallization, close to U_p = 0.02. Figure 4.5 clearly shows the transition from homogeneous melt to microphase separated state by giving a peak at the transition point. This result is in agreement with the experimental observation of double crystalline PLLA-*b*-PCL diblock copolymer where miscible melt at 165°C, initially converted into a microphase separated lamellar morphology at 100°C before crystallization [13].

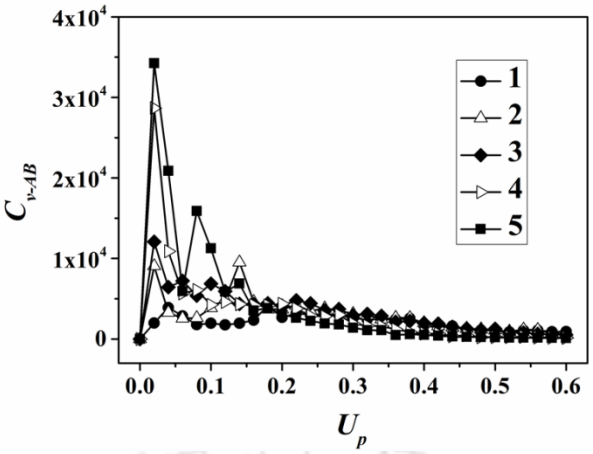

Figure 4.5 Change in specific heat of A-B demixing energy, C_{v-AB} with U_p for λ = 1, 2, 3, 4 and 5.

To get better idea, we again run our simulations from U_p = 0 to U_p = 0.02 with a step size 0.002 which is presented in Figure 4.6. Interestingly, the relative location of microphase separation point (viz., $U_p^{\#}$) varies with segregation strength λ. $U_p^{\#}$ shows decreasing trend with increasing value of λ (Figure 4.7). With the increment of segregation strength, repulsive interaction between two blocks increases, which accelerates microphase separation at a relatively higher temperature (viz., lower U_p).

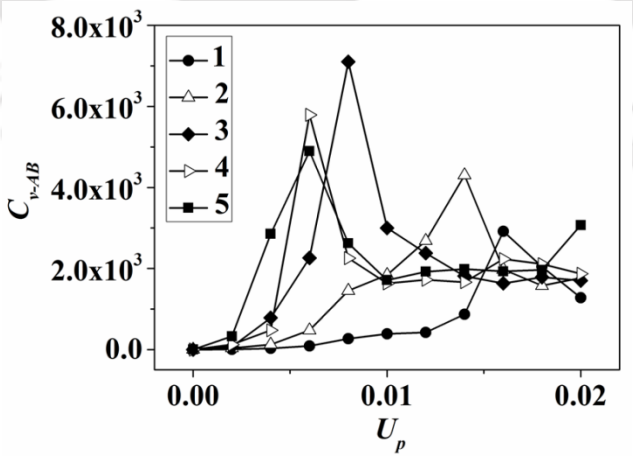

Figure 4.6 Change in specific heat of A-B demixing energy, C_{v-AB} with U_p (U_p = 0 to 0.06, with a step cooling of 0.002) for λ = 1, 2, 3, 4 and 5.

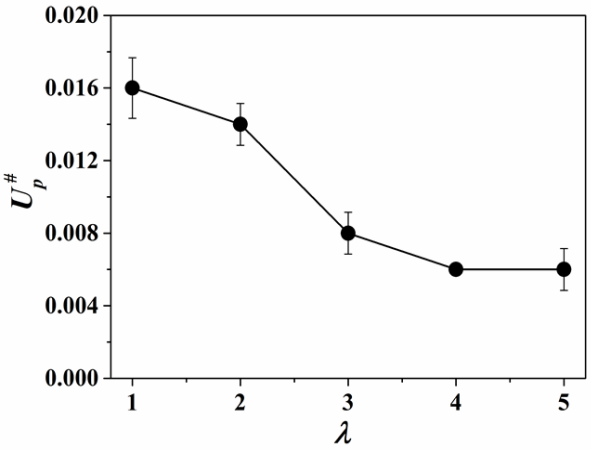

Figure 4.7 Change in microphase separation point, $U_p^{\#}$ with λ.

As segregation strength χN can be estimated as: $(q-2)\times U_{AB}\times N$, the value of χN = 32 (~ 10) for λ = 1 and 96 (~ 100) for λ = 3, at U_p = 0.02. Therefore, we may consider $\lambda \leq 2$ as weak segregation and $\lambda > 2$ as strong segregation. Figure 4.8 exhibits the snapshots of microphase separated melt from simulation at U_p = 0.02 and U_p = 0.1 for λ = 1 (weak segregation) and 3 (strong segregation). Microphase separation at strong segregation (λ = 3 - 5) initiates larger confinement which prevents crystal growth.

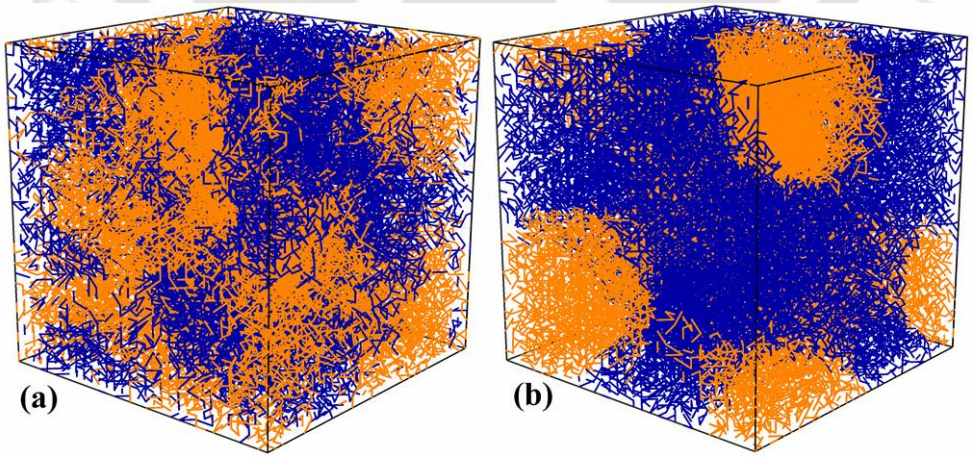

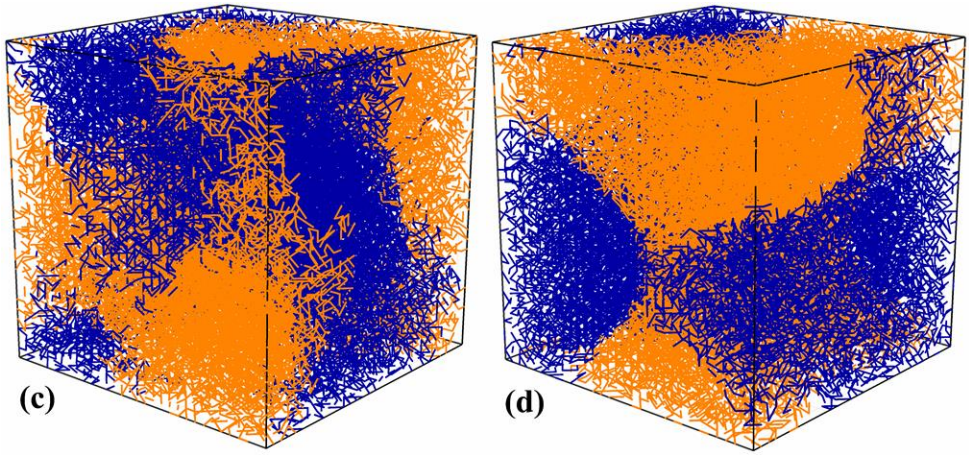

Figure 4.8 Snapshots of microphase separated melt for (a) weak segregation (λ = 1) at U_p = 0.02, (b) weak segregation (λ = 1) at U_p = 0.1, (c) strong segregation (λ = 3) at U_p = 0.02 (d) strong segregation (λ = 3) at U_p = 0.1. Blue and orange line represents segments of A- and B-block respectively.

We have computed mean square radius of gyration, $\langle R_g^2 \rangle$ as a function of U_p for U_p = 0 to 0.02 (Figure 4.9), to correlate the trend with $C_v - AB$ data (Figure 4.6). $\langle R_g^2 \rangle$ abruptly rises at a temperature, close to that where $C_v - AB$ indicates a peak during microphase separation. The abruptness in $\langle R_g^2 \rangle$ value increases with increasing values of λ, from 0 to 5, which correlates to the trend of $C_v - AB$ with λ.

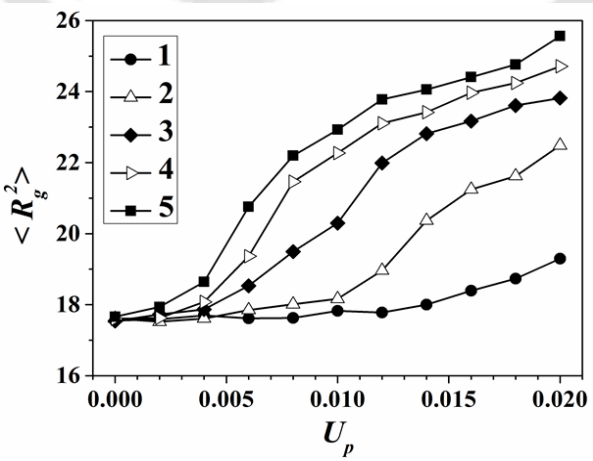

Figure 4.9 Change in mean square radius of gyration, $\langle R_g^2 \rangle$ with U_p (U_p = 0 to 0.06, with a step cooling of 0.002) for λ = 0, 1, 2, 3, 4 and 5.

4.2.1.3 Development of Crystallinity

We notice the crystallization behaviour of symmetric diblock copolymer for a series of λ (viz., λ = 0, 1, 2, 3, 4 and 5). Figure 4.10a displays the variation of crystallinity of A-block, X_A with U_p. X_A shows an abrupt increase in its value at $U_p \sim 0.3$ for all λ and extends up to saturated value, X_A^{sat} at $U_p \sim 0.5$. The saturation crystallinity declines with increasing λ. X_A^{sat} reduces from 0.76 at $\lambda = 0$ to 0.31 at $\lambda = 5$. This reduction in crystallinity with an increase in λ signifies that with the increase of λ, system proceeds from soft confinement to hard confinement. As a result, chain mobility decreases and hence crystallinity decreases.

We detect a similar trend for the crystallinity of B-block, X_B with U_p (Figure 4.10b). As we have modelled B-block with lower melting point, the crystallization of B-block proceeds at a higher U_p value (viz., lower temperature) compared to A-block. Figure 4.10b displays an abrupt increase in its value at $U_p \sim 0.4$ and reaches almost a saturated value, X_B^{sat} at $U_p \sim 0.55$. The saturation crystallinity, X_B^{sat} also monotonically declines with λ. However, the saturation crystallinity of A-block is higher than that of B-block for all value of λ. The difference in crystallinity establishes that B-block crystallizes within the confinement created by A-block and hence crystallization of B-block slows down giving rise to lower crystallinity compared to A-block. On the other side, the change in crystallinity at $\lambda = 4$ and 5 are quite substantial: X_A^{sat} = 0.36 and 0.31 whereas, X_B^{sat} = 0.23 and 0.20 respectively. So, the higher segregation strength (λ = 4 and 5) produces hard confinement for B-block monomers resulting poor crystallinity. We also evaluate the trend of overall crystallinity, X_c (combined crystallinity of A- and B-block units) as a function of U_p (Figure 4.10c). The graph clearly highlights two different regimes for two crystallizable blocks. For all values of λ, X_c increases abruptly at $U_p \sim 0.3$ (where A-block starts to crystallize), and extends up to saturation crystallinity at $U_p \sim 0.55$, after a marginal increase (where A-block almost reaches the saturated crystallinity and B-block begins to crystallize) at $U_p \sim 0.35$. The overall saturation crystallinity also decreases monotonically with increasing segregation strength from 0.73 for $\lambda = 0$ to 0.68, 0.63, 0.57, 0.3 and 0.25 for λ =1, 2, 3, 4 and 5 respectively. The inter-block segregation strength dramatically inhibits the crystalline domain to develop.

During the crystallization of higher segregation strength (viz., λ = 3 to 5), repulsive interaction between blocks leads to phase segregation with the formation of a large number of smaller size microdomains of both the blocks. As a result, crystallization is confined within these micro-domains and produces less crystalline structure (viz., confined crystallization). Our simulation results are in line with experimental observations for various diblock copolymers, where, crystallization of the second block is inhibited due to confinement created by the crystallization of first block resulting in less crystalline materials [7, 13, 14].

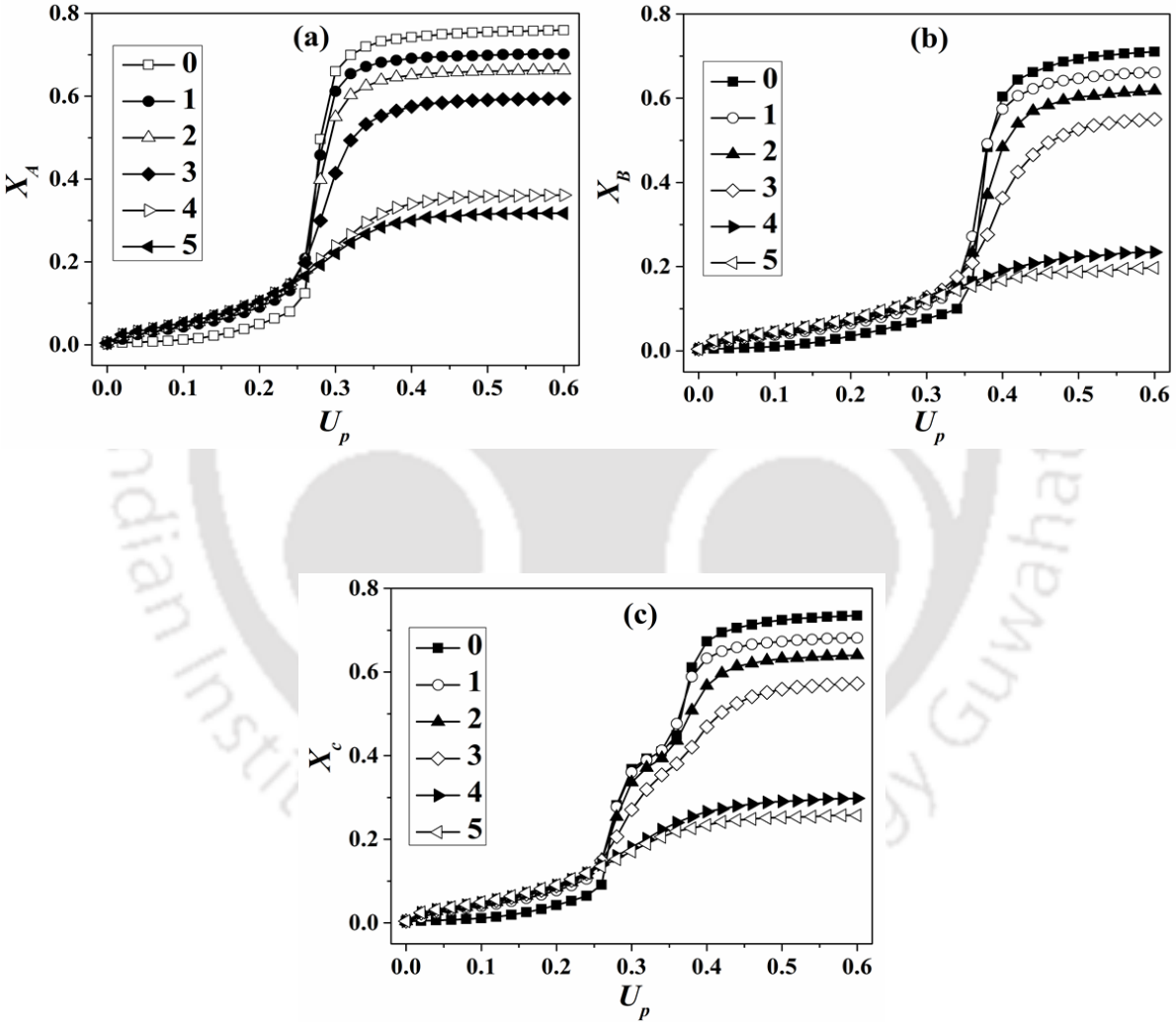

Figure 4.10 Change in crystallinity (X) of (a) A-block, (b) B-block and (c) Overall with U_p for λ = 0, 1, 2, 3, 4 and 5.

We express chain mobility as mean square displacement of center of mass averaged over all polymer chains (d_{cm}^2) and we plot chain mobility with U_p at different values of λ in Figure 4.11. At higher segregation, the chain mobility is mostly restricted which minimizes the diffusion of crystalline segments towards the growth front resulting less crystallinity.

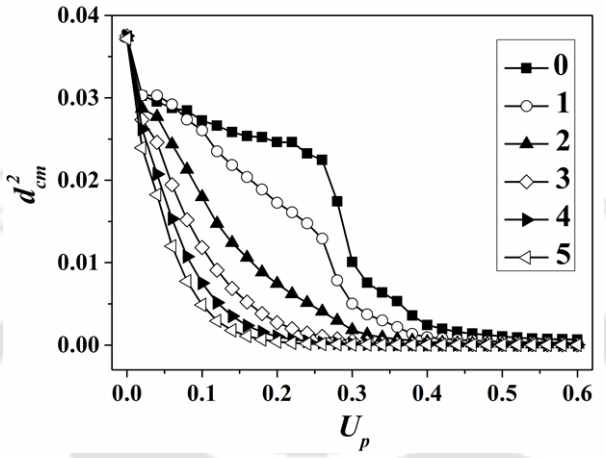

Figure 4.11 Change in mean square displacement (d_{cm}^2) with U_p (~1/T) for λ = 0, 1, 2, 3, 4 and 5.

Reheating from U_p = 0.6 to U_p = 0 with a heating step 0.02 reveals hysteresis on melting (Figure 4.12). This pattern is quite similar for non-equilibrium, first order phase transition in bulk polymers [25, 27].

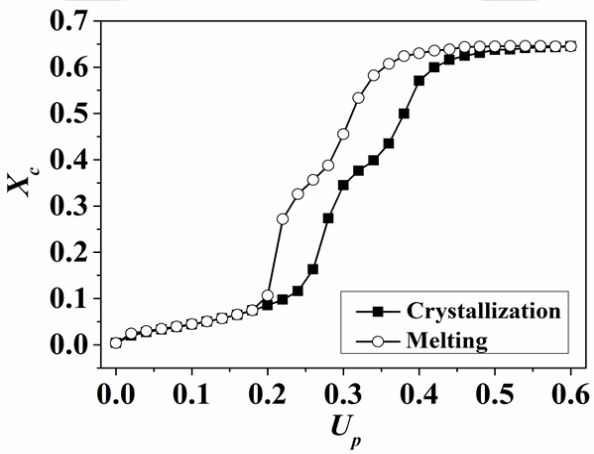

Figure 4.12 Change in fractional crystallinity, X_c with U_p (~1/T) for λ = 2, during crystallization and melting of diblock copolymer displaying hysteresis.

4.2.1.4 Structural Analysis

We evaluate the average crystallite size and the average lamellar thickness as a function of U_p. We notice a wider distribution of crystallites size compared to that of lamellar thickness. The dimension of crystallite size is much higher than the lamellar thickness of crystallites, representing the formation of two dimensional crystals. We observe the change in average crystallite size over the entire range of U_p at different λ values for A-block (Figure 4.13a) and B-block (Figure 4.13b). We detect that the average crystallites size of both A, $\langle S_A \rangle$ and B-block, $\langle S_B \rangle$ increases with increasing U_p and saturates at $U_p \geq 0.55$. The increment in the value of $\langle S_A \rangle$ and $\langle S_B \rangle$ is noticeable for lower values of λ ($\lambda \leq 3$), whereas for higher values of λ (viz., λ = 4 and 5), the increase in $\langle S_A \rangle$ and $\langle S_B \rangle$ is not visible. At high segregation strength, the growth of crystalline domains is restricted producing smaller size crystals, which is similar to crystallinity trend (Figure 4.10).

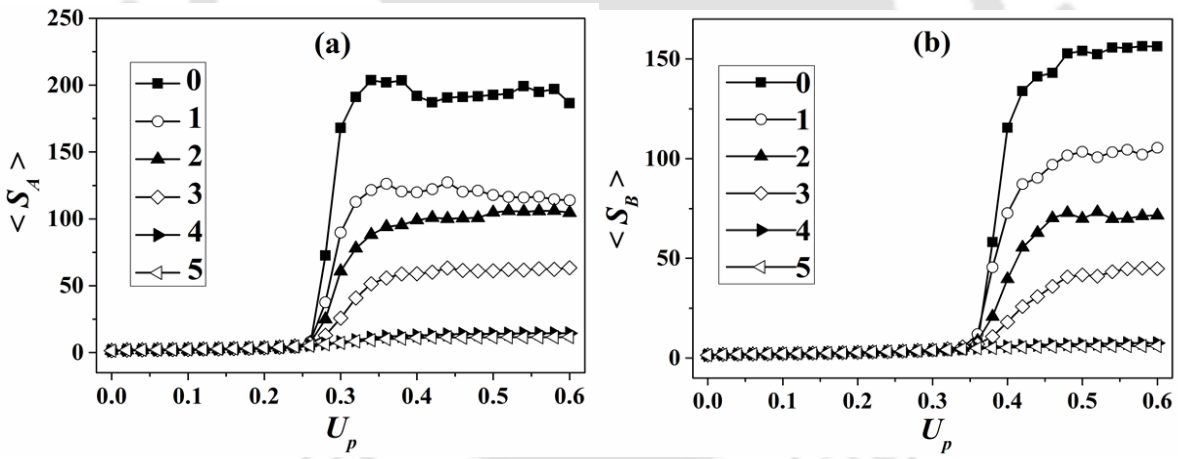

Figure 4.13 Change in average crystallites size, $\langle S \rangle$ of (a) A-block and (b) B-block with U_p at λ = 0, 1, 2, 3, 4 and 5.

For better understanding, we also study the average lamellar thickness of A- and B-block, $\langle l_A \rangle$ and $\langle l_B \rangle$ respectively as a function of U_p. The lamellar thickness of both A-block (Figure 4.14a) and B-block (Figure 4.14b) declines with increasing value of λ, suggesting the formation of thinner crystals against the normal tendency of crystal thickening of

homopolymer. High segregation strength (viz., λ > 3), provides smaller size microdomains of individual block, which upon crystallization transform to smaller and thinner crystals.

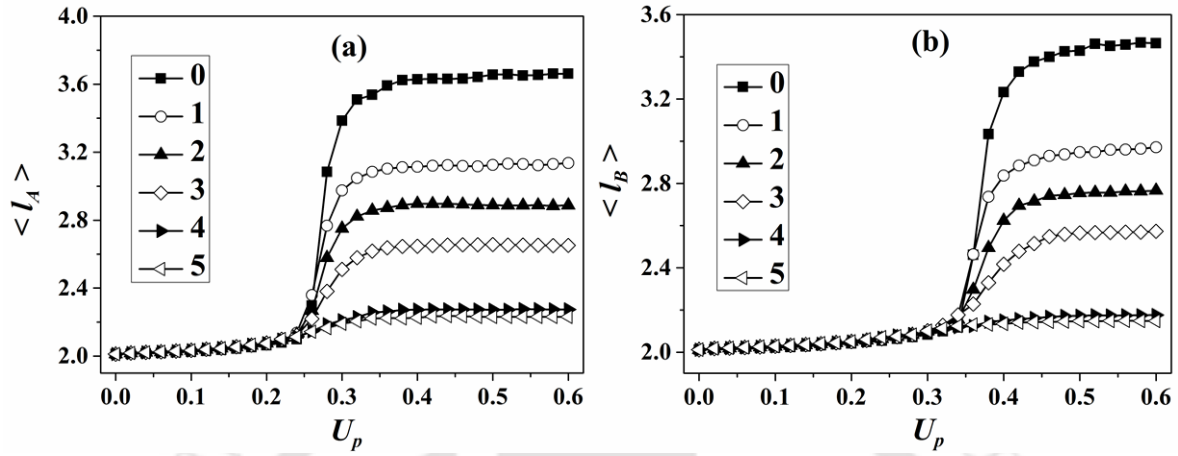

Figure 4.14 Change in lamellar thickness, $\langle l \rangle$ of (a) A-block (b) B-block with U_p at λ = 0, 1, 2, 3, 4 and 5.

During crystallization, block incompatibility enables the formation of phase separated domains which generates strong tension in the block junction resulting chain stretching. This stretching in the junction hampers the crystals from being thickened, producing smaller and thinner crystals. We also observe a significant increase in the mean square radius of gyration of the chain during crystallization in Figure 4.15.

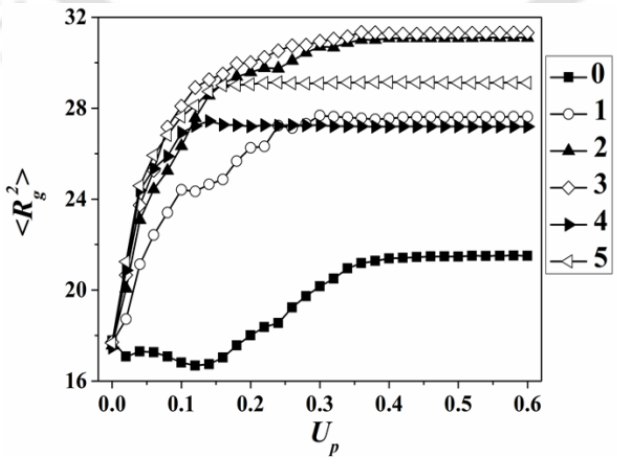

Figure 4.15 Change in mean square radius of gyration, $\langle R_g^2 \rangle$ with U_p for λ = 0, 1, 2, 3, 4 and 5.

With the increment of λ (viz., segregation strength), the repulsive interaction between A- and B-block units increases. As a result, the effective chain mobility decreases and the formation of smaller size domains are favoured over the formation of larger size domain, which involves the diffusion of chain segments towards the growth font (Figure 4.11). Figure 4.16 exhibits the snapshots for λ = 1, at U_p = 0.3 and U_p = 0.6. At U_p = 0.3, A-block is almost crystallized forming lamellar morphology, leaving space for B-block to crystallize. When U_p is increased to 0.6, B-block crystallizes within the confinement created by A-block. To understand the development of crystalline morphology as a function of λ (λ = 0, 1, 2, 3, 4 and 5), we display the snapshots from our simulation at U_p = 0.6 in Figure 4.17. The decrease in crystallinity with smaller crystallite size is evident from these snapshots.

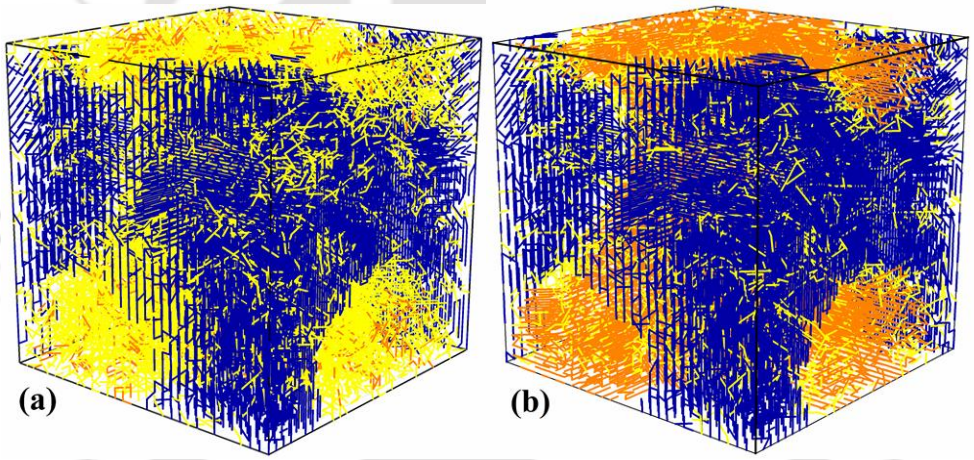

Figure 4.16 Snapshots of semi-crystalline structure for λ = 1 for (a) U_p = 0.3 and (b) U_p = 0.6, during non-isothermal crystallization. Blue lines represent crystalline bonds of A-block, orange lines represent crystalline bonds of B-block and yellow lines represent non-crystalline bonds of both the blocks.

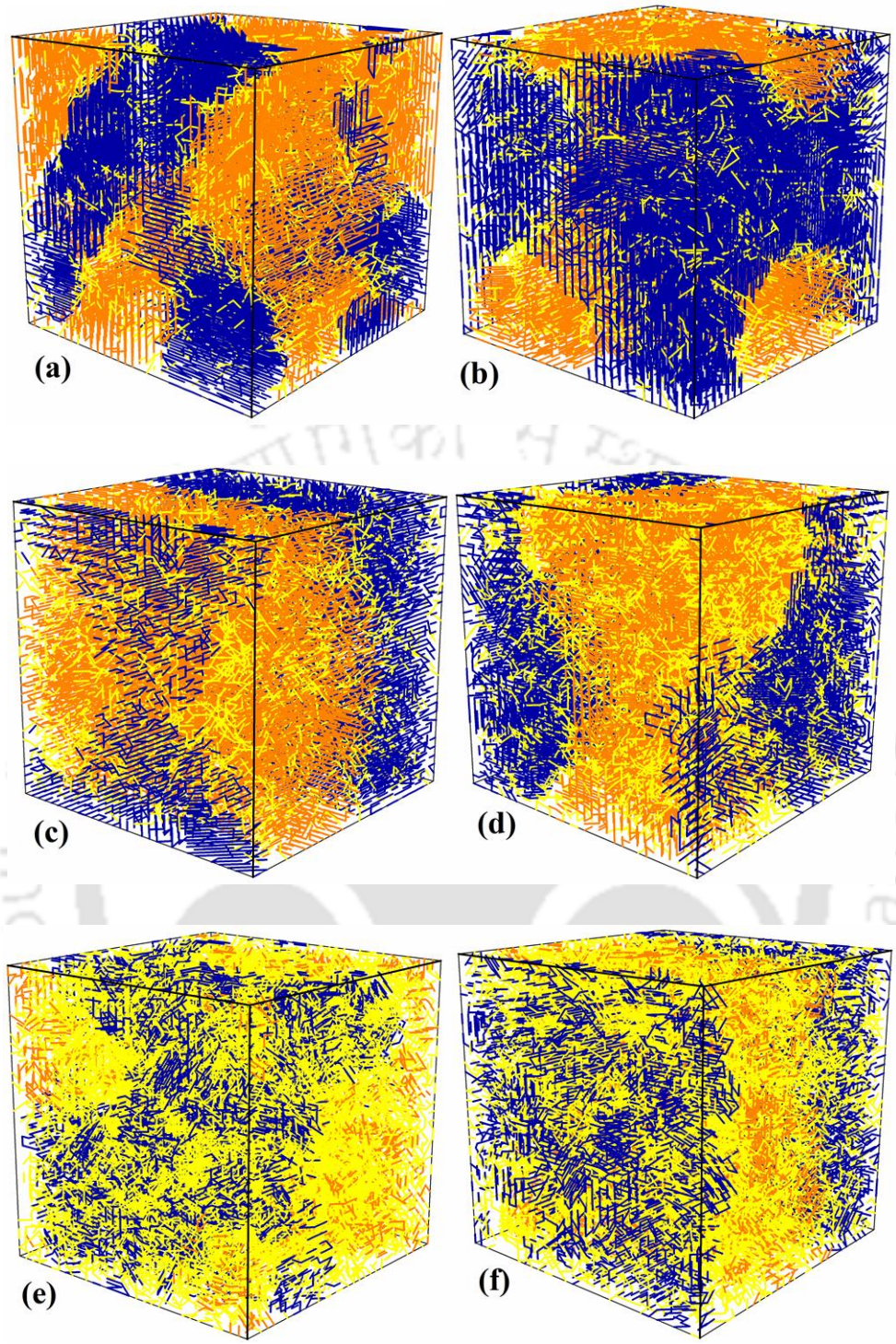

Figure 4.17 Snapshots of semi-crystalline structure at U_p = 0.6 for (a) λ = 0, (b) λ = 1, (c) λ = 2, (d) λ = 3, (e) λ = 4 and (f) λ =5. Blue lines represent crystalline bonds of A-block, orange lines represent crystalline bonds of B-block and yellow lines represent non-crystalline bonds of both the blocks.

4.2.2 Isothermal Crystallization

4.2.2.1 One-step Cooling

To explore isothermal one-step cooling, we quench our sample system from an athermal state (U_p = 0) to U_p = 0.6 directly and anneal for 10^5 MCS. We observe the evolution in the overall crystallinity (Figure 4.18a) with Monte Carlo steps (MCS) for all values of λ. We also estimate scaled crystallinity, $X_c^* = \left(X_c - X_c^i\right)/\left(X_c^f - X_c^i\right)$, ranges from 0 to 1, with λ (Figure 4.18b). X_c^i represents the initial crystallinity of the isothermal annealing, and X_c^f represents the final crystallinity of isothermal annealing (viz., X_c at the end of $1\times10^5 MCS$). The development of isothermal crystallinity with MCS reveals that the transition kinetics of diblock copolymer with two crystallisable blocks follows a distinct pathway for different magnitude of λ. For λ = 0, the overall crystallinity of isothermal crystallization is almost identical to that of the non-isothermal crystallization. However, with increasing value of λ, the overall crystallinity is reduced monotonically. For example, isothermal crystallization at λ = 1, 2, 3, 4 and 5 develops an overall crystallinity of 0.55, 0.22, 0.08, 0.05 and 0.03 respectively (Figure 4.18). The corresponding overall crystallinity during non-isothermal crystallization is 0.68, 0.64, 0.57, 0.30 and 0.26 respectively (Figure 4.10c). From the above data, we can conclude that when the segregation strength is high, the isothermal crystallization offers extremely poor crystallinity due to the lack of stability needed for equilibrium chain folding.

In Figures 4.19a and 4.19b, we compare the initial development of crystallinity (up to 1000 MCS) for A- block and B-block individually at λ = 0 and λ = 2 respectively. For λ = 0, the primary stage of crystallinity of both blocks is indistinguishable till ~ 10 MCS, after that A-block follows a different pathway with higher crystallinity than that of the B-block. The phenomenon is provoked by the higher driving force of A-block towards crystallization. For λ = 2, from the preliminary stage, both blocks follow different trajectories with A-block producing higher crystallinity than that of the B-block. At λ = 2, due to higher segregation strength, microphase separation occurs at a very early stage and as a result, the time evolution of crystallinity proceeds through different trajectories for A- and B-blocks.

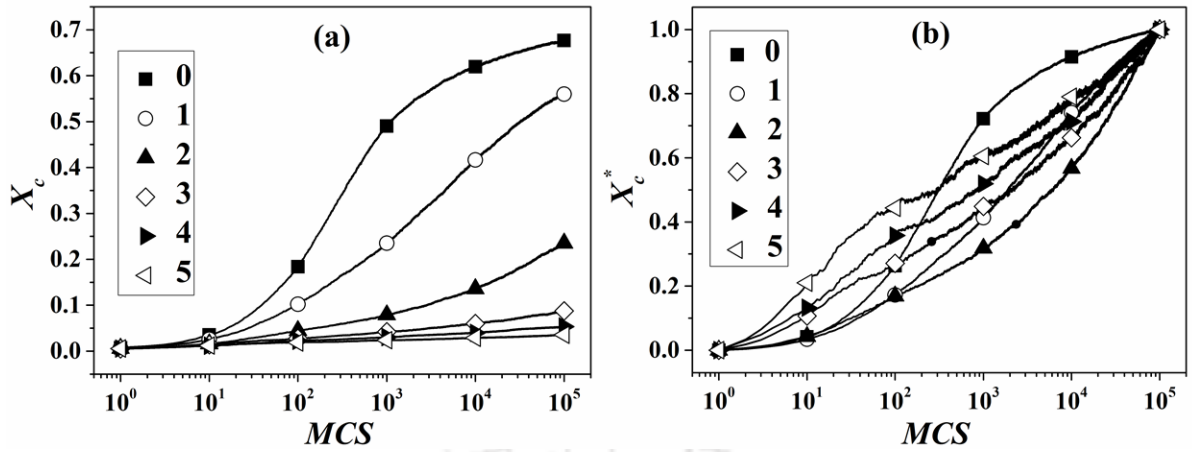

Figure 4.18 Change in (a) overall crystallinity and (b) scaled crystallinity with Monte Carlo Steps (*MCS*) for λ = 0, 1, 2, 3, 4 and 5 during isothermal one-step crystallization.

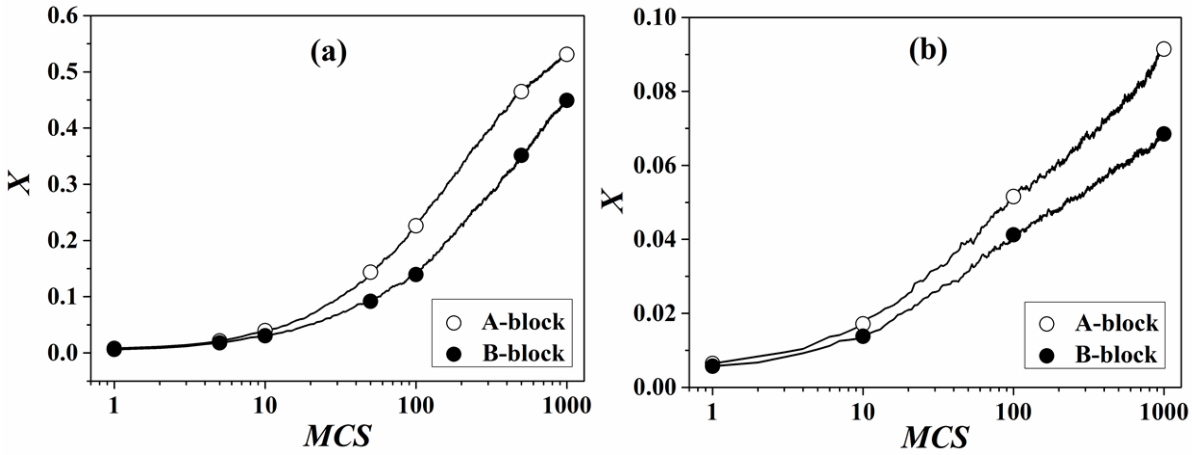

Figure 4.19 Development of initial crystallinity for individual A- block and B-block at (a) λ = 0 and (b) λ = 2 with Monte Carlo Steps during isothermal crystallization.

The condition of crystallization (isothermal vs. non-isothermal) has an enormous influence on final crystal morphology. Time evolution of crystallinity can be delivered by the Avrami equation [28].

$$\left(1 - X_c^*\right) = \exp\left(-kt^n\right)$$

Where, X_c^* represents the scaled value of overall crystallinity. We calculate Avrami index, *n* (which specifies the type of crystal geometry), with different values of λ, based on the primary crystallization, which is considered as the enlargement of crystallinity up to 20%

[29]. The value of *n* for both blocks exists in the range 0.6 to 1.2 (Figure 4.20), designating homogeneous nucleation with first order transition kinetics. The crystallization behaviour of several amorphous-crystalline diblock copolymers has been examined where the crystallization of one block is confined within lamellar microdomains of another block [30-32]. When the crystallization is confined in glassy (hard) microdomain structures, it follows a first order transition kinetics with homogeneous nucleation with the Avrami index close to 1.0 [31]. Confinement effect which is developed due to segregation strength compels both blocks to grow within small microdomains resulting into two dimensional growths. However, for higher segregation strength, where the development of crystallinity is very poor, it is difficult to investigate accurately the dimensionality of the crystals.

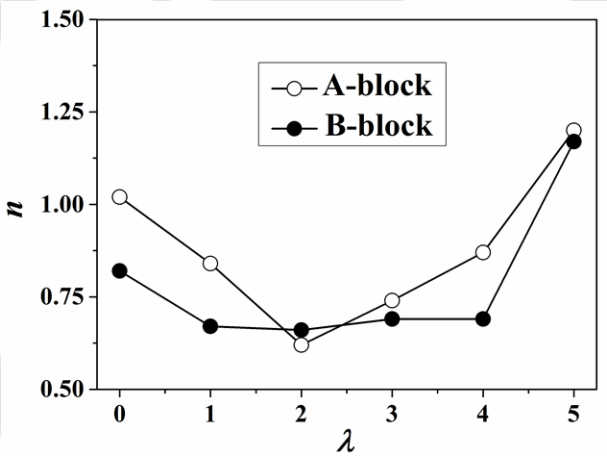

Figure 4.20 Change in Avrami index (n) with λ for A-block and B-block after isothermal annealing at U_p = 0.6.

We capture the final snapshots of crystal morphology at U_p = 0.6 during isothermal one-step crystallization in Figure 4.21. Isothermal crystallization with high segregation (λ >2) produces very poor crystallinity which is evident from following snapshots. During isothermal crystallization, the crystallization driving force (viz., in terms of temperature difference) is adequate for both the blocks. Therefore, both the blocks compete with each other for crystallization which leads to coincident crystallization. The above observation is in accord with PPDX-*b*-PCL diblock copolymer, where crystallization kinetics of both the blocks overlapped [20, 23].

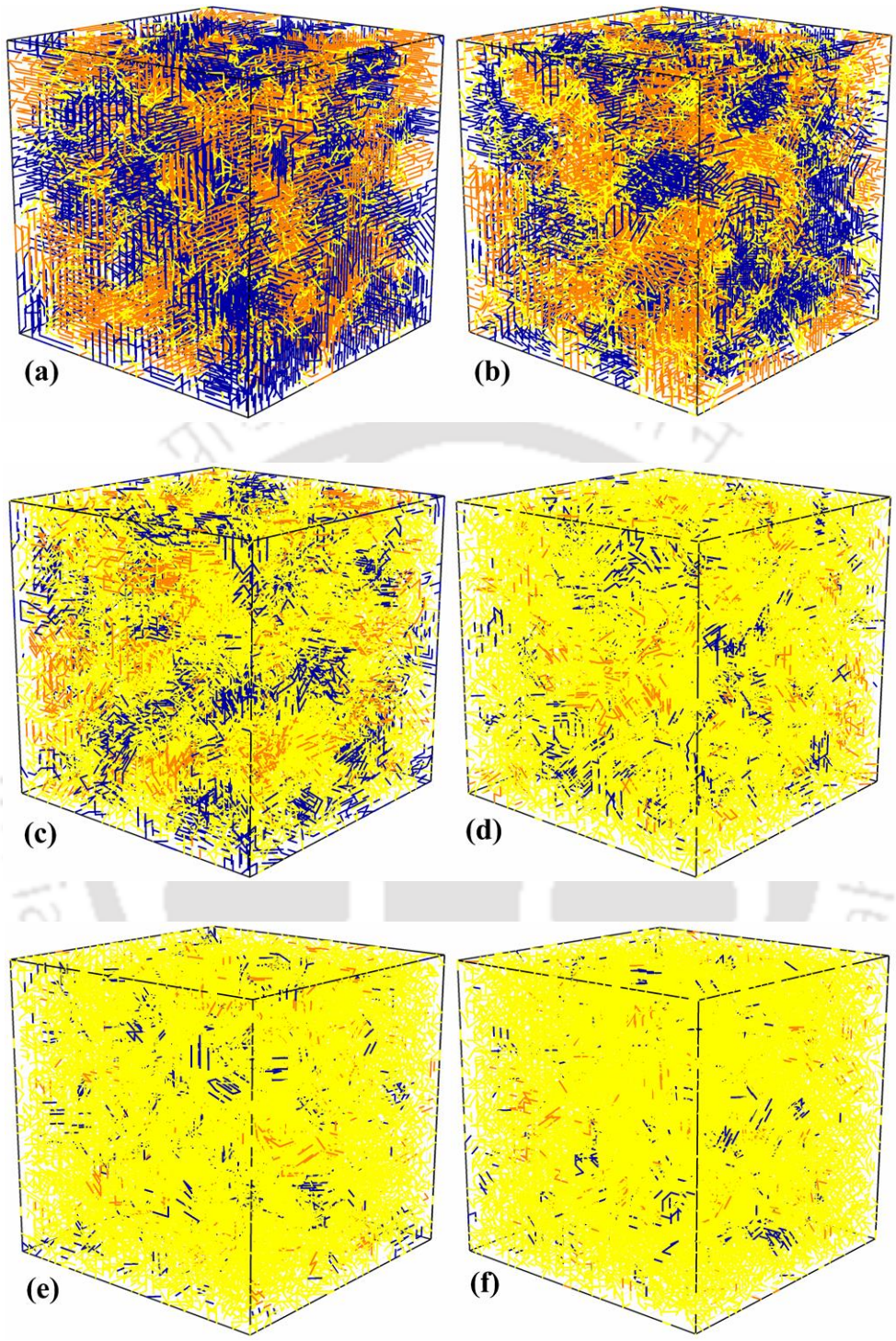

Figure 4.21 Snapshots of semi-crystalline structure at U_p = 0.6 during isothermal crystallization for (a) λ = 0, (b) λ = 1, (c) λ = 2, (d) λ = 3, (e) λ = 4 and (f) λ =5. Blue lines represent crystalline bonds of A-block, orange lines represent crystalline bonds of B-block and yellow lines represent non-crystalline bonds of both the blocks.

4.2.2.2 Two-step Cooling

To apprehend the effect of quench depth on the development of crystalline structure, we implement isothermal cooling in two steps. During the first step, we quench the equilibrated melt from $U_p = 0$ to $U_p = 0.3$ and annealed for 1×10^5 MCS and in the second step, we quench to $U_p = 0.6$ from $U_p = 0.3$ and annealed for 1×10^5 MCS. At $U_p = 0.3$ (temperature above the melting point of B-block), A-block crystallizes while B-block is still in a molten state. When we quench to $U_p = 0.6$ from $U_p = 0.3$, B-block crystallizes within the confined space created by A-block crystal. We compare the value of saturation crystallinity of A-block and B-block initiated by isothermal two-step and one-step crystallization in Table 4.1 and Table 4.2 respectively. We notice a considerable improvement in the saturation crystallinity of A-block in two-step quenching compared to one-step quenching (viz., direct quench to $U_p = 0.6$). However, we detect a minimal change in the saturation crystallinity of B-block when we compare one-step and two-step quenching. But high segregation provides poor crystallinity for both the blocks.

Table 4.1 Comparison in saturation crystallinity of A-block (X_A^{sat}) for λ = 0, 1, 2, 3, 4, and 5 during two-step and one-step isothermal crystallization.

Segregation strength (λ)	Two-step cooling at U_p = 0.3	Two-step cooling at U_p = 0.6	One-step cooling at U_p = 0.6
0	0.72	0.77	0.69
1	0.67	0.70	0.57
2	0.50	0.55	0.26
3	0.20	0.22	0.09
4	0.13	0.13	0.06
5	0.08	0.08	0.03

Table 4.2 Comparison in saturation crystallinity of B-block (X_B^{sat}) for λ = 0, 1, 2, 3, 4, and 5 during two-step and one-step isothermal crystallization.

Segregation strength (λ)	Two-step cooling at U_p = 0.3	Two-step cooling at U_p = 0.6	One-step cooling at U_p = 0.6
0	0.07	0.68	0.66
1	0.10	0.57	0.55
2	0.11	0.30	0.20
3	0.11	0.12	0.07
4	0.08	0.08	0.04
5	0.06	0.06	0.03

We interpret the above observation as follows. When we quench the sample to a temperature below the melting point of A-block (but above the melting point of B-block), crystallization of A-block occurs without much of hindrance from B-block units. In the next stage, we quench the sample to a temperature below the melting point of B-block where the crystallization of B-block does not experience interference from A-block, since A-block has already developed crystalline domain leaving spaces (viz., confined space) for the B-block units to crystallize. Therefore, the mode of crystallization in two-step quenching is sequential crystallization, which is similar with the isothermal crystallization of PPL-*b*-PE diblock copolymer where both blocks crystallize separately [10]. In one-step crystallization, we quench our sample to a temperature below the melting point of both A- and B-block (U_p = 0.6), where both the block compete with each other to crystallize, since the driving force for the crystallization is adequate for the crystallization of both the blocks. Therefore, the mode of crystallization in one-step quenching can be designated as coincident crystallization, where both the blocks crystallize simultaneously. This observation is in close agreement with the isothermal crystallization of PPDX-*b*-PCL diblock copolymer where crystallization kinetics

of two blocks are overlapped [20]. In one-step isothermal crystallization, inter-block entanglement also plays a pivotal role in suppressing the development of crystalline structure. When we quench directly to U_p = 0.6 (from an equilibrated melt at U_p = 0), the crystallization of A-block is hindered by the inter-block entanglement, and the interplay between microphase separation and crystallization resulting suppression of saturation crystallinity of A-block. But the amount of saturation crystallinity of B-block is almost similar in both the cooling process. The saturation crystallinity of B-block is 0.57 and 0.55 for λ =1 (Table 4.2) in two-step and one-step isothermal crystallization respectively, suggesting that the effective driving force for the crystallization is almost same irrespective of the mode of quenching. Thus, two-step quench gives a better crystallization than one-step quench for first crystallizable block.

We also compare the development of lamellar thickness of A-block and B-block during isothermal two-step and one-step quenching in Table 4.3 and 4.4 respectively. Analysis based on the evolution of lamellar thickness demonstrates that the lamellar thickness of A-block at U_p = 0.6 during one-step cooling is less compared to its value at U_p = 0.3 during two-step cooling (Table 4.3), which is in accord with the Hoffman-Weeks formulation [33] and recent experimental observation on the PCL-*b*-PE diblock copolymer [9]. However, the lamellar thickness of B-block when measured at U_p = 0.6 by one- and two-step cooling, are almost identical. We interpret this finding as follows. The development lamellar thickness is largely determined by the degree of undercooling $\left(\Delta T = T_m^{\alpha} - T\right)$. When we quench the sample system to U_p = 0.6, the effective ΔT for B-block remains same in one- and two-step cooling. Therefore, the crystal thickening (development of crystal thickness) remains almost same (Table 4.4) for both the cooling processes. Moreover, the crystallization of B-block is confined by the space created by A-block crystals, restricting the crystal thickening of B-block. As a result, B-block produces lamellae with comparable thickness during one-step and two-step isothermal crystallization. Our simulation result is in close agreement with the recent experimental observation by Sakurai et al. [9], on isothermal crystallization of the PCL-*b*-PE diblock copolymer, where the long range order is almost constant when crystallized below 35°C (25 °C $\leq T_c \leq$ 35 °C). The final crystal morphology at λ =1 during two-step cooling is available in Figure 4.22.

Table 4.3 Comparison in average lamellar thickness of A-block for λ = 0, 1, 2, 3, 4 and 5 during two-step and one-step isothermal crystallization.

Segregation strength (λ)	Two-step cooling at U_p = 0.3	Two-step cooling at U_p = 0.6	One-step cooling at U_p = 0.6
0	3.67	3.91	3.02
1	3.10	3.28	2.50
2	2.54	2.72	2.19
3	2.18	2.23	2.10
4	2.11	2.13	2.06
5	2.07	2.08	2.05

Table 4.4 Comparison in average lamellar thickness of B-block for λ = 0, 1, 2, 3, 4 and 5 during two-step and one-step isothermal crystallization.

Segregation strength (λ)	Two-step cooling at U_p = 0.3	Two-step cooling at U_p = 0.6	One-step cooling at U_p = 0.6
0	2.08	3.00	3.0
1	2.09	2.49	2.50
2	2.09	2.18	2.15
3	2.09	2.10	2.08
4	2.07	2.07	2.05
5	2.06	2.06	2.04

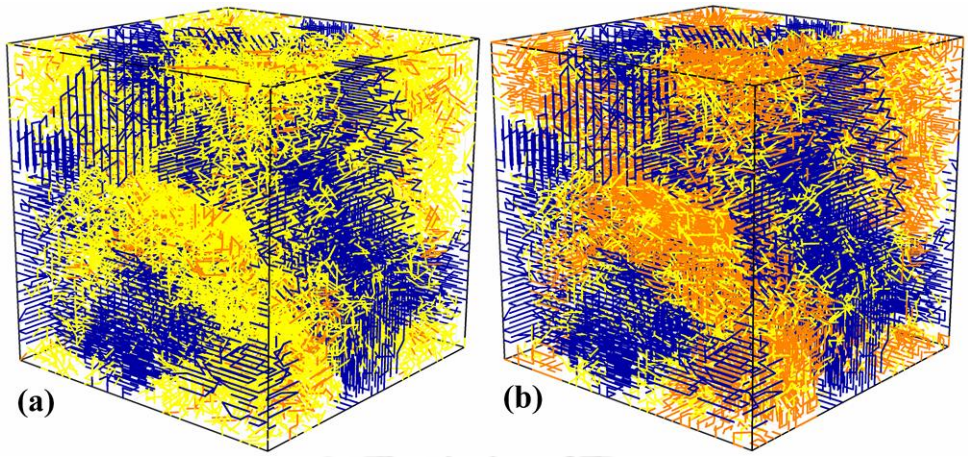

Figure 4.22 Snapshots of semi-crystalline structures for λ = 1 (a) at U_p = 0.3, (b) at U_p = 0.6 during two-step isothermal crystallization. Blue lines represent crystalline bonds of A-block, orange lines represent crystalline bonds of B-block and yellow lines represent non-crystalline bonds of both the blocks.

4.3 Summary

We present Monte Carlo simulation results on the crystallization behavior of symmetric diblock copolymer from a homogeneous melt state to a phase separated crystalline state. Segregation strength, λ (viz., demixing energy between A- and B-block units) is one of the pivotal factors to determine crystallinity and final morphology of diblock copolymer crystal. With increasing value of λ (from 0 to 5), we observe a gradual decrease in crystallinity associated with smaller and thinner crystals of both the blocks. In our model, A-block has higher crystallization driving force, and hence crystallizes first, forming lamellar morphology. The crystalline lamella of A-block generates confinement for the crystallization of B-block. Therefore, the crystallinity of B-block is suppressed compared to A-block. We notice a significant increase in the mean square radius of gyration of the polymer chain during crystallization, which is due to the tension at the block junction induced by the segregation strength. Higher the value of λ, higher is the influence of the chain stretching at the block junction which leads to the formation of smaller size domains and restricts the development of crystal growth. With increasing λ, microphase separation takes place at a relatively higher temperature (viz., lower U_p).

Isothermal crystallization establishes that the crystallization pathway is strongly influenced by the segregation strength (λ). The value of Avrami index(n), which is close to 1.0, denotes homogeneous nucleation with two dimensional crystals, where the process of crystallization is influenced by spatial confinement. Two-step isothermal crystallization produces sequential crystallization whereas one-step exhibits coincident crystallization. Two-step, compared to one-step quenching yields higher crystalline materials in A-block. In one-step quenching (at U_p = 0.6), both the blocks compete with each other towards the crystallization resulting in the formation of less crystalline materials in the first crystallizable block. However, the crystallinity of the second block in one-step and two-step quenching is close to each other suggesting that the effective driving force for the crystallization is almost same irrespective of the mode of quenching. Lamellar thickness of A-block, $\langle l_A \rangle$ at U_p = 0.6 (one-step cooling) is less than that of at U_p = 0.3 (during two-step cooling), which is in accord with the Hoffman-Weeks relation. However, the lamellar thickness of B-block is almost same irrespective of one-step or two-step cooling. Therefore, controlling the crystallization pathway (viz., non-isothermal crystallization, single step and two-step isothermal crystallization) is a viable option to tune crystalline morphology of diblock copolymers.

References

1. Darling SB. Prog. Polym. Sci. 2007;32:1152-1204.
2. Bates FS and Fredrickson GH. Annu. Rev. Phys. Chem. 1990; 41:525-557.
3. Bates FS and Fredrickson GH. Phys. Today 1999; 52(2):32-38.
4. Leibler L. Macromolecules 1980;13(6):1602-1617.
5. Sun L, Liu Y, Zhu L, Hsiao BS, and Avila-Orta CA. Polymer 2004;45:8181-8193.
6. Nojima S, Akutsu Y, Akaba M, and Tanimoto S. Polymer 2005; 46 4060–4067.
7. Nojima S, Kiji T, and Ohguma Y. Macromolecules 2007;40(21):7566-7572.
8. Myers SB and Register RA. Macromolecules 2008;41(18):6773-6779.
9. Sakurai T, Ohguma Y, and Nojima S. Polym. J. 2008;40(10):971-978.
10. Nojima S, Fukagawa Y, and Ikeda H. Macromolecules 2009;42(24):9515-9522.
11. Muller AJ, Balsamo V, Arnal ML, Jakob T, Schmalz H, and Abetz V. Macromolecules 2002;35(8):3048-3058.
12. Huang L, Kiyofuji G, Matsumoto J, Fukagawa Y, Gong C, and Nojima S. Polymer 2012;53:5856-5863.
13. Hamley IW, Castelletto V, Castillo RV, Muller AJ, Martin CM, Pollet E, and Dubois P. Macromolecules 2005;38(2):463-472.
14. Castillo RV, Muller AJ, Lin M-C, Chen H, Jeng U-S, and Hillmyer MA. Macromolecules 2008;41(16):6154-6164.
15. Sun J, He C, Zhuang X, Jing X, and Chen X. J Polym Res 2011;18:2161–2168.
16. Nojima S, Akutsu Y, Washino A, and Tanimoto S. Polymer 2004;45:7317-7324.
17. Maglio G, Migliozzi A, and Palumbo R. Polymer 2003;44:369-375.
18. Laredo E, N.Prutsky, Bello A, Grimau M, Castillo RV, and Muller AJ. Eur. Phys. J. E 2007;23:295-303.
19. Kim KS, Chung S, Chin IJ, Kim MN, and Yoon JS. J. Appl. Polym. Sci. 1999;72:341-348.
20. Albuerne J, Marquez L, Muller AJ, Raquez JM, Degee P, Dubois P, Castelletto V, and Hamley IW. Macromolecules 2003;36(5):1633-1644.
21. Muller AJ, Albuerne J, Marquez L, Raquez J-M, Degee P, Dubois P, Hobbs J, and Hamley IW. Farad. Discuss. 2005;128:231-252.
22. Li Y, Ma Y, Li J, Jiang X, and Hu W. J. Chem. Phys. 2012;136:104906-104901-104906-104907.

23. Muller AJ, Albuerne J, Esteves LM, Marquez L, Raquez J-M, Degee P, Dubois P, Collins S, and Hamley IW. Macromol. Symp. 2004;215:369-382.
24. Cong Y, Liu H, Wang D, Zhao B, Yan T, Li L, Chen W, Zhong Z, Lin M-C, Chen H-L, and Yang C. Macromolecules 2011;44:5878-5882.
25. Dasmahapatra AK, Nanavati H, and Kumaraswamy G. J. Chem. Phys. 2009;131:074905-074901-074905-074910.
26. D.L.Goodstein. States of Matter: Dover, New York, 1985.
27. Luo C and Sommer J-U. Phys. Rev. Lett. 2009;102(14):147801.
28. Avrami M. J. Chem. Phys. 1939;7:1103-1112.
29. Lorenzo AT, Arnal ML, Albuerne J, and Müller AJ. Polym. Test. 2007;26(2):222-231.
30. Loo Y-L, Register RA, and Ryan AJ. Macromolecules 2002;35(6):2365-2374.
31. Ho R-M, Lin F-H, Tsai C-C, Lin C-C, Ko B-T, Hsiao BS, and Sics I. Macromolecules 2004;37(16):5985-5994.
32. Shiomi T, Tsukada H, Takeshita H, Takenaka K, and Tezuka Y. Polymer 2001;42:4997-5004.
33. Marand H, Xu J, and Srinivas S. Macromolecules 1998;31(23):8219-8229.

Chapter 5

Effect of Block Asymmetry on Crystallization

In this chapter, we present Dynamic Monte Carlo simulation results on the crystallization and morphological evolution of a diblock copolymer. We follow the effect of block asymmetry on crystallization during non-isothermal as well as isothermal crystallization. We implement two different levels of segregation. At weak segregation, the value of segregation strength (λ) is 1 and for high segregation, the value of λ is 4.

5.1 Literature Review

The crystallization of amorphous-crystalline diblock copolymer has been widely explored in the last few decades [1-22]. However, the complex behaviour associated with the crystallization of double crystalline diblock copolymer needs further attention. In double crystalline diblock copolymer, the final crystal morphology is determined by the competition between two blocks towards crystallization along with microphase separation. Diblock copolymer usually exhibits the sequential crystallization mechanism, where the difference between melting points ofthe two blocks is relatively large [23-30]. During crystallization of double crystalline diblock copolymer, high melting block crystallizes first generating spatial confinement for the crystallization of the low melting block ensuing less crystallinity in the second block [23-27, 29, 31-36]. However, in some cases, they may crystallize simultaneously known as coincident crystallization [30, 31, 37-40].

Primarily, the interplay between crystallization and microphase separation dictates the final crystal morphology of the semi crystalline diblock copolymers. Apart from that, crystallization temperature (T_c), degree of immiscibility (viz., value of χ), and block composition are the other crucial factors which effect the crystallization of diblock copolymer to a large extent. By altering the block length ratio, one can easily influence the sequence of crystallization and crystal orientation of final crystal morphology [33, 34]. For instance, the crystallization behaviour of linear poly(ethylene)-*block*-hydrogenated poly(norbornene) (LPE-*b*-hPN) diblock copolymer, where the melting points of two blocks are adjacent

(~150°C), is largely tuned by the relative block length ratio. In hPN rich diblock copolymer, hPN crystallizes primarily whereas in LPE rich diblock copolymer, LPE crystallizes first, followed by the hPN block [33]. Moreover, numerous experimental studies confirm that the crystal orientation is equally influenced by the block length ratio. The first crystallizable block generates a structural template in which the crystallization of the second block is confined with a perpendicular orientation [34]. Similarly, during crystallization of poly(ethylene glycol)-*block*-poly(ε-caprolactone) (PEG-*b*-PCL) diblock copolymer, the block with higher composition crystallizes first [41].

Several interesting morphological evolution have been observed during the crystallization of asymmetric diblock copolymers. For example, PCL-*b*-PE diblock copolymer exhibits confined crystallization during isothermal crystallization where PE block crystallizes first ensuing lamellar morphology, which confines the crystallization of the PCL block [25, 26]. However, block composition strongly dominates the crystallization behaviour. When the block composition of PE is less than 56%, PCL block partially interrupts the lamellar morphology of previously crystallized PE block, as the crystalline layers of PE block deliver soft confinement during crystallization of the PCL block. When the composition of PE block is larger than 76%, the lamellar morphology of the crystalline PE block remains intact as it offers hard confinement during crystallization of the PCL block [36]. Isothermal crystallization of poly(*p*-dioxanone)-*b*-PCL (PPDX-*b*-PCL) diblock copolymer discloses that when the composition of the PCL block is large enough (~ 60 – 77 %), the crystallization rate of PCL block (in terms of crystallization half time) is enhanced, as the previously crystallized PPDX block turns into a nucleating agent to accelerate the crystallization of PCL block. However, when the composition of PCL block is ≤ 50%, the previously crystallized PPDX block enforces topological restrictions (viz., confinement) which suppress the crystallization of PCL block. On top of that, the hydrolytic degradation of PPDX is minimized by PCL block, but the increased resistance to hydrolysis is a complex function of block composition [39]. Degree of asymmetry of the block composition impacts the crystallization and melting temperatures of the constituent blocks [29, 31, 41, 42]. For instance, poly (L-lactic acid) (PLLA) in PLLA-*b*-PCL diblock copolymer shows higher crystallization and melting temperature with increasing content of PLLA. On the other hand, at lower composition of PLLA, the reverse phenomena are noticeable with the reduced crystallization rate, which is endorsed by the PCL block (major component) as it acts as a diluent, and causes the depression of crystallization and melting temperatures of PLLA block [29]. Kinetic analysis

based on Avrami equation indicates the evolution of 3-dimensional sphurelitic superstructure with Avrami index 2.5 – 3, for most of the block compositions, whereas the diblock copolymer containing 10 wt.% PLLA forms axialites (viz., non-spherical and irregular superstructures) with Avrami index 1.0 [29]. Similar diluent effects on the PLLA blocks have been detected for miscible PLLA-*b*-PEO diblock copolymer with the increasing composition of poly(ethylene oxide) (PEO) block [43, 44].

5.2 Results and Discussion

We are going to start our discussion by exploring the effect of block composition on crystallization of double crystalline diblock copolymer during non-isothermal crystallization. We limit our discussion with two levels of segregation strengths: $\lambda = 1$ for weak and $\lambda = 4$ for strong segregation. Subsequently, we discuss transition kinetics over a wide range of block composition by isothermal crystallization with both the segregation levels.

5.2.1 Non-Isothermal Crystallization

5.2.1.1 Monitoring Phase Transition

To simulate crystallization of diblock copolymer, we first generate an equilibrated high temperature melt at $U_p = 0$ (T = ∞, athermal state), where both the blocks are miscible. Figure 5.1 displays the snapshots of homogeneous melt composed of A- and B-type units at x_B = 0.125, 0.25, 0.375, 0.625, 0.75 and 0.875 respectively (blue lines represent A-block and orange lines represent B-block segments). The snapshots clearly signify an isotropic orientation of polymer chains at $\lambda = 1$.

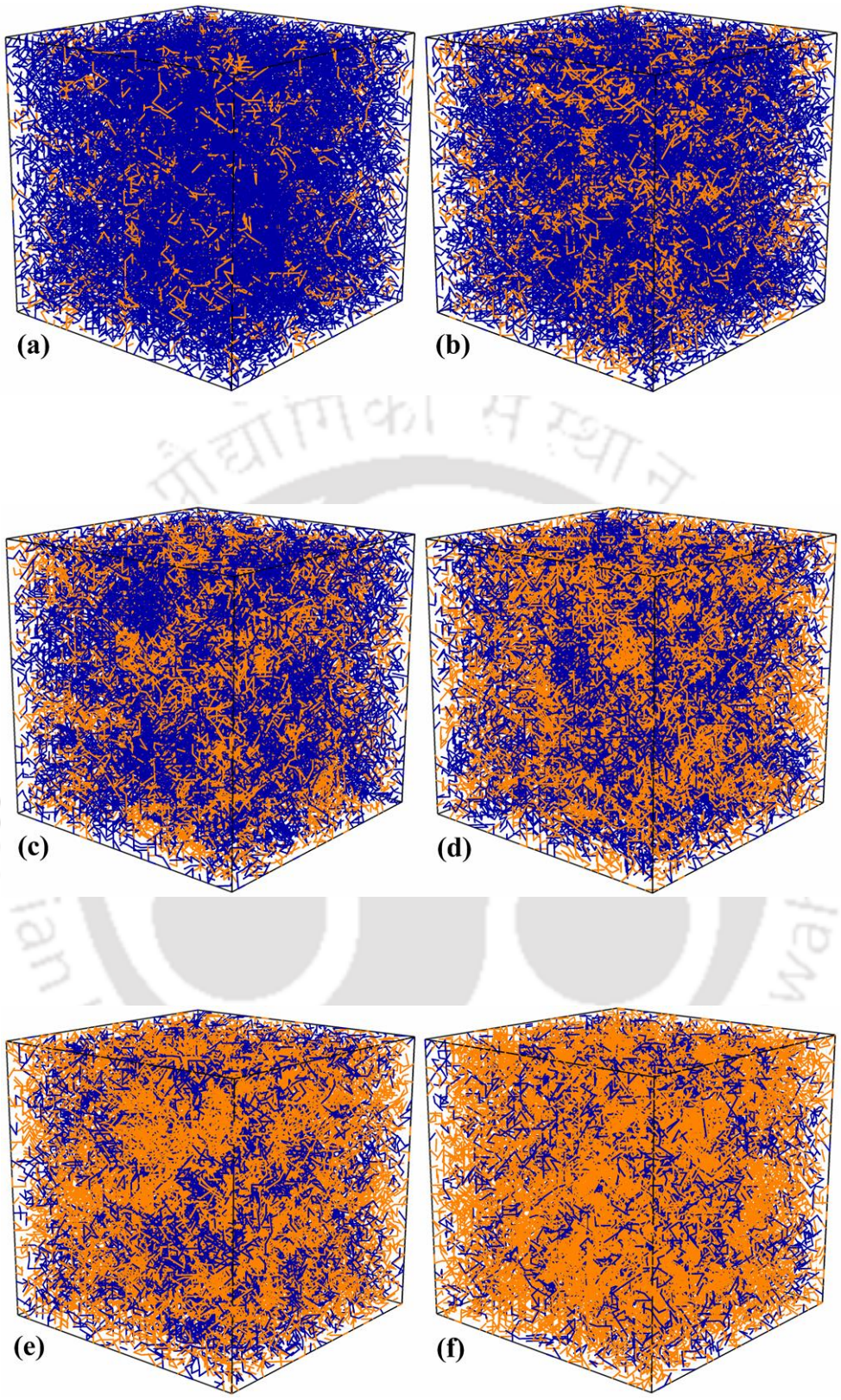

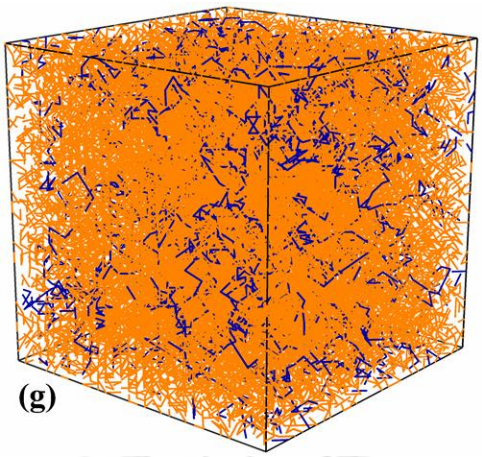

Figure 5.1 Snapshots of the simulation box at U_p = 0 representing homogeneous melt of diblock copolymer for (a) x_B = 0.125, (b) x_B = 0.25 (c) x_B = 0.375 (d) x_B = 0.50 (e) x_B = 0.625 (f) x_B = 0.75 and (g) x_B = 0.875. Blue and orange line represents segments of A- and B-block respectively.

We cool the homogenous melt from U_p = 0 to U_p = 0.6 with a step size of 0.02 to implement non-isothermal crystallization which generates parallel alignment of polymer chains indicating ordered crystalline regions. We observe the transition of diblock copolymer by tracking the change in specific heat (C_v) calculated from energy fluctuations as a function of U_p. During crystallization, C_v display a peak at a certain value of U_p reflecting transition point from a homogeneous disordered melt to an ordered crystalline state [45-47]. We plot C_v vs. U_p over an extensive range of block compositions (viz., x_B = 0.125 to x_B = 0.875) in Figure 5.2 at two diverse range of segregation strength (viz., λ =1 and 4). As the crystallization driving force of the A-block is greater than the B-block, they introduce a sequential crystallization mechanism, which is determined by the presence of two different transition peaks at two different values of U_p. The previous result is in accord with the experimental results of PE-*b*-PEO diblock copolymer which offers sequential crystallization at two different temperatures which are 95.4 °C for PE block and 12.9 °C for PEO block [23].

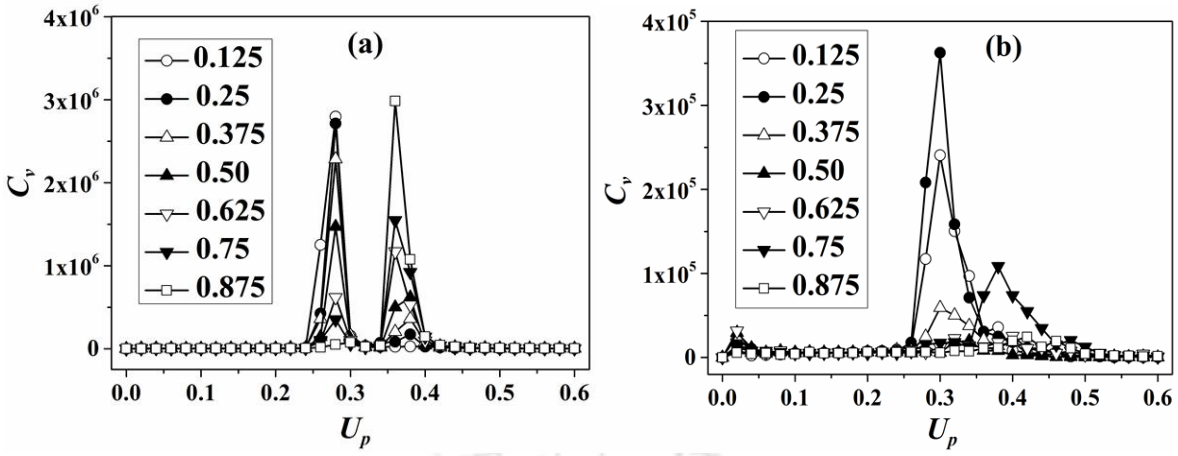

Figure 5.2 Change in specific heat (C_v) with U_p for different block compositions (x_B) at (a) weak segregation (λ = 1) and (b) strong segregation (λ = 4).

We estimate the change in the crystallization temperatures (U_p^*) of two blocks in weak segregation limit in Figure 5.3a. We notice that the crystallization temperatures of A-block (U_{pA}^*) remain similar for all block compositions except at x_B = 0.875, where it generates higher value of U_p (U_p^* = 0.3). The above observation represents that, there is a small depression in crystallization temperature ($U_p \sim 1/T$) of A-block at x_B = 0.875. As the primary stage of crystallization is motivated by the thermodynamic driving forces (viz., degree of cooling), the transition point of A-block is unaffected with most of the block compositions, because the crystallization driving force (ΔT) is almost comparable for all the compositions investigated. However, at x_B = 0.875, a small depression in crystallization temperature of A-block is detected which is influenced by the dilution effect of the B-block. At higher x_B, B-block acts like a "solvent" for A-block. To follow this non-intuitive and unexpected trend, we simulate the mobility of polymer chains by calculating mean square displacement of the centre of mass in terms of U_p. During the crystallization of A-block (viz., $U_p \sim 0.28$), the mean square displacement of the centre of mass of the A-block (d_{cm}^2 of A-block) increases at higher x_B (Figure 5.4) compared to that of the B-block. Higher mobility makes the chain segments less attractive towards crystallization at that temperature (viz., less thermal driving force). On lowering the temperature further (viz., higher U_p), A-block starts to crystallize owing to the fact that it has now higher thermal driving force towards crystallization. On the other hand, we notice that the crystallization temperature of

B-block increases (viz., decline of U_p) with increasing block length (Figure 5.3a), and the mean square displacement of the centre of mass of the B-block (d_{cm}^2 of B-block) decreases with composition (Figure 5.4). The presence of higher fraction of the B-block assists the formation of larger size domains with reduced chain mobility. For this reason, the crystallization occurs at a relatively higher temperature while the thermodynamic driving force for the crystallization is relatively less (viz., at a higher temperature). This observation is in line with the experimental results of PLLA-*b*-PCL diblock copolymer where the crystallization temperature of PLLA block increases with the increased composition of PLLA blocks [29, 35]. In the PEO-*b*-PCL diblock copolymer, the crystallization temperature of PCL block also rises with an increasing weight fraction of PCL block in the copolymer [42]. Similarly, in PLLA-*b*-PEG diblock copolymer, the crystallization temperature of PLLA block increases with increasing molecular weight of PLLA block [43]. We also notice the transition points in terms of U_p for both the blocks at $\lambda = 4$ (higher segregation strength) in the Figure 5.3b. The transition points for both the blocks show a non-monotonic trend with composition (Figure 5.3b) due to the effect of strong segregation, which causes hard confinement and developing large numbers of microdomains in the phase separated melt. On top of that, due to the strong confinement, chain mobility of both the blocks is highly restricted at strong segregation (viz., $\lambda = 4$), which is in accord with Figure 5.4.

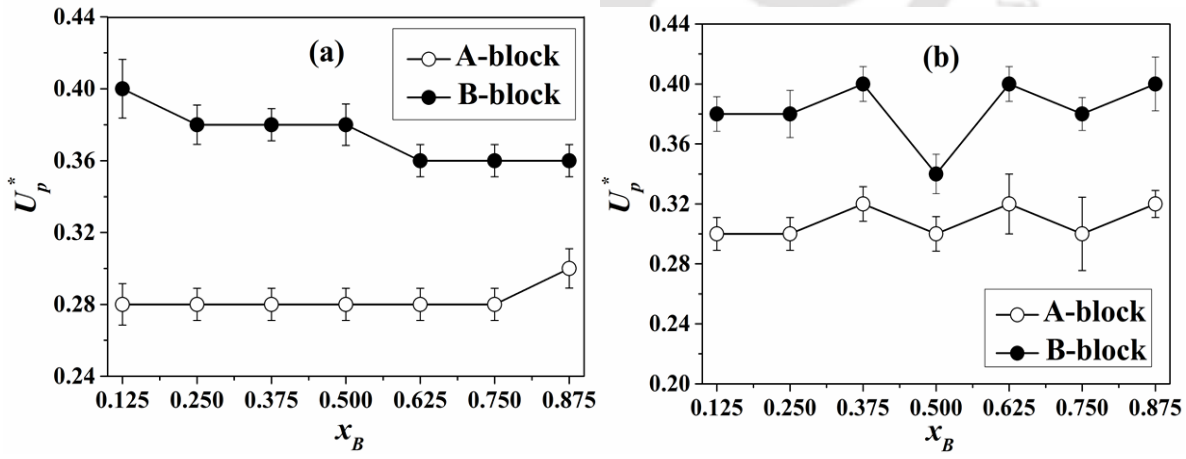

Figure 5.3 Change in transition points (U_p^*) for A- and B-block with block composition (x_B) at (a) $\lambda = 1$ and (b) $\lambda = 4$.

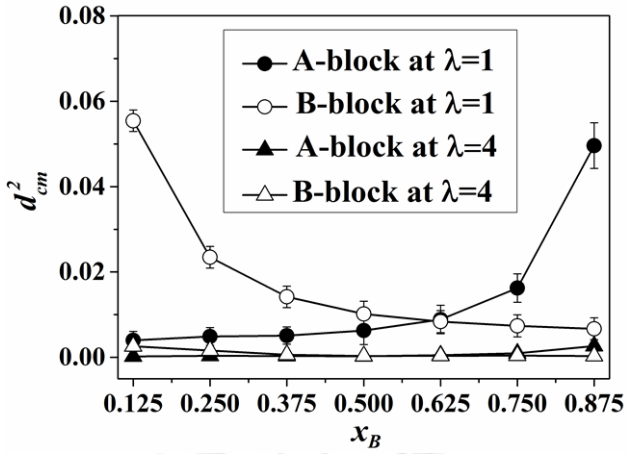

Figure 5.4 Change in mean square displacement of centre of mass (d^2_{cm}) of A- and B-block with x_B at U_p = 0.3.

5.2.1.2 Locating Microphase Separation

Typically in a diblock copolymer, immiscibility between two blocks results into microphase separation with numerous morphological patterns [3, 4, 6-8, 11-14]. Therefore, the energy fluctuation based on A-B contacts also exhibits a peak at the transition point [47]. Figure 5.5 summarizes the plots of C_{v-AB} with U_p at a wide range of block composition which leads to the location of microphase separation for weak as well as strong segregation.

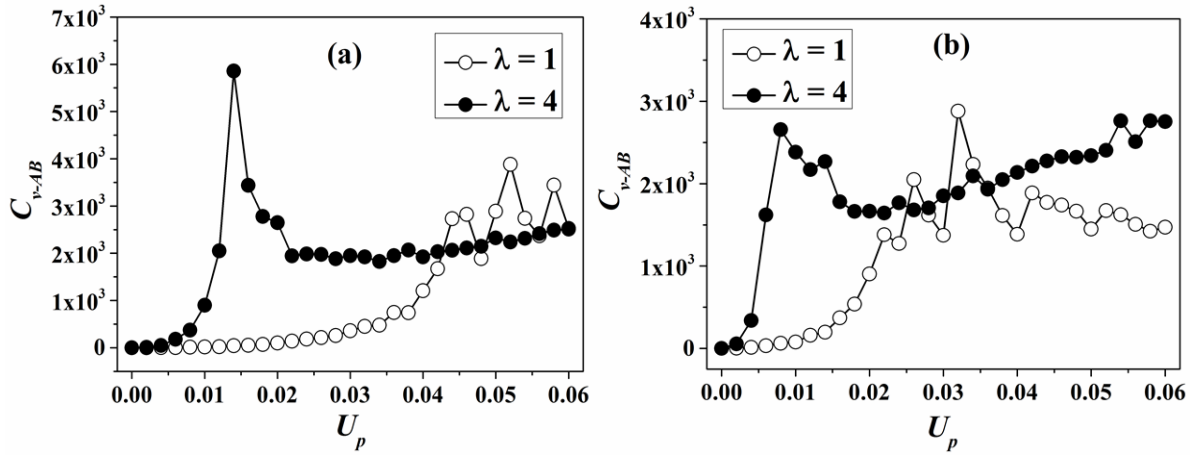

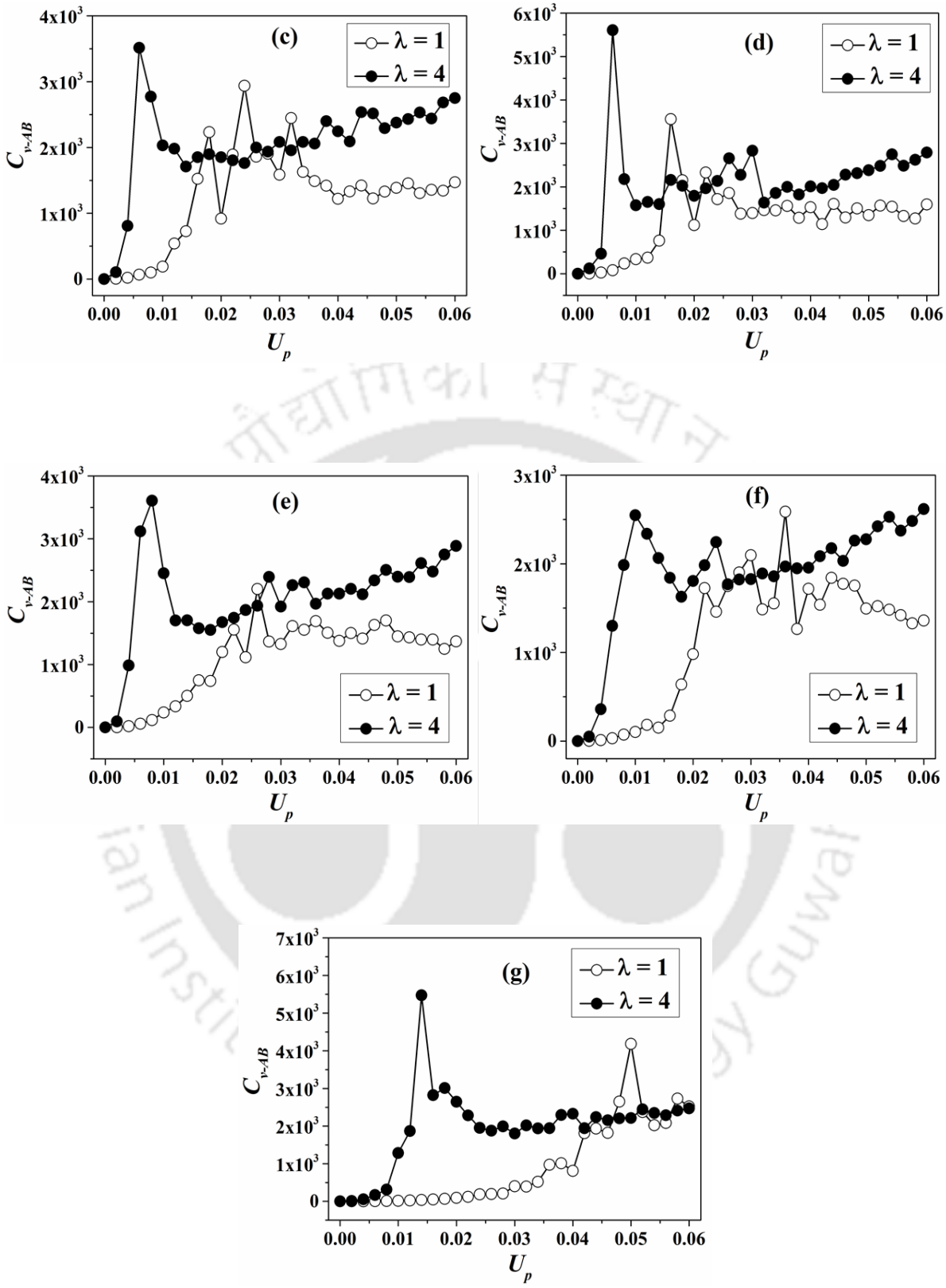

Figure 5.5 Change in specific heat of A-B demixing energy ($C_v - AB$) with U_p for (a) x_B = 0.125, (b) x_B = 0.25 (c) x_B = 0.375, (d) x_B = 0.50, (e) x_B = 0.625, (f) x_B = 0.75 and (g) x_B = 0.875 within weak segregation (λ = 1) and strong segregation (λ = 4).

We estimate the value of microphase separation points ($U_p^{\#}$) with block compositions (x_B) in Figure 5.6 at two different segregation strengths. At weak segregation (viz., λ = 1), the relative location of microphase separation point fluctuates with block composition of B (x_B) whereas at strong segregation (viz., λ = 4), the microphase separation points are ~ 0.01 which signifies that the relative location of microphase separation point is independent of block composition of B (x_B). During high segregation strength, composition enforces a minimal effect on microphase separation point, because segregation between two blocks plays a crucial role to develop microphase separation. At weak segregation, the degree of microphase separation is controlled by the block length (viz., composition), whereas, at strong segregation, demixing energy dominates over composition. From Figure 5.6, we can conclude that, the value of $U_p^{\#}$ declines from 0.052 for x_B = 0.125 to 0.016 for x_B = 0.50 and again 0.05 for x_B = 0.875. The above data reveals that the microphase separation is retarded (viz., happens at a lower temperature) with the increase of the degree of asymmetry in the diblock copolymer. The above observation is in good agreement with ethylene-*b*-ethylethylene (E-*b*-EE) diblock copolymer, where microphase separation (measured in terms of order-disorder transition temperature, T_{ODT}) is affected by composition. Diblock copolymer with 0.25, 0.49 and 0.75 weight fraction of ethylene exhibits T_{ODT} at 255, 121 and 148 °C respectively [3]. Similarly, PLLA-*b*-PCL diblock copolymer shows T_{ODT} at 175 and 220 °C for the sample having 37.4 and 46 weight % PCL block respectively [48]. The snapshots of microphase separated melt at U_p = 0.1 from x_B = 0.125 to 0.875 at weak segregation limit are available in Figure 5.7, and at strong segregation limit are available in Figure 5.8 where the development of phase segregated melt microdomains are clearly visible.

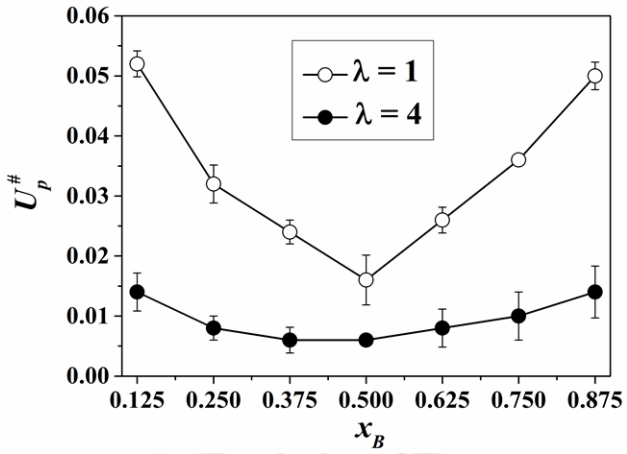

Figure 5.6 Change in microphase Separation point ($U_p^{\#}$) with block composition (x_B) at two different segregation levels.

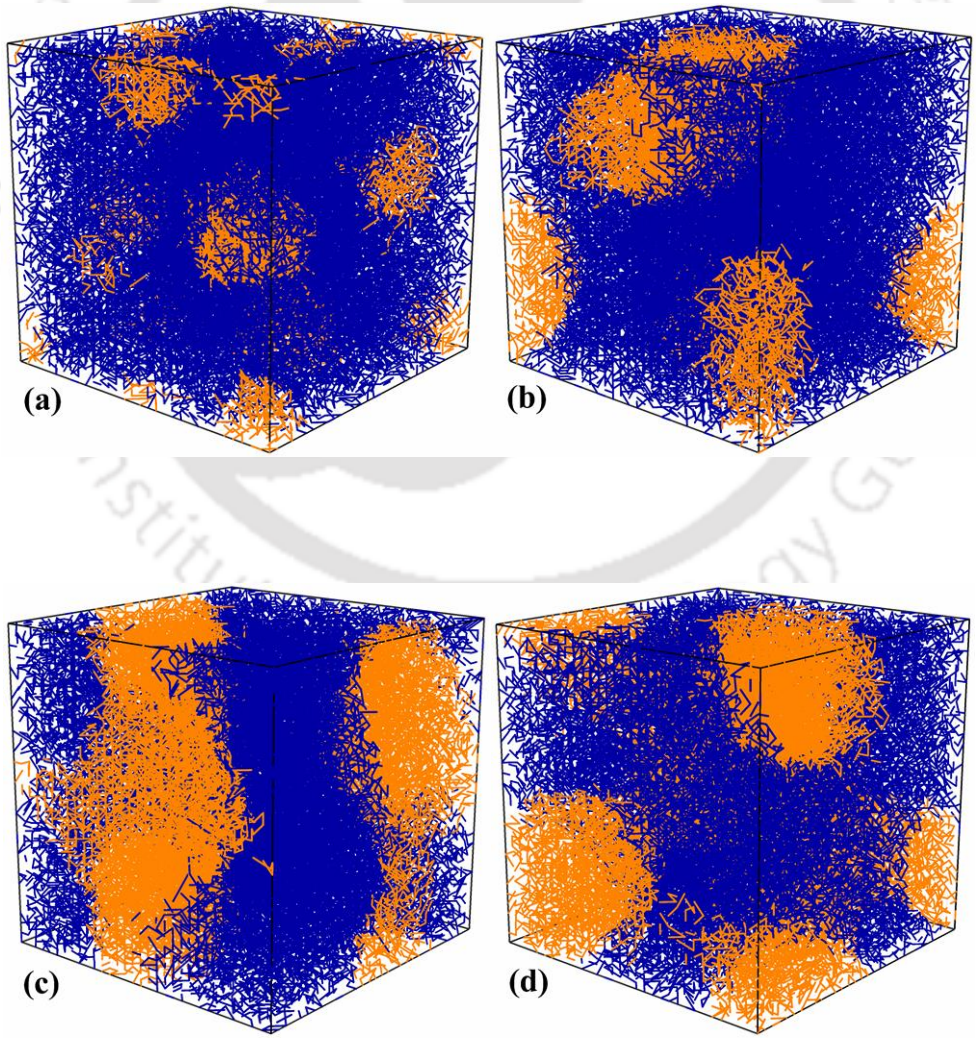

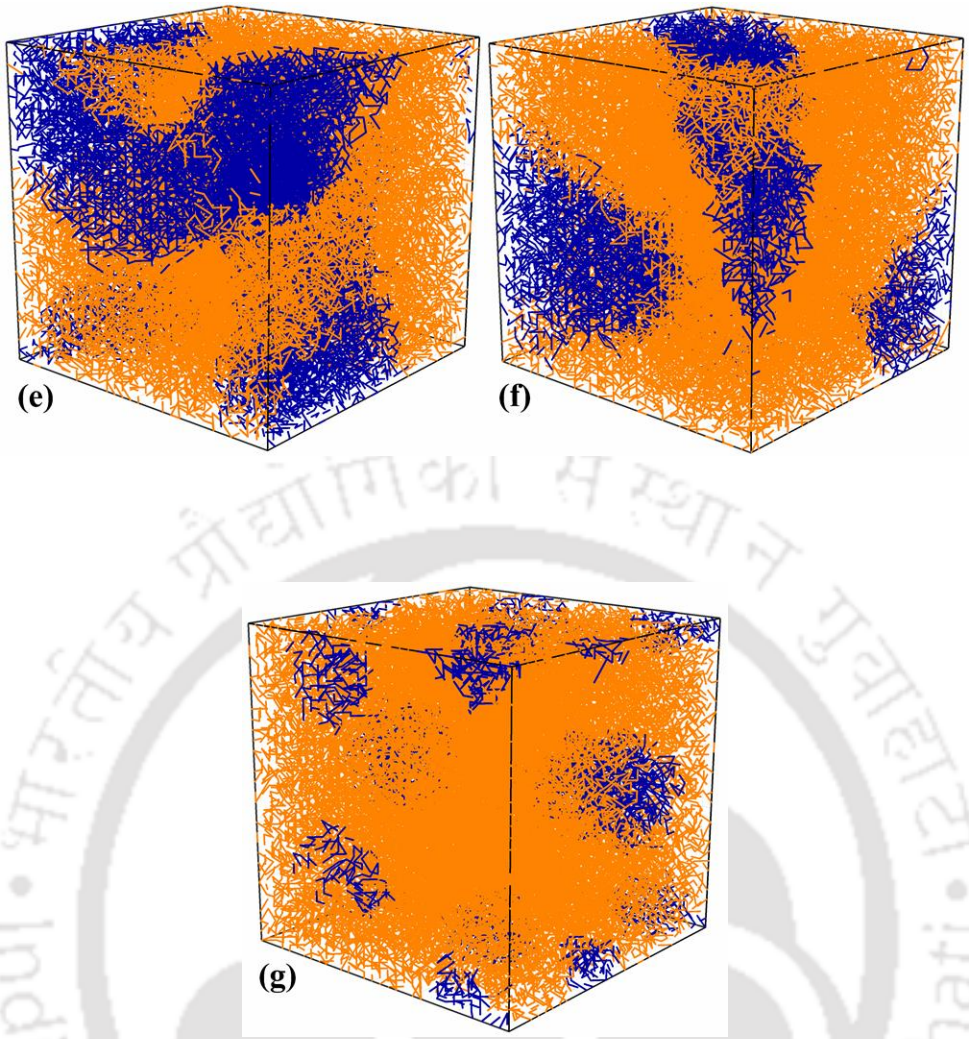

Figure 5.7 Snapshots of microphase separated melt at U_p = 0.1 for (a) x_B = 0.125, (b) x_B = 0.25, (c) x_B = 0.375, (d) x_B = 0.50 (e) x_B = 0.625, (f) x_B = 0.75 and (g) x_B = 0.875 within weak segregation limit. Blue and orange line represents segments of A- and B-block respectively.

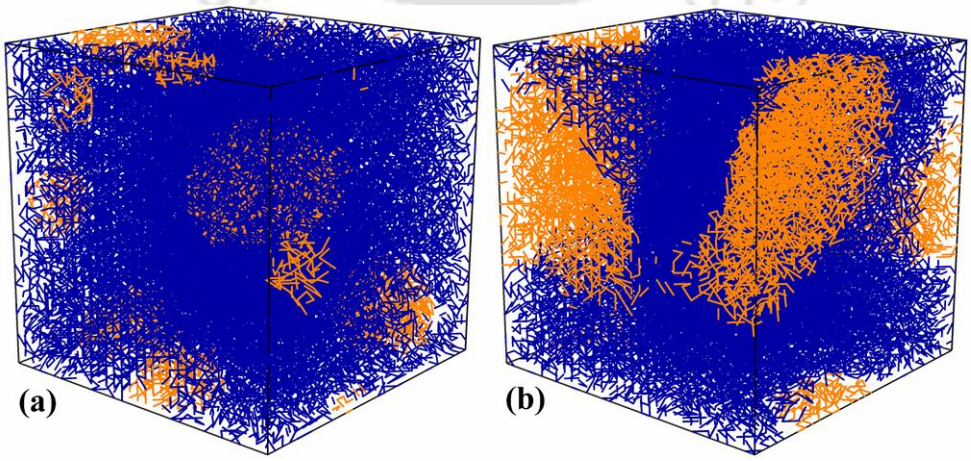

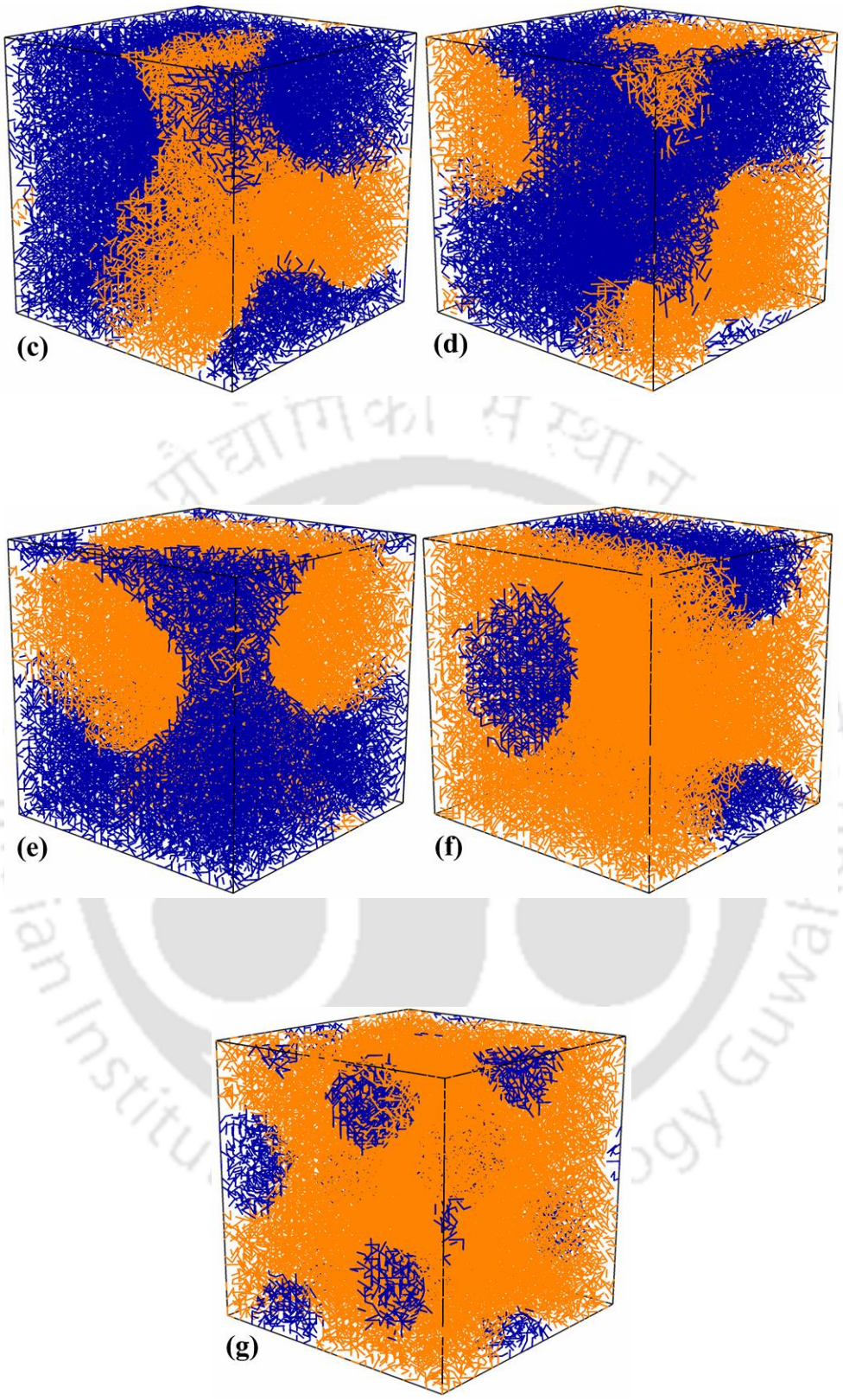

Figure 5.8 Snapshots of microphase separated melt at U_p = 0.1 for (a) x_B = 0.125, (b) x_B = 0.25, (c) x_B = 0.375, (d) x_B = 0.50 (e) x_B = 0.625, (f) x_B = 0.75 and (g) x_B = 0.875 within strong segregation limit. Blue and orange line represents segments of A- and B-block respectively.

5.2.1.3 Development of Crystallinity

We observe the evolution of crystallinity during non-isothermal crystallization as a function of block composition at two different segregation levels. We calculate the change in overall crystallinity (X_c) with U_p in Figure 5.9a at weak segregation. Overall crystallinity is considered as the weighted average of the summation of crystallinity of A- and B-block (viz., $X_c = x_A \times X_A + x_B \times X_B$). With the enlarged value of U_p, the overall crystallinity gradually increases and at $U_p \sim$ 0.3, it shows an abrupt change in its value to reach saturation crystallinity where there is no significant change in crystallinity. The change in crystallinity of A-block (X_A) and B-block (X_B) individually with U_p for λ = 1 is presented in Figure 5.9b and 5.9c respectively. The saturation crystallinity of A-block, B-block and overall at U_p = 0.6 are summarized in Figure 5.10 as a function of the block composition of B (x_B). At weak segregation, overall crystallinity does not differ too much with the block composition (Figure 5.10). The values are almost 0.70 for all the block compositions explored. This occurs due to the similar driving force for all block compositions during crystallization which is primarily dominated by the degree of cooling. The saturation crystallinity of A-block is almost independent of block composition, whereas the saturation crystallinity of B-block monotonically increases with the increasing composition of the B-block (viz., x_B). The values of saturation crystallinity of A-block at λ = 1 are 0.72, 0.71, 0.71, 0.70, 0.70, 0.71 and 0.71 for x_B = 0.125, 0.25, 0.375, 0.50, 0.625, 0.75 and 0.875 respectively. As we simulate each composition within the same degree of cooling, the crystallization driving force in each case is identical. Therefore, the development of crystallinity of A-block over a wide range of composition appears to be independent of x_B. On the other hand, the saturation crystallinity of the B-block at λ = 1 is 0.60, 0.63, 0.66, 0.66, 0.67, 0.68 and 0.69 for x_B = 0.125, 0.25, 0.375, 0.50, 0.625, 0.75 and 0.875 respectively. As the crystallization driving force of A-block (viz., high melting point) is more than the B-block, the saturation crystallinity of B-block is always less than the A-block. With increased value of block composition of B, the saturation crystallinity of B-block increases due to the enhanced number of B-block units. The above observation is in good agreement with the experimental results of the PCL-*b*-PE [36] and PEO-*b*-PCL [42] diblock copolymers, wherein the crystallinity of PE and PCL block increases with increasing their content in PCL-*b*-PE and PEO-*b*-PCL diblock copolymer respectively. The snapshots of the final crystalline structure (viz., at U_p = 0.6) for x_B = 0.125

to x_B = 0.875 are presented in Figure 5.11 within weak segregation (λ = 1). The blue and orange lines represent the crystalline segments of A- and B-block, respectively, and yellow lines represent the non-crystalline segments of both the blocks.

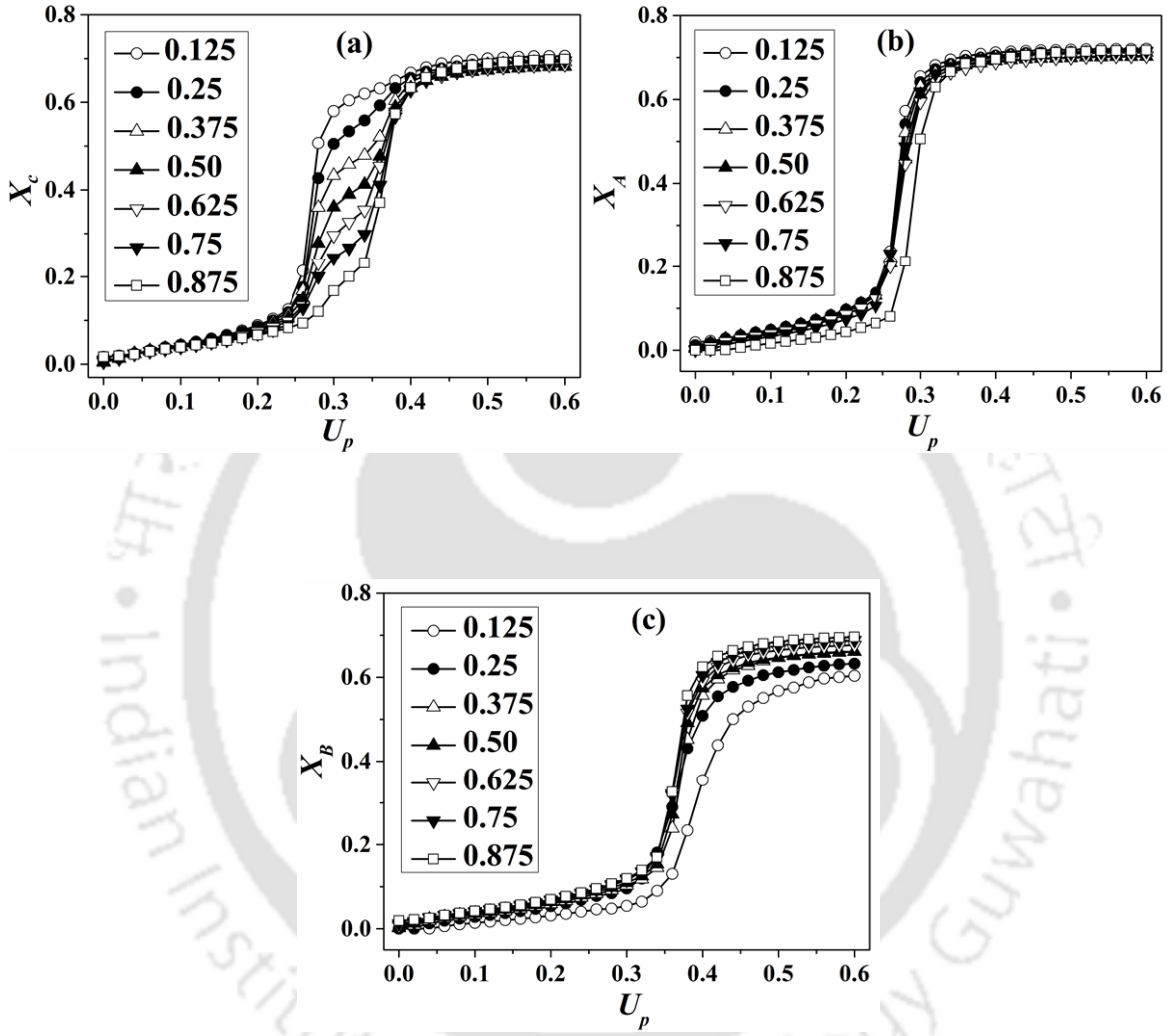

Figure 5.9 Change in (a) overall crystallinity (X_c), (b) crystallinity of A-block (X_A) and (c) crystallinity of B-block (X_B) with U_p at λ =1 for different block compositions (x_B).

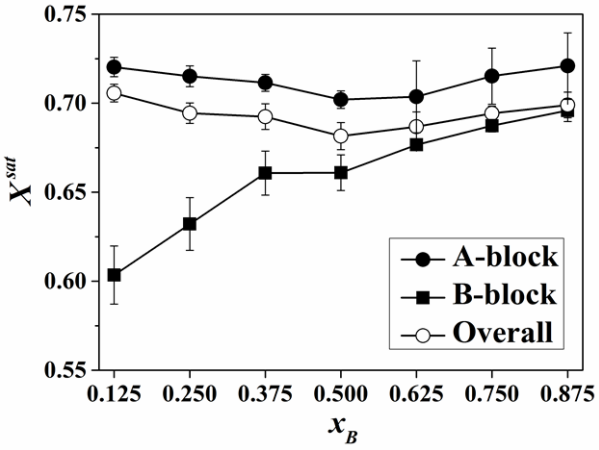

Figure 5.10 Change in saturation crystallinity at U_p = 0.6 with block compositions (x_B).

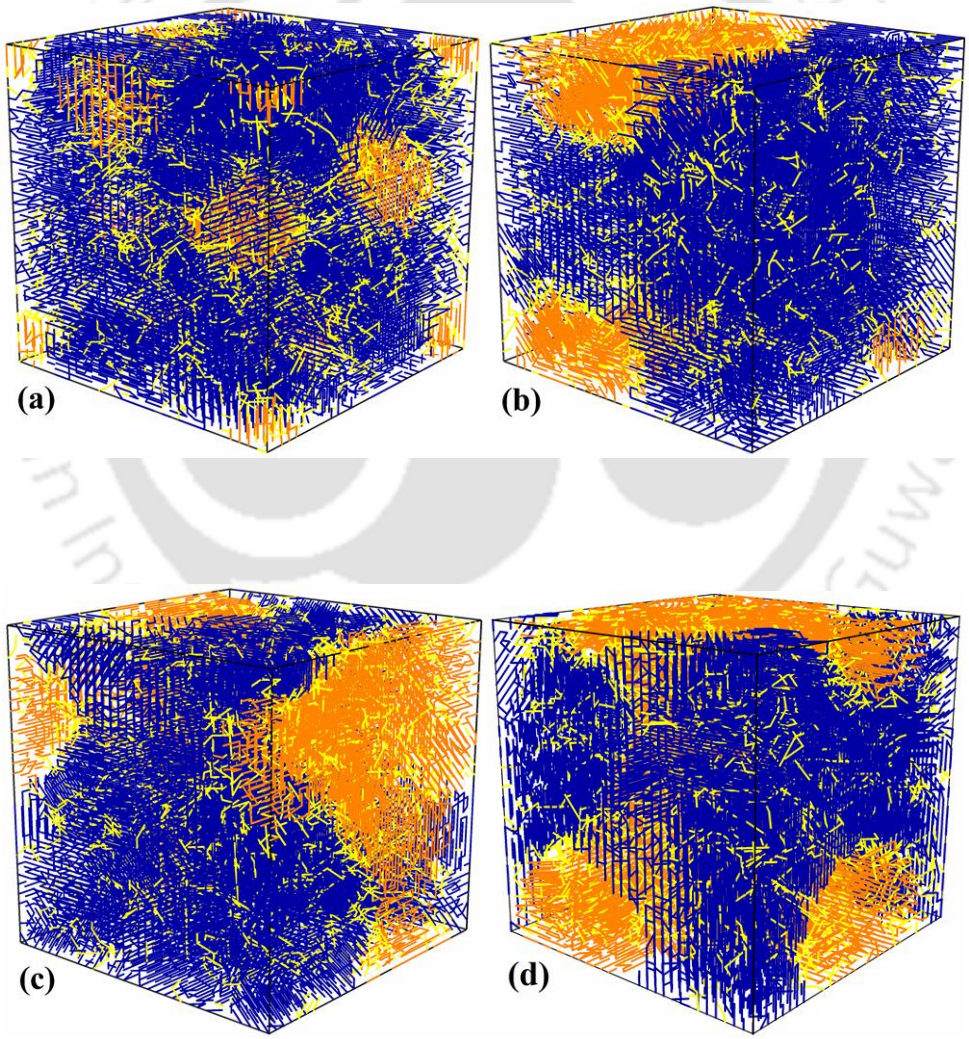

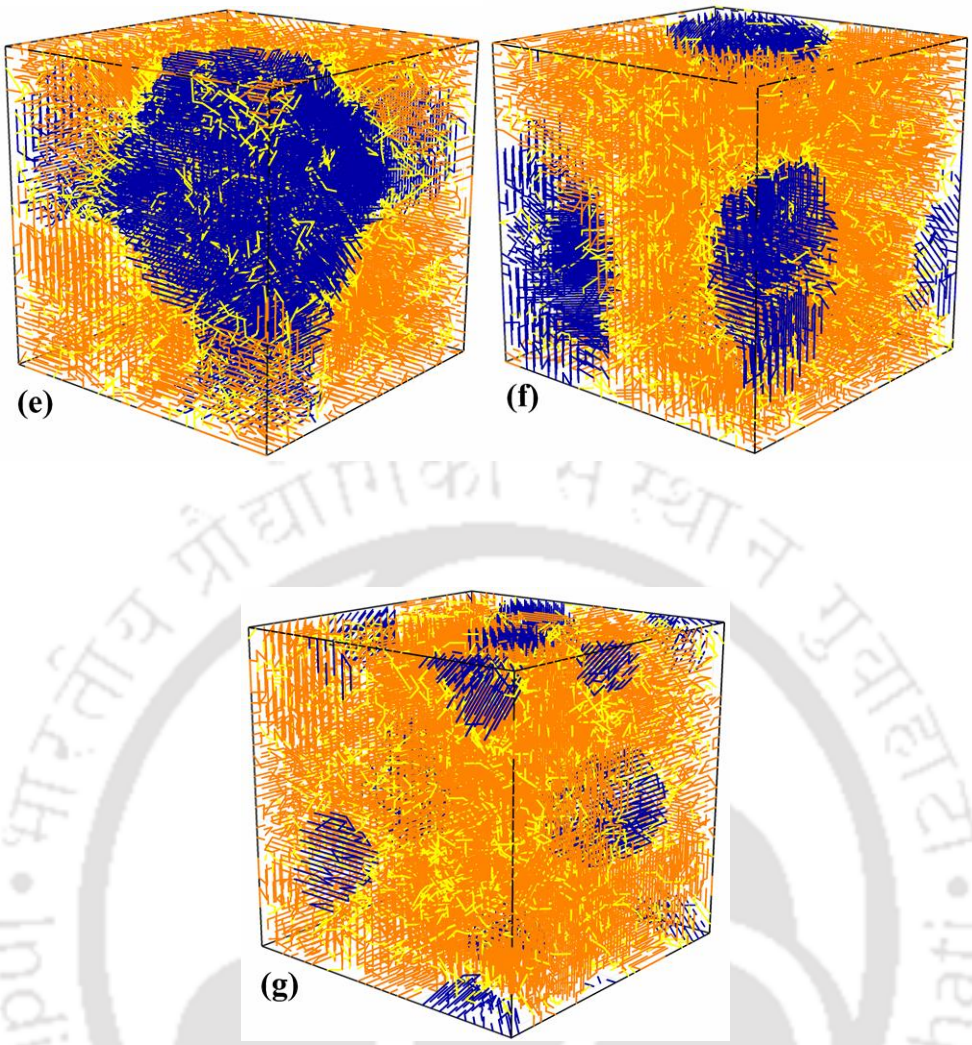

Figure 5.11 Snapshots of semi crystalline structures at λ = 1 for (a) x_B = 0.125, (b) x_B = 0.25, (c) x_B = 0.375, (d) x_B = 0.50, (e) x_B = 0.625, (f) x_B = 0.75 and (g) x_B = 0.875 during non-isothermal crystallization. Blue and orange lines represent crystalline bonds of A- and B-block respectively; yellow lines represent non-crystalline bonds of both the blocks.

At strong segregation (viz., λ = 4), the development of overall crystallinity as a function of U_p is available in Figure 5.12a. Similarly, the changes in crystallinity of A-block and B-block with U_p are available in Figure 5.12b and 5.12c respectively. We also plot the value of saturation crystallinity (X^{sat}) with respect to block composition (x_B) in Figure 5.13. The overall crystallinity covers a wide range from 0.3 to 0.6 with a non-monotonic trend as a function of x_B. The values of saturation crystallinity of A-block at λ = 4 are 0.56, 0.60, 0.50, 0.36, 0.43, 0.46 and 0.25 for x_B = 0.125, 0.25, 0.375, 0.50, 0.625, 0.75 and 0.875

respectively. On the other side, the values of saturation crystallinity of the B-block at $\lambda = 4$ are 0.15, 0.44, 0.31, 0.23, 0.36, 0.50 and 0.41 for $x_B = 0.125$, 0.25, 0.375, 0.50, 0.625, 0.75 and 0.875 respectively. The saturation crystallinity at $\lambda = 4$ is always lesser than the saturation crystallinity at $\lambda = 1$ for all the block compositions. At $\lambda = 4$, the inter-block segregation strength is strong enough to confine the crystallization within the large number of microdomains created during microphase separation, and as a result crystallization is strongly suppressed. The snapshots for $x_B = 0.125$ to 0.875 at the end of crystallization (viz., at $U_p = 0.6$) are presented in Figure 5.14 at $\lambda = 4$. The snapshots clearly demonstrate that at strong segregation, the crystallinity decreases regardless of composition.

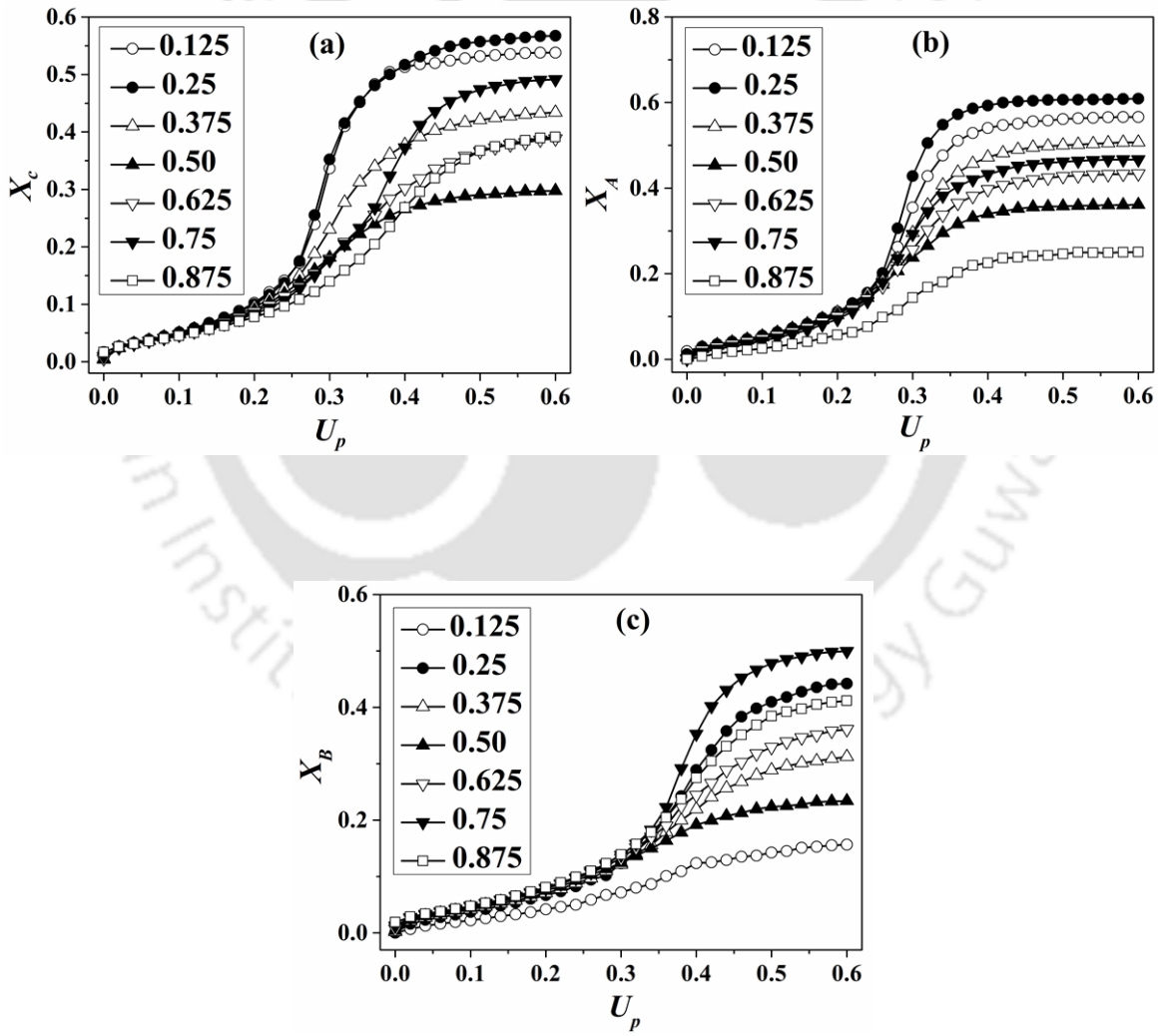

Figure 5.12 Change in (a) overall crystallinity (X_c), (b) crystallinity of A-block (X_A) and (c) crystallinity of B-block (X_B) with U_p at λ =4 for different compositions (x_B).

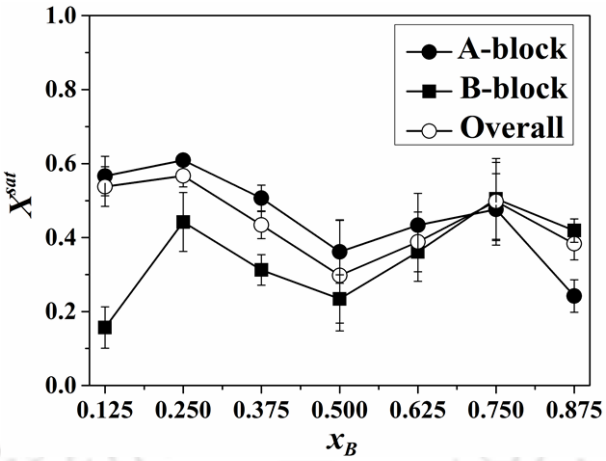

Figure 5.13 Change in saturation crystallinity at U_p = 0.6 with block compositions (x_B).

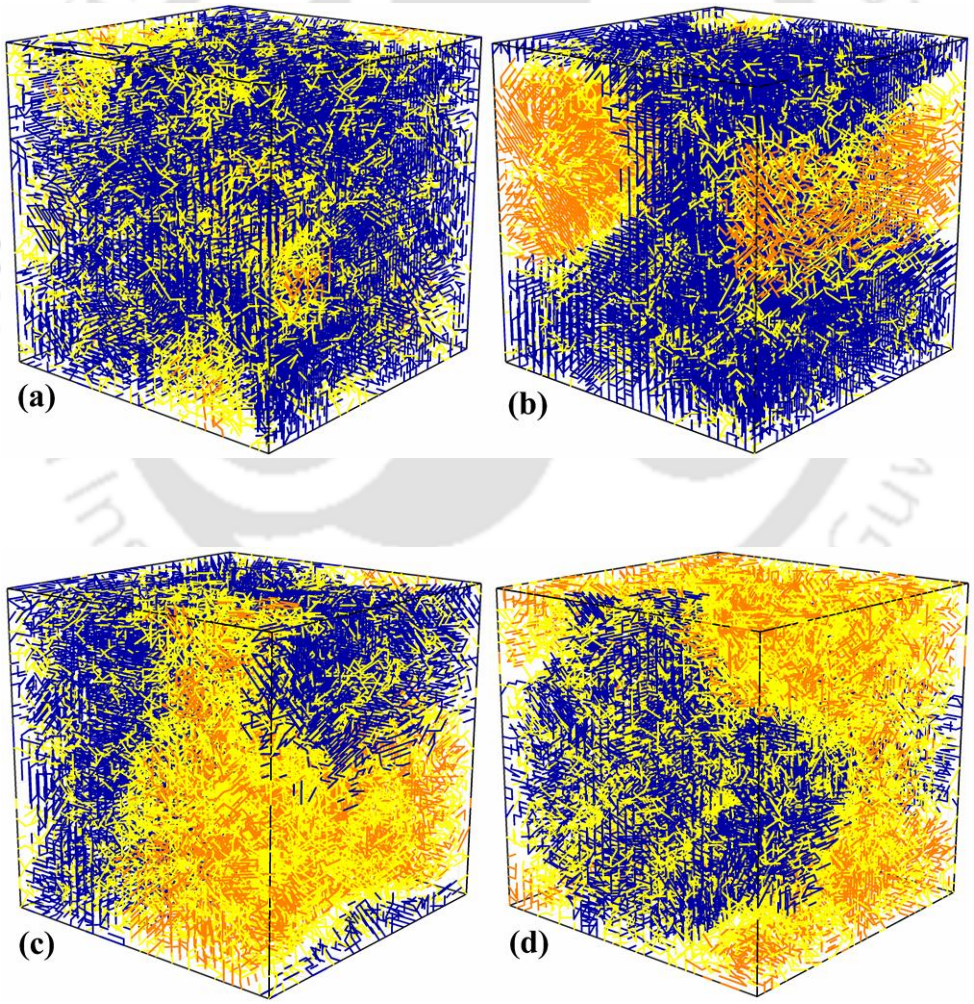

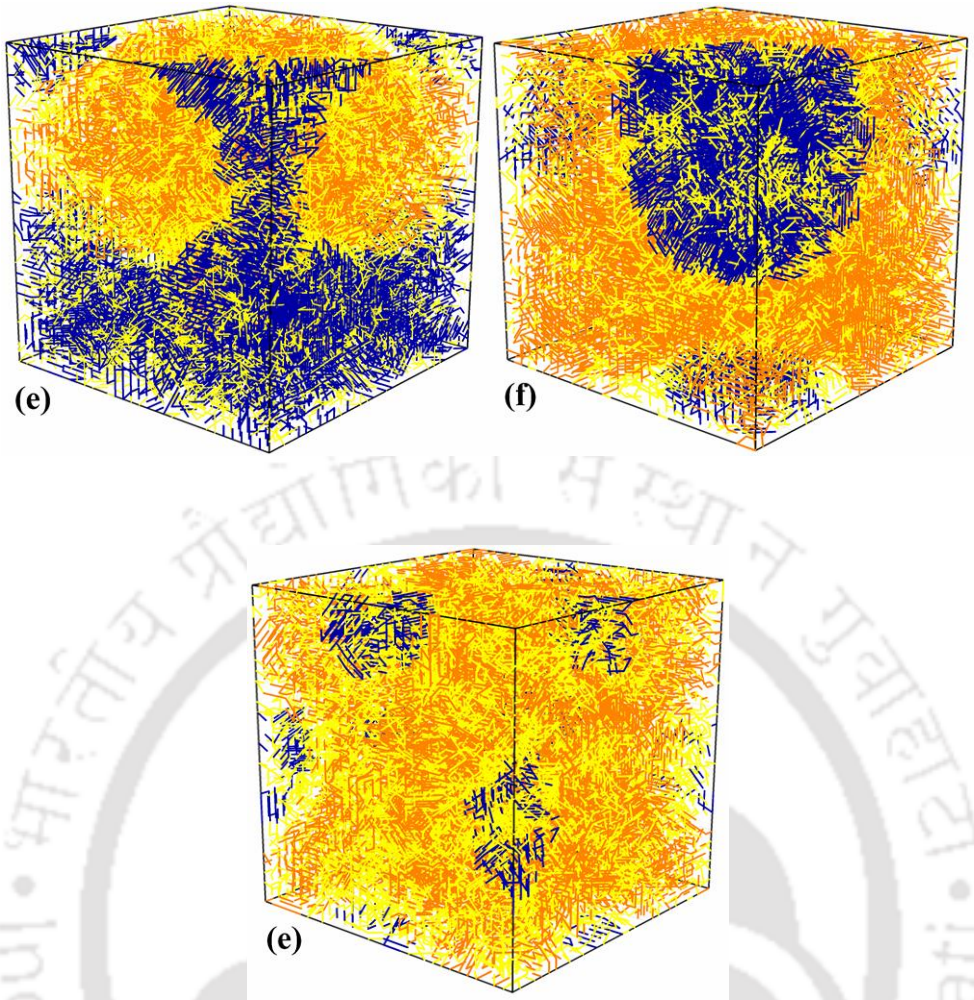

Figure 5.14 Snapshots of semi crystalline structures at λ = 4 for (a) x_B = 0.125, (b) x_B = 0.25, (c) x_B = 0.375, (d) x_B = 0.50, (e) x_B = 0.625, (f) x_B = 0.75 and (g) x_B = 0.875 during non-isothermal crystallization. Blue and orange lines represent crystalline bonds of A- and B-block respectively; yellow lines represent non-crystalline bonds of both the blocks.

5.2.1.4 Structural Analysis

We evaluate the average crystallites size and lamellar thickness individually for both the blocks as a function of U_p for all block compositions. There is a wider distribution in crystallites size than lamellar thickness, and the extent of lamellar thickness is smaller compared to crystallites size, signifying the development of two dimensional crystals. Figure 5.15a represents the change in average crystallite size (at U_p = 0.6) as a function of x_B for λ = 1. At weak segregation (viz., λ = 1), the crystallite size of A-block reveals a non-

monotonic trend, whereas the crystallite size of B-block monotonically increases with x_B (Figure 5.15a). The non-monotonic trend of A-block crystallites is endorsed by the dilution effect of B-block. When x_B is low (viz., $x_A > x_B$), the development of larger crystallites of A-block is naturally assisted as A-block is more crystallizable than B-block. But when x_B increases up to 0.5, the relative stability of microdomains of B-block in the phase separated melt increases and as a result, the formation of larger size crystallites of A-block is restricted. We also calculate the chain mobility of both the blocks separately by calculating the mean square displacement as a function of U_p in Figure 5.16. From figure 5.16, it is evident that the chain mobility of A-block is delimited by B-block up to block composition 0.5 ensuing smaller crystallites of A-block due to suppression of diffusion towards crystalline segments. This observation is in accord with SAXS results on PLLA-*b*-PCL diblock copolymer, which gives decreasing domain spacings of the PLLA block on increasing its content producing additional confinement for the crystallization of PCL block [29]. On further increasing of x_B (viz., x_B > 0.5), B-block now turns as the continuous phase and A-block acts as the disperse one. During crystallization of A-block (U_p ~ 0.3), B-block is still in a molten state, and behaves like a "solvent", weakening the topological restriction, which is reflected by the enhancement of mean square displacement of the centre of mass of B-block compared to A-block (Figure 4.16). This enhanced mobility of A-block helps the formation of larger size crystallites when $x_A < x_B$ as it is shown in Figure 5.15a.

For better understanding, we notice the change in average lamellar thickness of both the blocks as a function of compositions (Figure 5.15b). At weak segregation (viz., λ = 1), the lamellar thickness of A-block $\langle l_A \rangle$ does not differ with block compositions (x_B = 0.125, 0.25, 0.375 and 0.5, Figure 5.15b). However, at higher values of x_B (x_B > 0.5), the value of $\langle l_A \rangle$ significantly increases and it is endorsed by the dilution effect of the B-block. When the composition of the B-block is less than 0.5, the crystallization of A-block is typically dominated by the chain entanglement and follows "melt crystallization", where the diffusion of chain segmentsof A-block is delayed by intra- and inter-chain entanglement which is available in Figure 5.16, imposing folded chain crystals. On the other side, when x_B increases, A-block crystallizes within the matrix of the molten B-block, which act like a "solvent". The molten B-block enforces a marginal hindrance towards the diffusion of chain

segments of A-block, and we observe enhanced mobility of A-block compared to the B-block in Figure 5.16. The dilution effect introduces extended chain crystals, which is typically related to the increased value of $\langle l_A \rangle$ in Figure 5.15b. As a result, A-block crystallites thickens, giving rise to thicker crystals with larger crystallites size.

The average crystallites size $\langle S \rangle$ and lamellar thickness $\langle l \rangle$ of both the blocks give a non-monotonic trend with block compositions at strong segregation (Figure 5.17a and 5.17b). During strong segregation, demixing energy between two blocks plays a crucial role to determine crystal morphology and composition effect is overruled by the confinement effect.

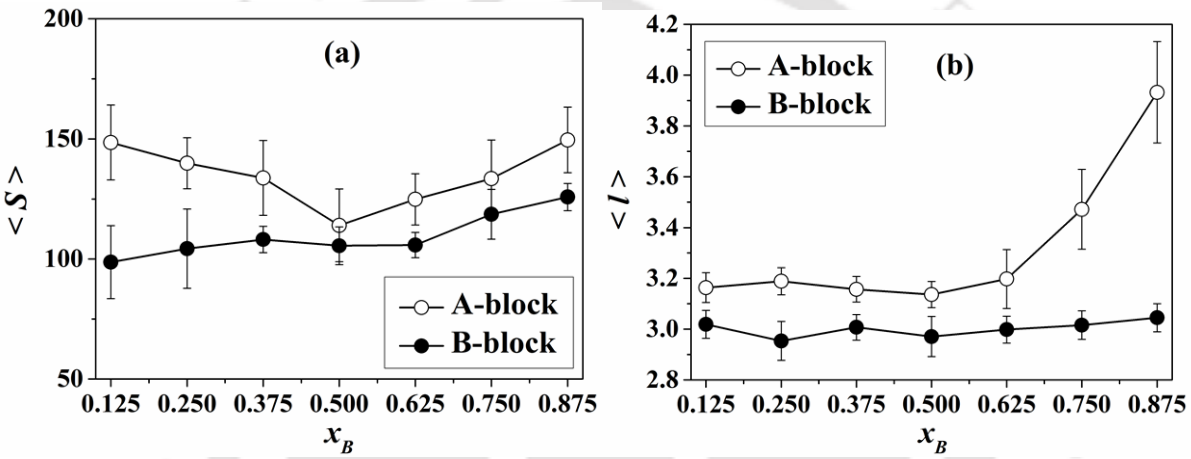

Figure 5.15 Change in (a) average crystallites size $\langle S \rangle$ and (b) average lamellar thickness $\langle l \rangle$ of A- and B-blocks with block compositions (x_B) at λ =1.

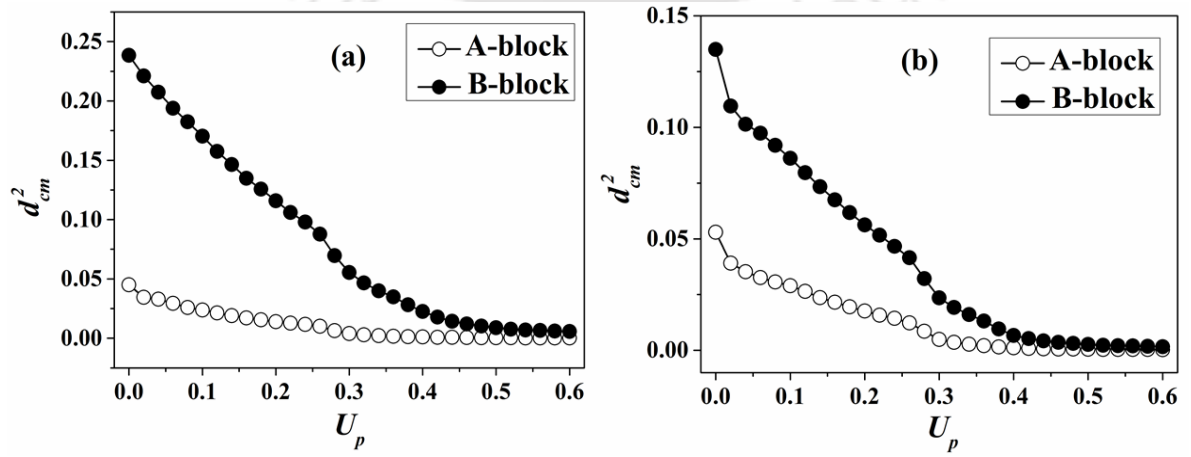

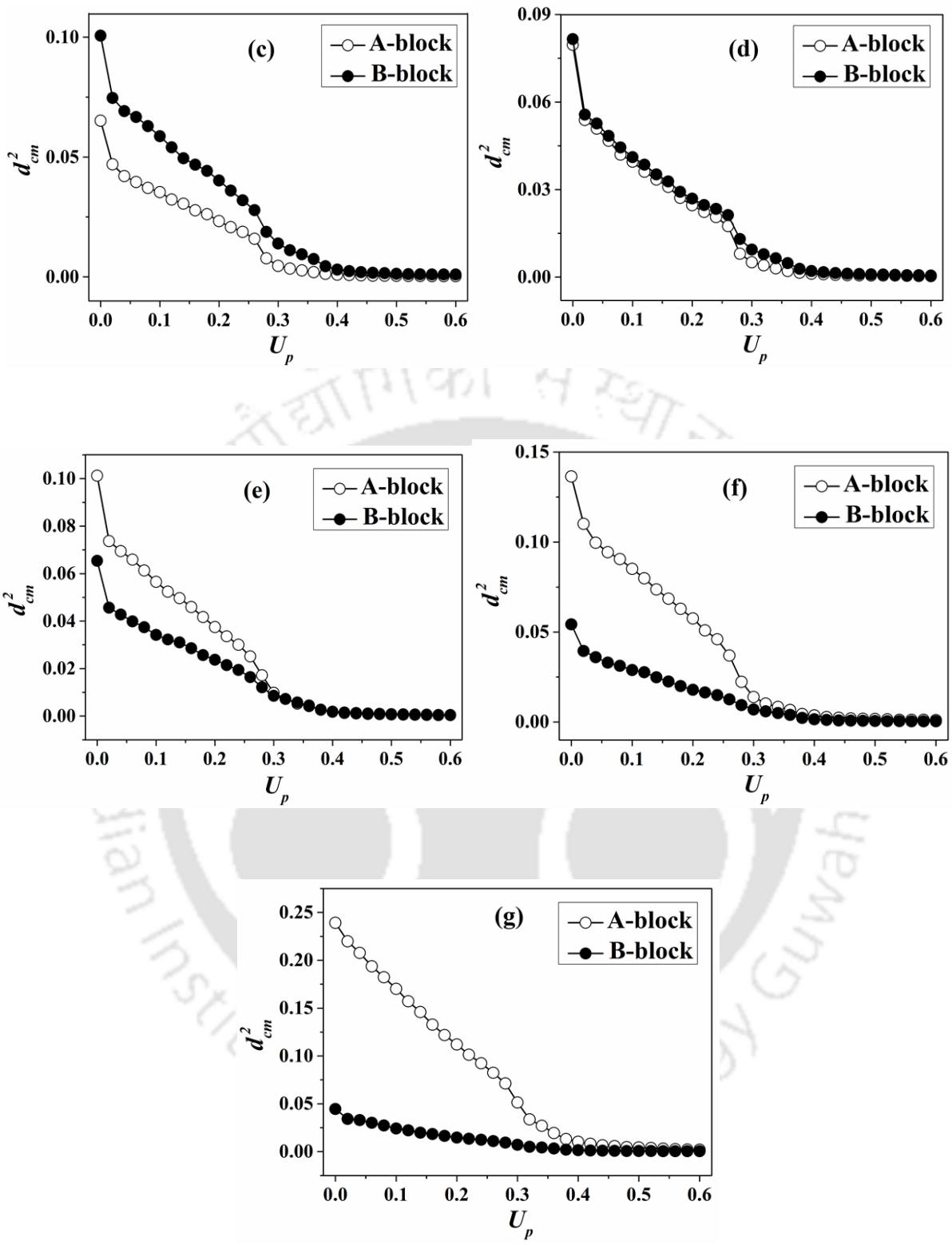

Figure 5.16 Change in mean square displacement of centre of mass (d^2_{cm}) of A- and B-block with U_p at weak segregation (λ=1) for (a) x_B= 0.125, (b) x_B = 0.25, (c) x_B = 0.375, (d) x_B = 0.50, (e) x_B= 0.625, (f) x_B = 0.75 and (g) x_B= 0.875.

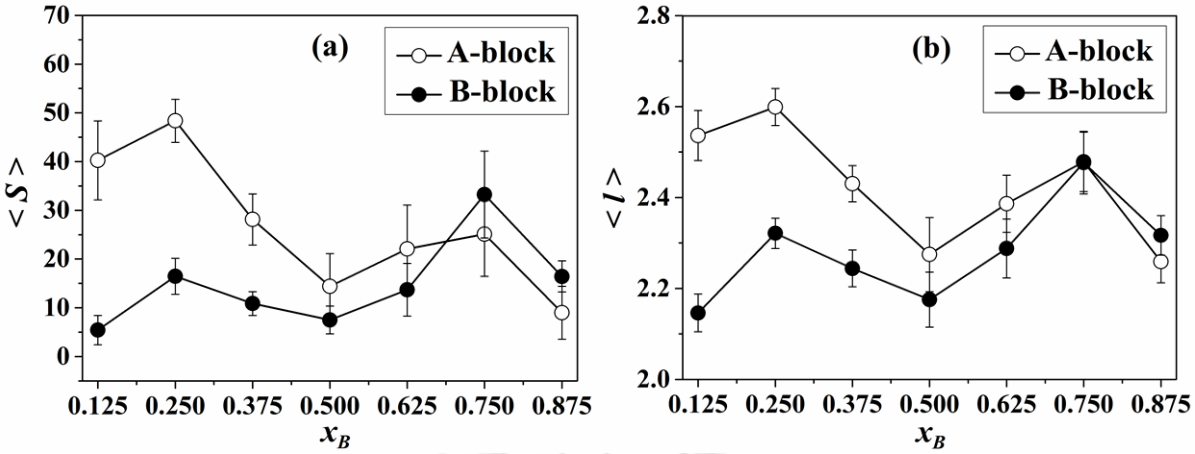

Figure 5.17 Change in (a) average crystallites size $\langle S \rangle$ and (b) average lamellar thickness $\langle l \rangle$ of A- and B-blocks with block compositions (x_B) at λ = 4.

5.2.2 Isothermal Crystallization

5.2.2.1 One-step Cooling

To follow the transition kinetics, we quench our sample from $U_p = 0$ to $U_p = 0.6$ and allow the system to anneal for 10^5 Monte Carlo steps (MCS). Figure 5.18 represents the development of overall crystallinity (X_c) as a function of MCS for all the block compositions in weak segregation as well as strong segregation. Overall crystallinity is considered as the summation of weighted average crystallinity of A- and B-blocks. The overall crystallinity indicates a non-monotonic trend with composition at both the levels of segregation; however, it establishes the dependence of transition kinetics on composition. During one-step isothermal cooling, as the driving force for crystallization (viz., in terms of the temperature difference) is adequate for both the blocks, they compete with each other which lead to the coincident crystallization. This observation is in accord with the isothermal crystallization of PPDX-*b*-PCL diblock copolymer, where the crystallization kinetics of both the blocks are overlapping [37, 38].

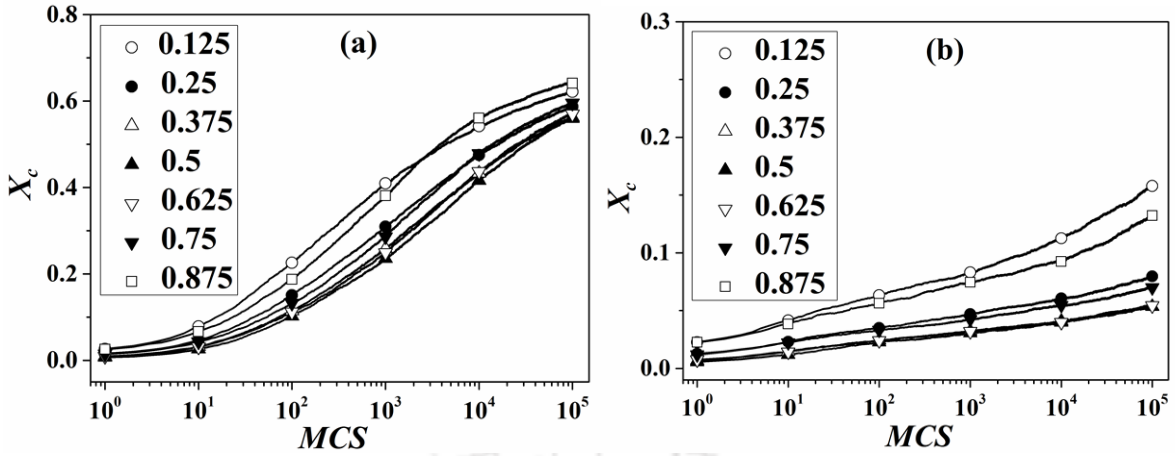

Figure 5.18 Change in Overall Crystallinity (X_c) with Monte Carlo steps (MCS) on isothermal one step crystallization at (a) λ = 1 and (b) λ =4.

To get an insight on the transition kinetics, nucleation type (viz., homogeneous or heterogeneous) and crystal geometry, we investigate the evolution of isothermal crystallization with the help of the Avrami equation [49, 50].

$$(1 - X) = \exp(-kt^n)$$

Where, X is the crystallinity, k and n are constants. The value of Avrami index (n) designates the type of crystal geometry. We estimate the value of Avrami index (n) based on the primary crystallization, which is considered as the development of crystallinity up to 20% [50]. At the weak segregation limit, the values of Avrami index of both the blocks are within the limit of 0.5 to 1.5 (Figure 5.19a) which signifies first order transition kinetics with homogenous nucleation. However, at the strong segregation limit, due to confinement effect the value of Avrami index is decreased to the range of 0.5 to 1 (Figure 5.19b). This result is in accord with the experimental observation of the crystallization of asymmetric double crystalline diblock copolymer, PLLA-*b*-PCL, which follows a homogeneous nucleation pathway with Avrami index close to 1.0 [29]. Similar phenomena have also been detected during the crystallization of crystalline-amorphous diblock copolymers, where the crystalline block is confined within the matrix of amorphous block, follows homogeneous nucleation pathway with Avrami index ~ 1.0. For example, the crystallization of PEO block in poly(ethylene oxide)-*b*-poly(styrene) (PEO-*b*-PS) or PCL block in PCL-*b*-PS diblock copolymer, is confined by the large numbers of isolated microdomains of PS block (viz., spheres or cylinders) and finally it crystallizes via homogeneous nucleation [14]. Similarly,

PLLA block in PLLA-*b*-PS diblock copolymer [15] and PE block in styrene-*b*-ethylene-*b*-butane random terpolymer [13] also obey similar mechanism with the Avrami index ~ 1.0. The final semi-crystalline structures of diblock copolymer after isothermal one-step crystallization are available in Figure 5.20 for weak segregation and Figure 5.21 for strong segregation. Blue and orange lines represent crystalline bonds of A- and B-block, respectively and yellow lines represent non-crystalline bonds of both the blocks. However, at strong segregation (viz., $\lambda = 4$), the development of crystallinity of both the blocks is confined which ranges from 3 to 10% in one-step cooling.

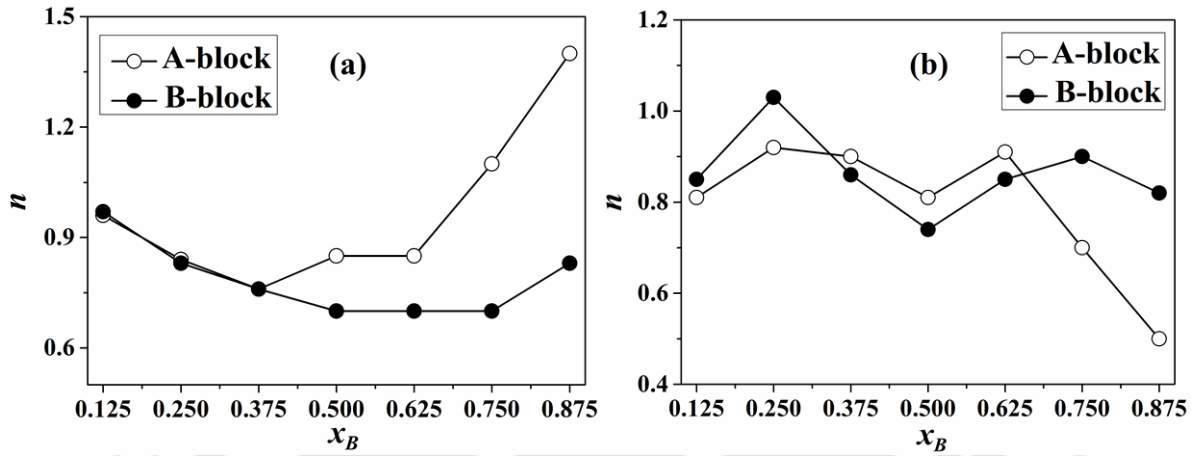

Figure 5.19 Change in Avrami index (n) with block composition (x_B) for A- and B-block at (a) λ = 1 and (b) λ =4.

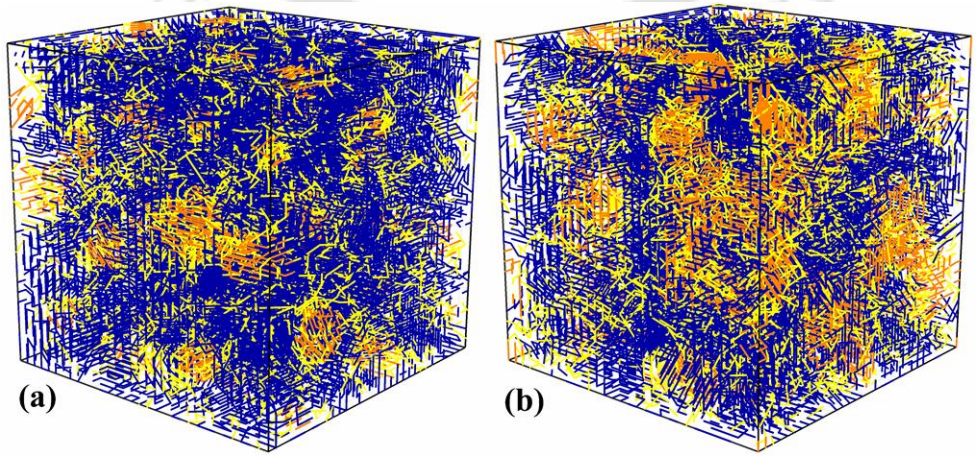

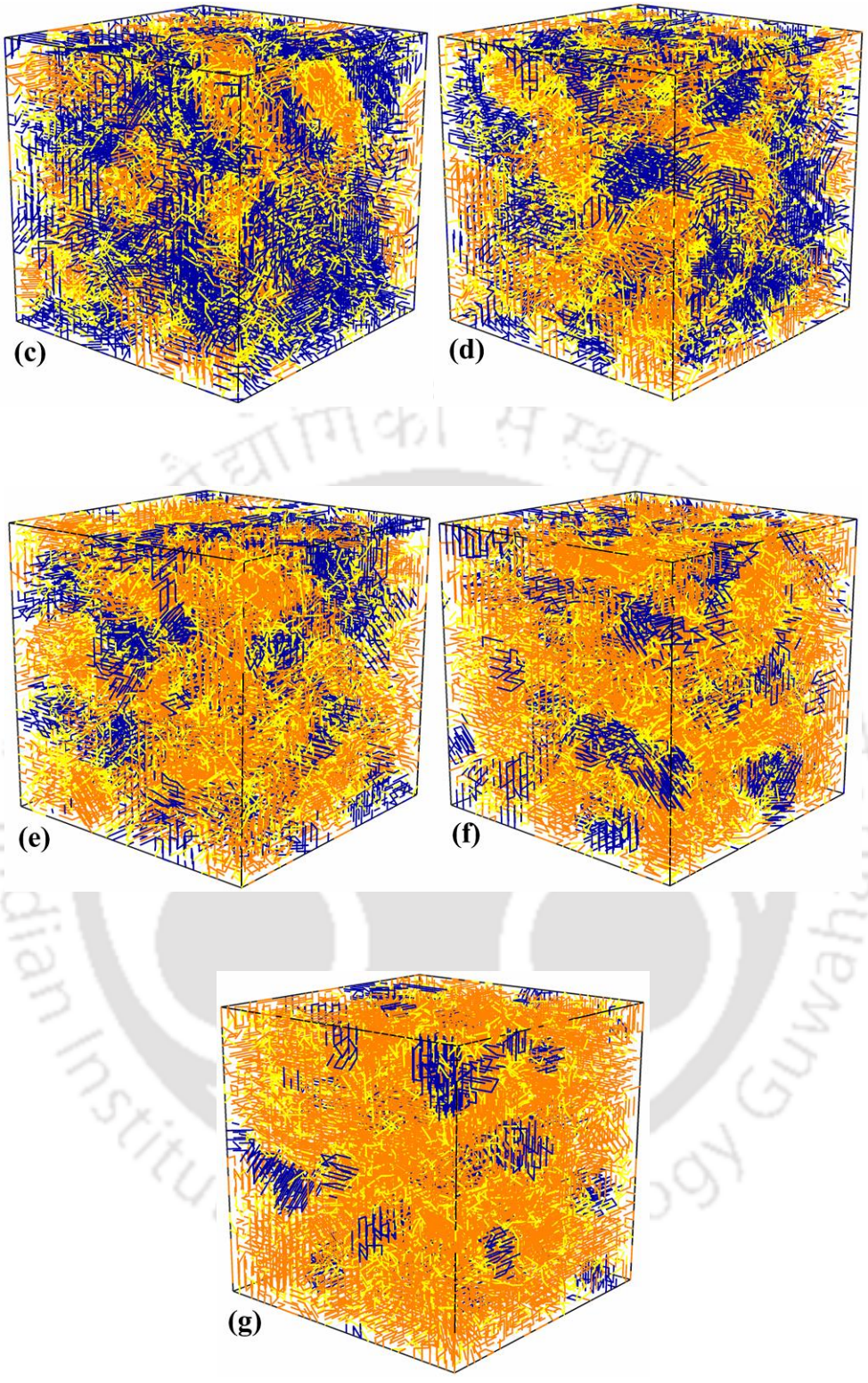

Figure 5.20 Snapshots of semi crystalline structures at λ = 1 for (a) x_B = 0.125, (b) x_B = 0.25, (c) x_B = 0.375, (d) x_B = 0.50, (e) x_B = 0.625, (f) x_B = 0.75 and (g) x_B = 0.875 during isothermal crystallization.

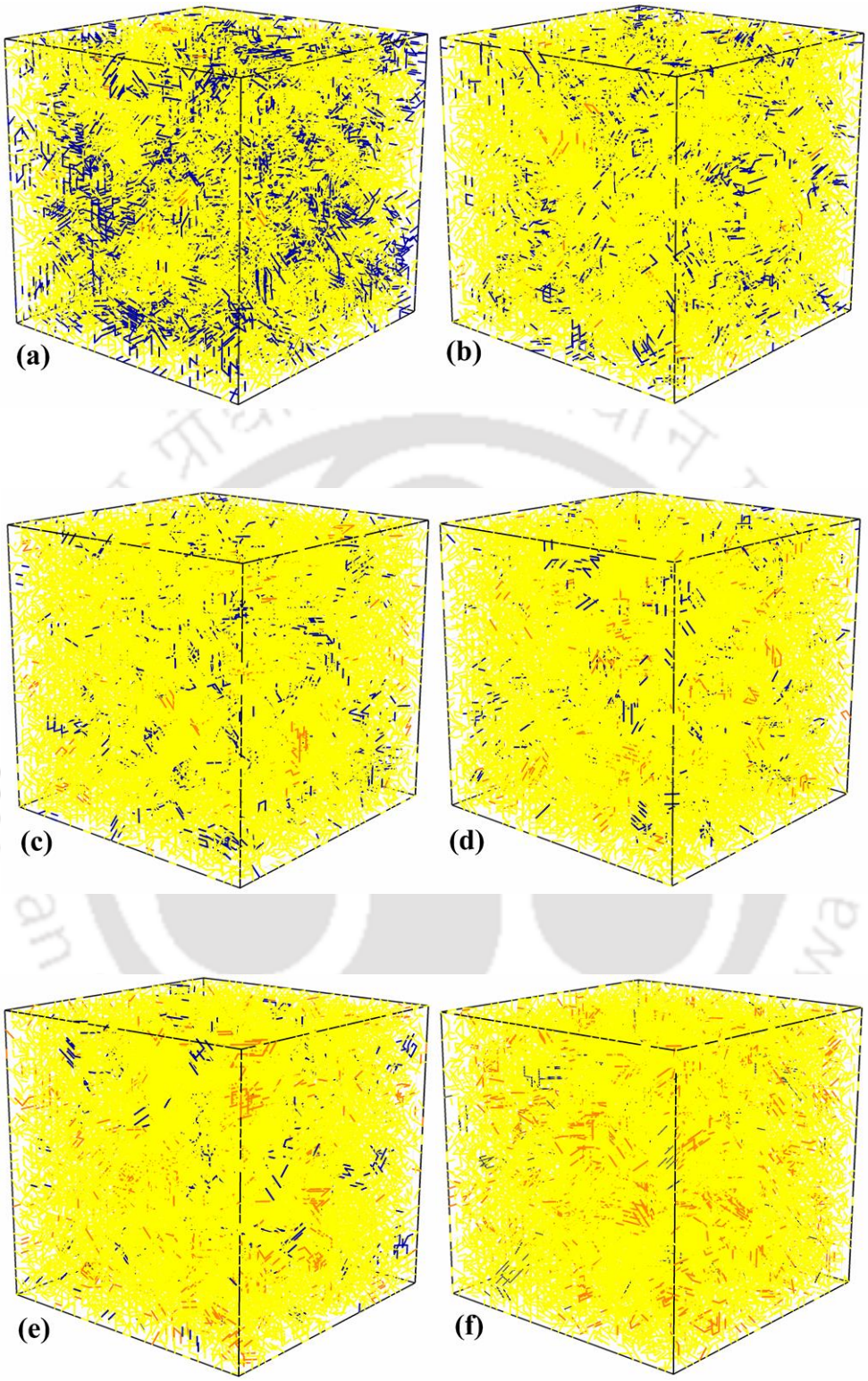

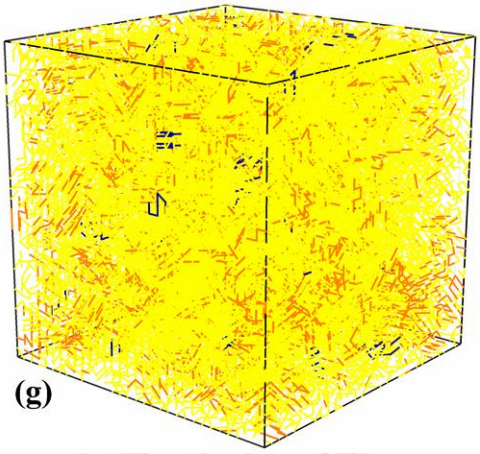

Figure 5.21 Snapshots of semi crystalline structures at λ = 4 for (a) x_B = 0.125, (b) x_B = 0.25, (c) x_B = 0.375, (d) x_B = 0.50, (e) x_B = 0.625, (f) x_B = 0.75 and (g) x_B = 0.875 during isothermal crystallization.

5.2.2.2 Two-step Cooling

In order to gain insight, we implement isothermal crystallization in two steps. We quench our sample from U_p = 0 to U_p = 0.3 in the first step, and from U_p = 0.3 to U_p = 0.6 in the second step, with annealing for 10^5 MCS in each step. During the first step of quenching at U_p = 0.3 (temperature below the melting point of A-block, but above the melting point of B-block) only A-block is going to crystallize and B-block is still in a molten state. During the second stage of quenching at U_p = 0.6 (temperature below the melting point of B-block), B-block crystallizes within the confined space created by A-block. Therefore, the mode of crystallization in two-step isothermal cooling is sequential crystallization. Table 5.1 compares the crystallinity of A-block during one- and two-step isothermal crystallization of a wide range of block compositions at λ = 1 (viz., weak segregation). The crystallinity of A-block is close to 0.71 for x_B up to 0.625 in two–step isothermal cooling, whereas, for x_B = 0.75 and 0.875, the crystallinity of A-block increases to 0.78. As the initial development of crystallinity is largely dominated by the degree of cooling, the crystallization of A-block is unaffected by block composition up to a certain point. However, at x_B = 0.75 and 0.875, dilution effect of B-block dominates the system, which reduces the topological restriction resulting in an increase in crystallinity of A-block. In the one-step isothermal cooling, the dilution effect is not prominent at higher composition. The above observation is basically

related with the change in mode of crystallization. In two–step isothermal crystallization, we observe a sequential crystallization similar to the non-isothermal crystallization. However, in one-step isothermal crystallization, we observe a coincident crystallization, where both the blocks compete for crystallization and develop crystallinity simultaneously. Table 5.2 compares the crystallinity of the B-block in two-step and one-step isothermal cooling at $\lambda = 1$ (viz., weak segregation). There is a monotonic increase in crystallinity of B-block with an increasing block length which is in line with the previous observation of non-isothermal crystallization. However, at strong segregation (viz., $\lambda = 4$), the final value of crystallinity for both the blocks are marginal which ranges from 3 to 30% in two–step isothermal cooling (Table 5.3 and Table 5.4). Therefore, it appears that the effect of block asymmetry on the development of crystallinity at strong segregation is negligible. The final crystalline structures of $x_B = 0.50$ at $U_p = 0.6$ are available in Figure 5.22.

Table 5.1 Comparison in fractional crystallinity (X_A) of A-block with block compositions of B (x_B), during two-stage and one-stage isothermal crystallization at weak segregation ($\lambda = 1$).

Composition	Two-step at $U_P = 0.3$	Two-step at $U_P = 0.6$	One step at $U_P = 0.6$
0.125	0.69	0.72	0.64
0.25	0.68	0.71	0.60
0.375	0.68	0.71	0.58
0.50	0.66	0.71	0.57
0.625	0.67	0.71	0.57
0.75	0.69	0.73	0.58
0.875	0.72	0.78	0.58

Table 5.2 Comparison in fractional crystallinity (X_B) of B-block with block compositions of B (x_B), during two-stage and one-stage isothermal crystallization at weak segregation (λ = 1).

Composition	Two-step at U_P = 0.3	Two-step at U_P = 0.6	One step at U_P = 0.6
0.125	0.05	0.53	0.50
0.25	0.08	0.56	0.53
0.375	0.10	0.58	0.53
0.50	0.10	0.58	0.55
0.625	0.12	0.60	0.57
0.75	0.12	0.62	0.60
0.875	0.12	0.66	0.65

Table 5.3 Comparison in fractional crystallinity (X_A) of A-block with block compositions of B (x_B), during two-stage and one-stage isothermal crystallization at strong segregation (λ = 4).

Composition	Two-step at U_P = 0.3	Two-step at U_P = 0.6	One step at U_P = 0.6
0.125	0.33	0.35	0.175
0.25	0.19	0.20	0.09
0.375	0.150	0.155	0.06
0.50	0.130	0.135	0.06
0.625	0.116	0.120	0.05
0.75	0.109	0.114	0.04
0.875	0.106	0.112	0.04

Table 5.4 Comparison in fractional crystallinity (X_B) of B-block with block compositions of B (x_B), during two-stage and one-stage isothermal crystallization at strong segregation (λ = 4).

Composition	Two-step at U_P = 0.3	Two-step at U_P = 0.6	One step at U_P = 0.6
0.125	0.050	0.056	0.033
0.25	0.070	0.073	0.036
0.375	0.077	0.080	0.036
0.50	0.085	0.088	0.045
0.625	0.10	0.103	0.057
0.75	0.122	0.127	0.08
0.875	0.131	0.150	0.14

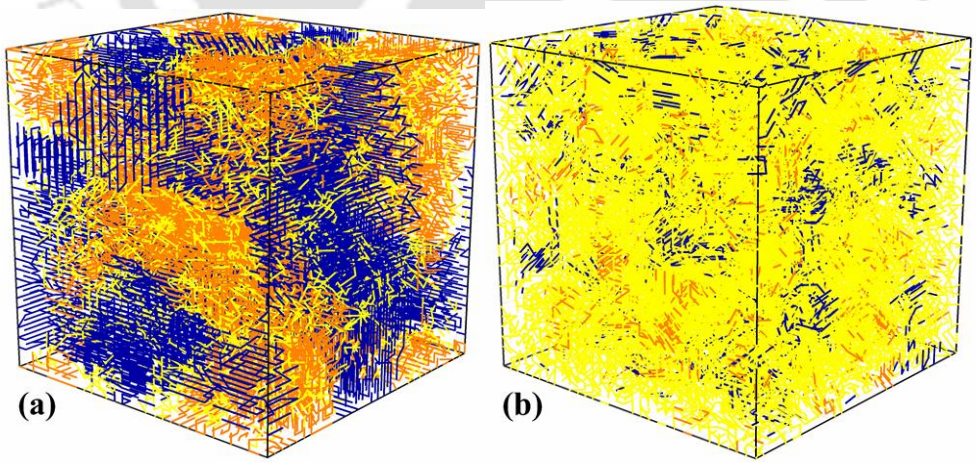

Figure 5.22 Snapshots of semi crystalline structures for x_B = 0.50 at (a) λ = 1 and (b) λ = 4 during isothermal two-step crystallization.

5.3 Summary

We investigate the effect of block asymmetry on crystallization of double crystalline diblock copolymer by dynamic Monte Carlo simulation at two different segregation levels. Diblock copolymer exhibits sequential crystallization mechanism regardless of composition during non-isothermal crystallization. At weak segregation (viz., λ = 1), we detect a small depression in crystallization temperature of A-block at x_B = 0.875, which is attributed to the dilution effect, imposed by B-block. We also notice a significant increase in chain mobility (in terms of mean square displacement of the centre of mass) of A-block at U_p = 0.3 compared to that of B-block at higher x_B. The crystallization temperature of the B-block monotonically rises with increasing block composition. At strong segregation, the transition points of both the blocks exhibit non-monotonic trend with block composition due to the confinement effect offered by large numbers of microdomains in microphase separated melt. The crystallinity of A-block remains identical over a wide range of block composition, whereas the crystallinity of B-block increases with increasing block length of B at weak segregation. However the crystallinity of both the blocks gives non-monotonic trend with x_B within strong segregation. The lamellar thickness of A-block significantly increases for x_B = 0.75 and 0.875 at λ = 1 which is attributed to the dilution effect enforced by B-block. When the composition of A-block is very small in the system, B-block behaves as a “diluent”, which reduces topological restriction favouring crystal thickening. But the lamellar thickness of both the blocks produces non-monotonic trend with composition within strong segregation.

Isothermal crystallization confirms the dependence of the compositions on transition kinetics for both the levels of segregations. The values of Avrami index establish the presence of homogeneous nucleation with the formation of two-dimensional crystals. The dilution effect is active in two-stage isothermal crystallization compared to one-stage crystallization due to changing mode of crystallization. Two-stage isothermal cooling follows sequential crystallization whereas one-stage cooling follows coincident crystallization. Therefore, by manipulating the block asymmetry with a proper choice of crystallization process, one can easily achieve the desired morphological pattern. The present findings on the composition-dependent morphological evolution would enable us in gaining insight of crystallization of diblock copolymer for targeted applications.

References

1. Rangarajan P and Register RA. Macromolecules 1993;26(17):4640-4645.
2. Rangarajan P, Register RA, Adamson DH, Fetters LJ, Bras W, Naylor S, and Ryan AJ. Macromolecules 1995;28(5):1422-1428.
3. Ryan kJ, Hamley IW, Bras W, and Bates FS. Macromolecules 1995;28(11):3860-3868.
4. Hamley IW, Fairclough JPA, Terrill NJ, Ryan AJ, Lipic PM, and Bates FS. Macromolecules 1996;29(27):8835-8843.
5. Hamley lW, Fairclough JPA, Ryan AJ, Bates FS, and Towns-Andrews E. Polymer 1996;37(19):4425-4429.
6. Nojima S, Kato K, Yamamoto S, and Ashida T. Macromolecules 1992;25(8):2237-2242.
7. Nojima S, Nakano H, and Ashida T. Polymer 1993;34(19):4168-4170.
8. Nojima S, Nakano H, Takahashi Y, and Ashida T. Polymer 1994;35(16):3479-3486.
9. Nojima S, Yamamoto S, and Ashida T. Polym. J. 1995;27(7):673-682.
10. Nojima S, Fujimoto M, Kakihira H, and Sasaki S. Polym. J. 1998;30(12):968-975.
11. Quiram DJ, Register RA, and Marchand GR. Macromolecules 1997;30(16):4551-4558.
12. Loo Y-L, Register RA, Ryan AJ, and Dee GT. Macromolecules 2001;34(26):8968-8977.
13. Loo Y-L, Register RA, and Ryan AJ. Macromolecules 2002;35(6):2365-2374.
14. Muller AJ, Balsamo V, Arnal ML, Jakob T, Schmalz H, and Abetz V. Macromolecules 2002;35(8):3048-3058.
15. Ho R-M, Lin F-H, Tsai C-C, Lin C-C, Ko B-T, Hsiao BS, and Sics I. Macromolecules 2004;37(16):5985-5994.
16. Fu J, Luan B, Pan C, Li B, and Han Y. Macromolecules 2005;38:5118 - 5127.
17. Lorenzo AT, Arnal ML, Muller AJ, Boschetti-de-Fierro A, and Abetz V. Macromolecules 2007;40(14):5023-5037.
18. Al-Husseina M and Jeu WHd. Polymer 2009;50:2149–2153.
19. Nakagawa S, Kadena K-i, Ishizone T, Nojima S, Shimizu T, Yamaguchi K, and Nakahama S. Macromolecules 2012;45:1892-1900.

20. Lin M-C, Chen H-L, Lin W-F, Huang P-S, and Tsai J-C. J. Phys. Chem. B 2012;116:12357 - 12371.
21. Kim YY, Ahn B, Sa S, Jeon M, Roth SV, Kim SY, and Ree M. Macromolecules 2013;46(20):8235-8244.
22. Chen L, Jiang J, Wei L, Wang X, Xue G, and Zhou D. Macromolecules 2015;48:1804 - 1812.
23. Sun L, Liu Y, Zhu L, Hsiao BS, and Avila-Orta CA. Polymer 2004;45:8181-8193.
24. Hamley IW, Castelletto V, Castillo RV, Muller AJ, Martin CM, Pollet E, and Dubois P. Macromolecules 2005;38(2):463-472.
25. Nojima S, Akutsu Y, Washino A, and Tanimoto S. Polymer 2004;45:7317-7324.
26. Nojima S, Akutsu Y, Akaba M, and Tanimoto S. Polymer 2005; 46 4060–4067.
27. Nojima S, Kiji T, and Ohguma Y. Macromolecules 2007;40(21):7566-7572.
28. Li L, Meng F, Zhong Z, Byelov D, Jeu WHd, and Feijen J. J. Chem. Phys. 2007;126:024904-1 - 024904-7.
29. Castillo RV, Muller AJ, Raquez J-M, and Dubois P. Macromolecules 2010;43(9):4149–4160.
30. Lin M-C, Chen H-L, Su W-B, Su C-J, Jeng U-S, Tzeng F-Y, Wu J-Y, Tsai J-C, and Hashimoto T. Macromolecules 2012;45:5114−5127.
31. Castillo RV, Muller AJ, Lin M-C, Chen H, Jeng U-S, and Hillmyer MA. Macromolecules 2008;41(16):6154-6164.
32. Kim KS, Chung S, Chin IJ, Kim MN, and Yoon JS. J. Appl. Polym. Sci. 1999;72:341-348.
33. Myers SB and Register RA. Macromolecules 2008;41(18):6773-6779.
34. Li S, Myers SB, and Register RA. Macromolecules 2011;44:8835-8844.
35. Hamley IW, Parras P, Castelletto V, Castillo RV, Mu¨ller AJ, Polleet E, Dubois P, and Martin CM. Macromol. Chem. Phys. 2006;207:941-953.
36. Nojima S, Ito K, and Ikeda H. Polymer 2007;48:3607-3611.
37. Albuerne J, Marquez L, Muller AJ, Raquez JM, Degee P, Dubois P, Castelletto V, and Hamley IW. Macromolecules 2003;36(5):1633-1644.
38. Muller AJ, Albuerne J, Esteves LM, Marquez L, Raquez J-M, Degee P, Dubois P, Collins S, and Hamley IW. Macromol. Symp. 2004;215:369-382.
39. Muller AJ, Albuerne J, Marquez L, Raquez J-M, Degee P, Dubois P, Hobbs J, and Hamley IW. Faraday Discuss. 2005;128:231-252.
40. Nojima S, Fukagawa Y, and Ikeda H. Macromolecules 2009;42(24):9515-9522.

41. Sun J, He C, Zhuang X, Jing X, and Chen X. J Polym Res 2011;18:2161–2168.
42. He C, Sun J, Ma J, Chen X, and Jing X. Biomacromolecules 2006;7(12):3482-3489.
43. Sun J, Hong Z, Yang L, Tang Z, Chen X, and Jing X. Polymer 2004;45:5969–5977.
44. Shin D, Shin K, Aamer KA, Tew GN, Russel TP, Lee JH, and Jho JY. Macromolecules 2005;38(1):104-109.
45. D.L.Goodstein. States of Matter: Dover, New York, 1985.
46. Dasmahapatra AK, Nanavati H, and Kumaraswamy G. J. Chem. Phys. 2009;131:074905-1-074905-10.
47. Kundu C and Dasmahapatra AK. Polymer 2014;55(3):958-969.
48. Kim JK, Park D-J, Lee M-S, and Ihn KJ. Polymer 2001;42:7429-7441.
49. Avrami M. J. Chem. Phys. 1939;7:1103-1112.
50. Lorenzo AT, Arnal ML, Albuerne J, and Müller AJ. Polym. Test. 2007;26(2):222-231.

Chapter 6

Crystallization from Microphase Separated Melt

In this chapter, we demonstrate the effect of thermal history in addition to block asymmetry on the crystallization of a double crystalline diblock copolymer originated by microphase separated melt. Microphase separation introduces self-assembled nanostructures which can successfully be modified by the process of annealing. Effect of annealing on the subsequent crystallization and morphological evolution is the main focus of the present study.

6.1 Literature Review

The confinement-induced crystallization in block copolymer has accelerated the recent development of nano technology as the intrinsic properties and final morphology of a crystal can successfully be tailored by judicious adjustment of constituent blocks [1-5]. The self-assembled microdomain characteristic of diblock copolymers is one of the convenient ways to achieve nanoscale confinement during crystallization [1, 6-12]. A diblock copolymer consists of two distinct repeat units which are in most of the cases thermodynamically incompatible [13]. This mutual incompatibility leads to microphase separation between blocks offering a large variety of morphologies including lamellar structure, hexagonally packed cylinder or body centred cubic phases that are stable over a wide range of compositions [14, 15]. Microphase separation in bulk provides ordered nanostructures which are advantageous for designing new functional materials for potential applications such as, in lithography, catalysis, filtration, photovoltaic, energy storage etc. [16-20].

The crystallization behaviour of amorphous-crystalline diblock copolymers has been considered as a prospective research topic during last few decades [6, 21-36]. Typically, crystallization happens after microphase separation and microphase separation offers confinement, which restricts crystallization in respective micro domains keeping melt morphology intact [1, 11, 12, 21, 22, 24, 26, 29, 31, 33, 37-39]. However, in some cases, the microphase structure of semi crystalline diblock copolymer is completely destroyed by the subsequent crystallization of crystalline block giving various morphological patterns [9, 22,

24, 26-28, 34, 40]**.** But the morphological perturbation of phase separated melt is typically driven by thermal history [9, 21, 22, 24, 26]. For example, asymmetric diblock copolymer of polyethylene-*block*-poly(3-methyl-1-butene) exhibits hexagonally packed cylindrical morphology in microphase separated melt. Faster cooling (cooling rate 10-20°C/min) confines crystallization within cylindrical microdomains; whereas slower cooling (cooling rate 8°C/min) ensures morphological perturbation by producing lamellar morphology [26]. Microphase separated melt structure of poly(ethylene glycol)-*block*-poly(butadiene) copolymer with weight fraction (f_{PEG}) of 0.7 also modifies from cylindrical to lamellar microstructure at high crystallization temperature (viz., T_c = 40°C) but the structure remains identical at low crystallization temperature (viz., T_c = 25°C) [24]. Symmetric diblock copolymer of polyethylene-*block*-(atactic polypropylene) shows spherulite growth with disruption of microphase separated lamellar structure when the crystallization temperature (T_c) is in between 95°C to 110°C. But when the crystallization temperature (T_c) is below 95°C, microphase separated lamellar structure preserves it morphology without spherulite growth [22].

Additionally, the crystallization behaviour of double crystalline diblock copolymer instigated by microphase separated melt also presents interesting morphological evolution [5, 7, 10, 35, 36, 41-43]. The nanoscale microdomains can be used as templates for producing long-range order within a polymer matrix. Thus, the incorporation of two different types of crystalline blocks in a diblock copolymer offers an effective way to explore polymer crystallization under confinement. During crystallization from microphase separated melt, polyethylene-*block*-poly(ε-caprolactone) diblock copolymer first exhibits an alternate lamellar structure of crystalline PE block and amorphous PCL block, and subsequently the crystallization of PCL block is followed later at a lower crystallization temperatures (T_c). When T_c < 30°C, the lamellar morphology of PE block remains intact after crystallization of PCL block, whereas at high crystallization temperature (45°C > T_c > 30°C), a morphological transition is observed where PE crystals are fragmentally dispersed in PCL lamellar morphology [7, 41, 42]. The crystallization process of Poly (L-lactide)-*block*-polyethylene (PLLA-*b*-PE) is confined within strongly segregated lamellar microdomain. In the first step of two-step crystallization process (190 °C to 130 °C), PLLA crystallizes first without morphological perturbation of melt microdomain, followed by PE block at 97 °C (in the second step from 130 °C to 97 °C). In one-step crystallization from 190 °C to 80 °C, PE

crystallizes at a much faster rate and dictates the final crystal morphology [5]. The orientation and nanostructures of semiconducting polymers play a pivotal role in determining performances of electronic and optoelectronic devices [43]. For example, the crystallization of conjugated diblock copolymer of poly (2,5-dihexyloxy-p-phenylene)-*block*-(3-hexythiophene) is mainly driven by the crystallization of P3HT which establishes final crystal morphology of the thin films. Higher block composition of P3HT promotes breakout crystallization, whereas lower block composition results in confined crystallization [43]. Similarly, asymmetric syndiotactic polypropylene-*block*-poly(ε-caprolactone) copolymer exhibits hexagonally packed cylindrical morphology in melt, which is completely disrupted, irrespective of the crystallization process, resulting crystalline lamellar morphology. However, in two-step crystallization, interactive crystallization is observed, whereas in one stage crystallization confined crystallization is prominent [10].

6.2 Results and Discussion

To simulate crystallization of diblock copolymer initiated by microphase separated melt, first we prepare a set of phase segregated melt morphology of various block compositions and then we crystallize it through non-isothermal as well as isothermal crystallization.

6.2.1 Preparation of Microphase Separated Melt

Finding a precise location of the microphase separation point is one of the important and challenging tasks in our simulation. Microphase separation creates self-assembled microdomain structures which offer spatial confinement within the system. Therefore, phase segregated melt morphology induces crystallization under confinement.

To monitor crystallization, we have considered three potential energies such as, parallel bond interaction energy (U_p), collinear bond interaction energy (U_c) and demixing energy (U_{AB}) between blocks, the strength of which is given by λ. This demixing energy promotes phase segregation via microphase separation before crystallization. Therefore, to

develop phase separated melt system, we consider only demixing energy and the change in energy per MC move is now modified as: $\Delta E = \Delta N_{AB} U_{AB}$

Then we simulate our system from U_p = 0 to U_p = 0.6 with a step size of 0.02 for different block compositions (x_B) ranging from 0.125 to 0.875 with the increment of 0.125. We plot C_{v-AB} (viz, C_v for A-B contacts) vs. U_p for all block compositions in Figure 6.1. C_{v-AB} gives a peak as fluctuations in energy and the U_p value associated with the peak is considered as microphase separation point ($U_p^{\#}$) [44, 45].

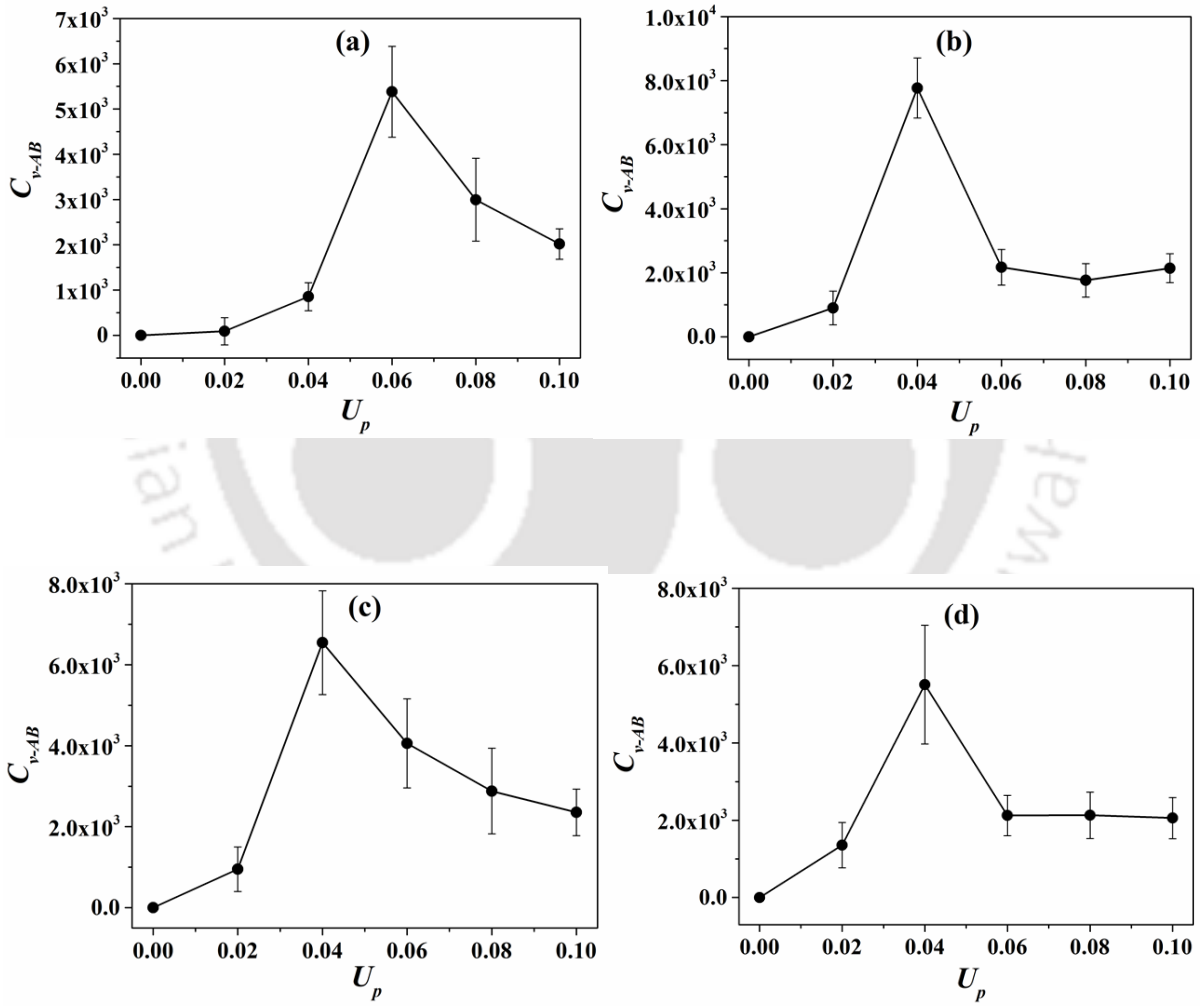

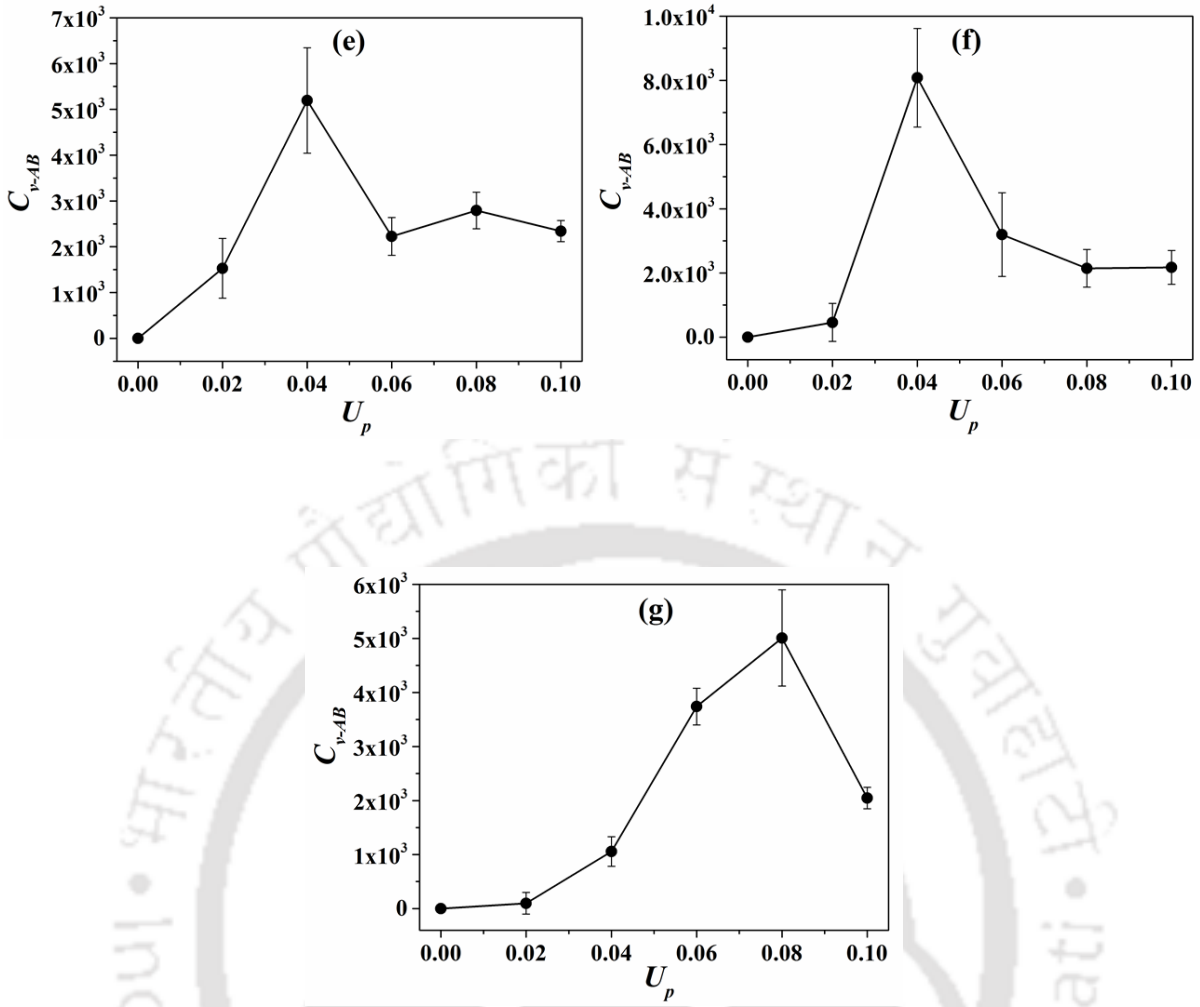

Figure 6.1 Change in specific heat of AB contacts (C_{v-AB}) with U_p for (a) x_B = 0.125, (b) x_B = 0.25, (c) x_B =0.375, (d) x_B = 0.50, (e) x_B = 0.625, (f) x_B = 0.75 and (g) x_B = 0.875.

Figure 6.2 summarizes the changes in microphase separation point ($U_p^{\#}$) with block compositions (x_B). For most of the compositions, $U_p^{\#}$ = 0.04 except for highly asymmetric blocks. For, x_B of 0.125 and 0.875, $U_p^{\#}$ = 0.06 and 0.08, respectively. From the above data, it appears that with the increase of block asymmetry, microphase separation takes place at a relatively lower temperature (viz., higher U_p). The above observation in line with poly(L-lactide)-*block*-poly(ε-caprolactone) diblock copolymer which exhibits microphase separation temperature (measured in terms of T_{ODT}) at 175 and 220°C for the sample having 37.4 and 46 wt% PCL block, respectively [46, 47]. Semi crystalline diblock copolymer with 0.25, 0.49, 0.75 wt% of ethylene shows T_{ODT} at 273, 121, 148°C respectively [25]. The snapshots of

phase separated melt morphology for all block compositions (x_B) at their respective microphase separation points are presented in Figure 6.3, where blue line represents A-block and orange line represents B-block, respectively.

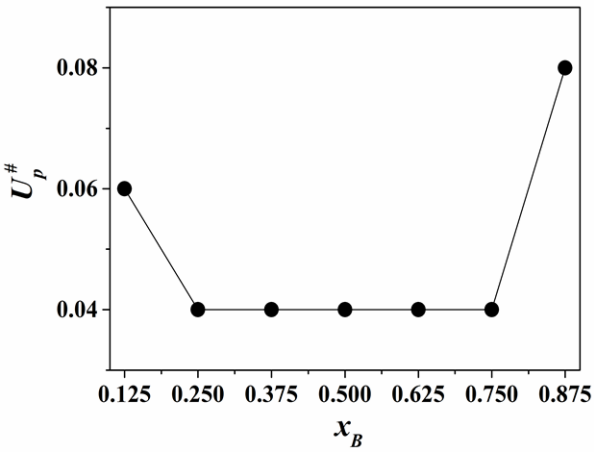

Figure 6.2 Change in microphase separation point ($U_p^{\#}$) with block composition (x_B).

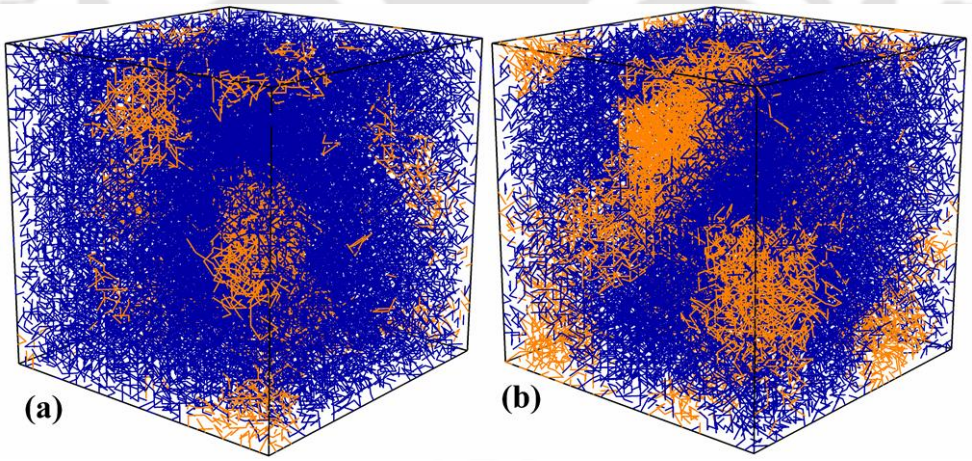

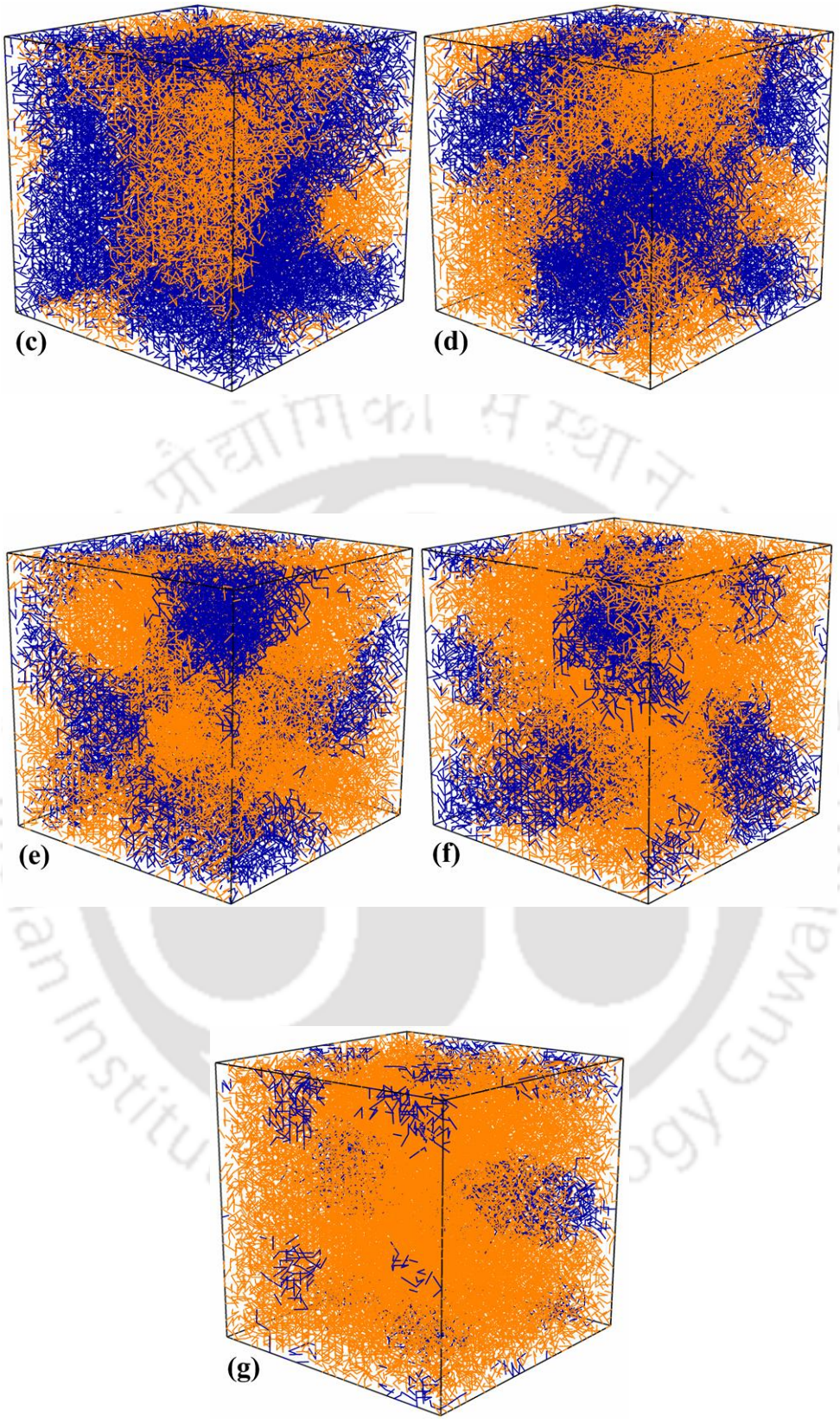

Figure 6.3 Snapshots of microphase separated melt for (a) x_B = 0.125, (b) x_B = 0.25, (c) x_B = 0.375, (d) x_B = 0.50, (e) x_B = 0.625, (f) x_B = 0.75 and (g) x_B = 0.875. Blue and orange line represents segments of A- and B-block respectively.

To generate phase separated melt, first we simulate our system for 10^4 *MCS* , out of which 5000 *MCS* is needed to equilibrate the system which is evident from R_g vs. *MCS* trend (Figure 6.4). Then we anneal the melt morphology for 10^6 *MCS* for all the compositions at their respective $U_p^{\#}$, to allow the chain molecules to relax further, disentangled and generate a better phase separated melt microstructure. The annealed temperature is much higher than the respective melting points. The similar process has been followed in semi crystalline diblock copolymer of polyethylene-*block*-atactic polypropylene where the samples are annealed at 150°C for one day before quenching in liquid nitrogen [33]. Similarly, in polyethylene oxide-*block*-polystyrene copolymer, the sample is annealed at 95°C for 12hours after solvent evaporation to ensure consistency of phase behavior [21]. Asymmetric diblock copolymer of polyethylene oxide-*block*-poly(1,4-butadiene) is first annealed at 80°C for 5 minutes before cooling to room temperature [34]. The snapshots of annealed melt morphology for various block compositions (x_B) are given in Figure 6.5, where blue line represents A-block and orange line represents B-block, respectively.

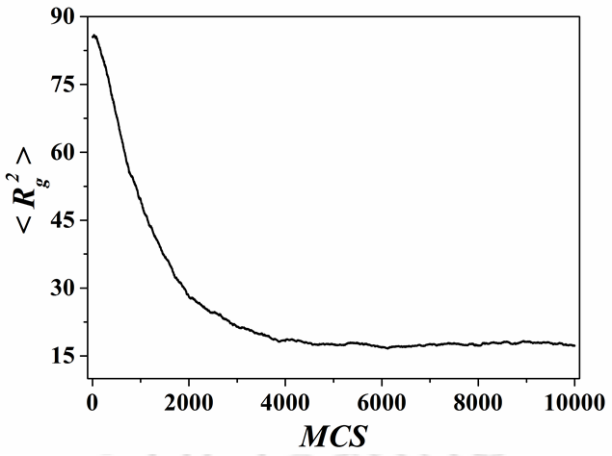

Figure 6.4 Change in mean square radius of gyration $\langle R_g^2 \rangle$ with Monte Carlo Steps at U_p = 0 for x_B = 0.50. There is no appreciable change in the value of $\langle R_g^2 \rangle$ beyond 5000 MCS and it is considered as the equilibration time.

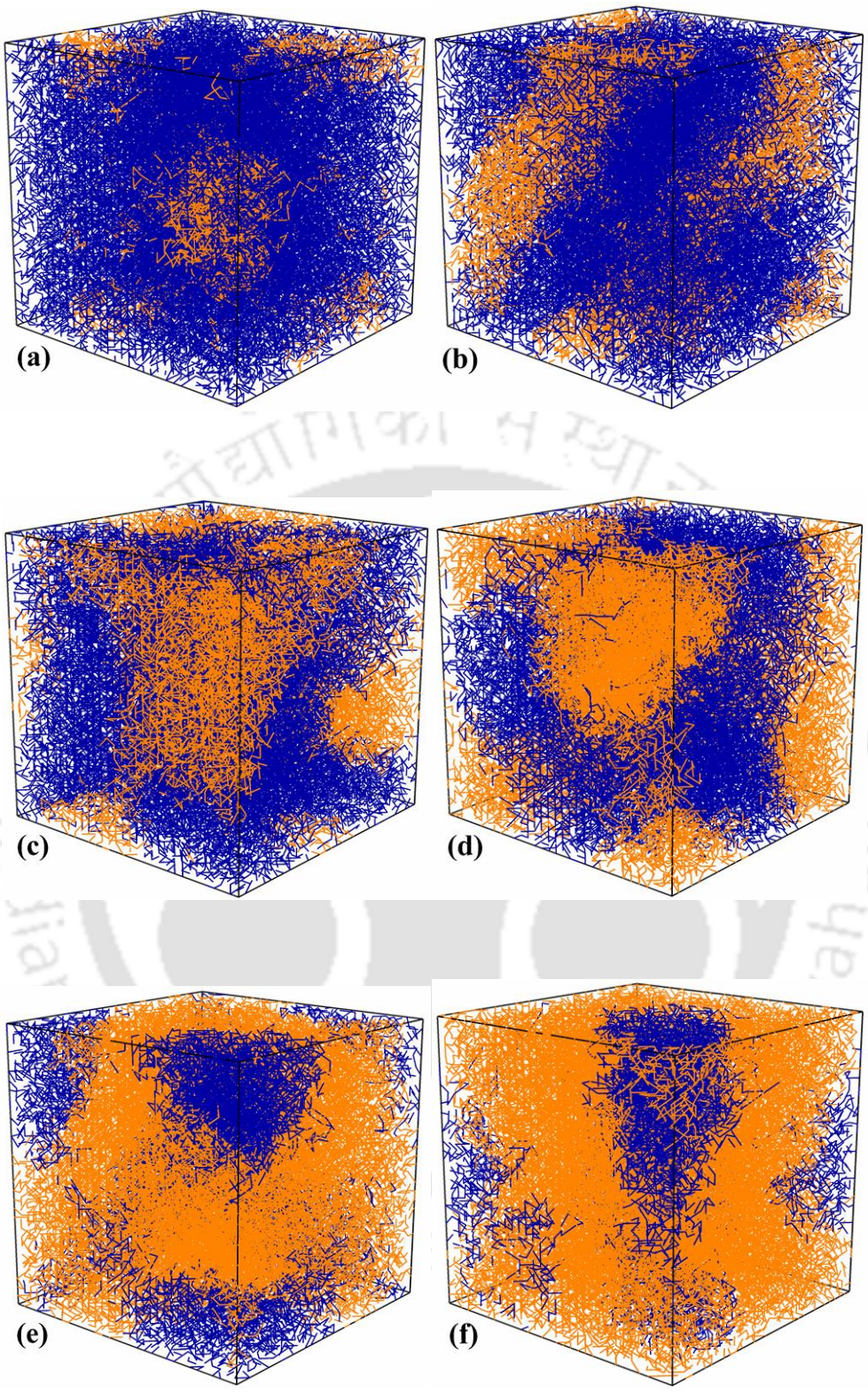

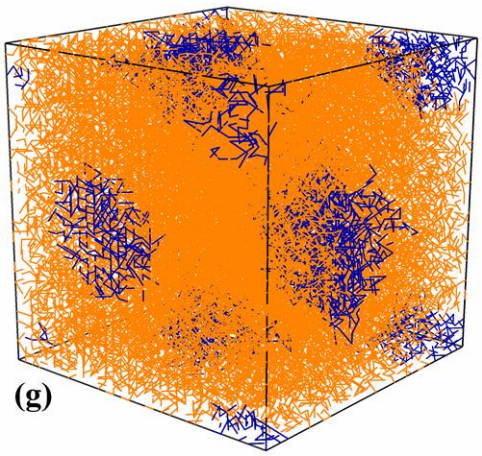

Figure 6.5 Snapshots of microphase separated annealed melt for (a) x_B = 0.125, (b) x_B = 0.25, (c) x_B = 0.375, (d) x_B = 0.50, (e) x_B = 0.625, (f) x_B = 0.75 and (g) x_B = 0.875.

6.2.2 Non-isothermal Crystallization

6.2.2.1 Development of Crystallinity

After generation of high temperature melt, we cool our sample system from the respective microphase separation point ($U_p^{\#}$) to U_p = 0.6 with a step size of 0.02 to implement the cooling process of non-isothermal crystallization. For block composition (x_B) of 0.125, we start simulation from U_p = 0.06 and for block composition (x_B) of 0.875, we start simulation from U_p = 0.08. For rest of the compositions, we start our simulation from U_p = 0.04 to simulate crystallization of diblock copolymer from microphase separated melt. We monitor crystallization by calculating overall crystallinity of diblock copolymer originated from microphase separated melt without annealing as well as with annealing. Overall crystallinity (X_c) is calculated as the weighted average of the summation of A-block (X_A) and B-block (X_B). The change in overall crystallinity (X_c) with U_p introduced by microphase separated melt without annealing and with annealing is available in Figure 6.6. In Figure 6.6, there is an abrupt increment of crystallinity at a certain value of U_p and after that there is no appreciable change in crystallinity (cf., saturation crystallinity, X^{sat}). The comparison in saturation crystallinity (X^{sat}) of both the blocks induced from two different

microphase separated melts with block compositions is given in Table 6.1. There is no significant difference in saturation crystallinity (X_A^{sat} and X_B^{sat}) between microphase separated melt without annealing and with annealing. This happens because the development of crystallinity is primarily driven by the degree of cooling (ΔT). For both type of melts, we use almost the same degree of cooling to implement non-isothermal crystallization. As we crystallize each composition within almost same of degree of cooling, the crystallization driving force in each composition is equal, resulting in the development of comparable crystallinity for all the compositions. However, the saturation crystallinity of B-block (X_B^{sat}) shows an increasing trend with increasing block composition (x_B). The enhanced number of B-units at higher x_B facilitates in producing crystalline materials with higher crystallinity. This observation is in accord with the experimental results on the crystallization of poly(ε-caprolactone)-*block*-polyethylene copolymers, wherein the crystallinity of PE blocks increases with an increment of PE content in PCL-*b*-PE diblock copolymer [41]. In order to follow the orientation of crystalline bonds with respect to Z-axis, we calculate bond order parameter (*P*) of individual blocks over all compositions. Figure 6.7 represents the change in bond orientation of individual blocks for different block compositions viz., (x_B = 0.25, 0.50 and 0.75) from microphase separated melt with and without annealing. From the above figures, it is evident that, annealed melt induces change in orientation of A-block compared to microphase separated melt without annealing; whereas there is no appreciable change in B-block during annealing. It happens because microphase separated melt (without annealing) induces morphological perturbation during non-isothermal crystallization. Therefore, the rearrangement of crystalline bonds is possible and it gives perpendicular orientation with respect to the Z-axis. However, annealed melt retains the melt morphology set during the annealing, no appreciable rearrangement of crystalline bonds is observed, and the orientation becomes parallel to the Z-axis. The confinement induced by crystallization of A-block makes B-block less facile for the re-arrangement of crystalline bonds.

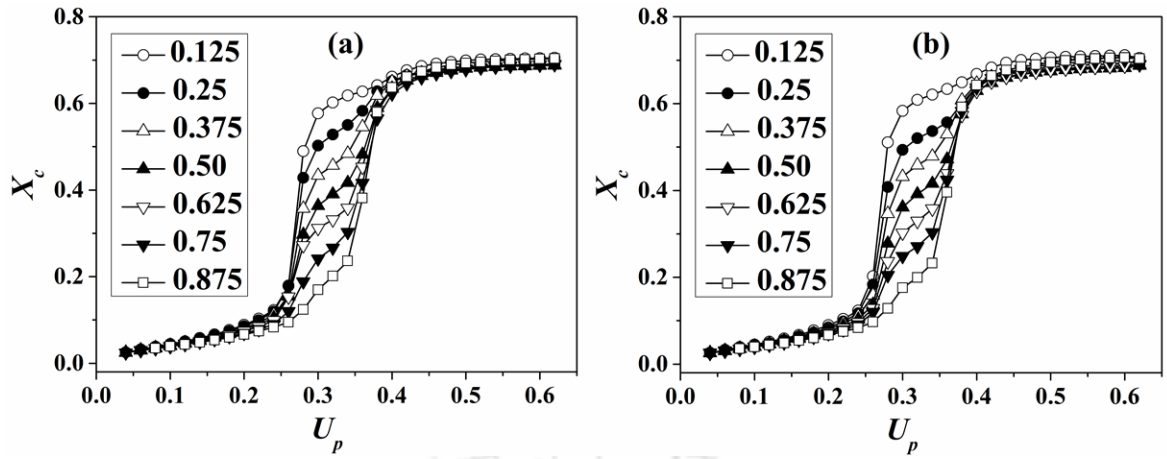

Figure 6.6 Change in overall crystallinity (X_c) with U_p for different x_B induced from microphase separated melt (a) without annealing and (b) with annealing.

Table 6.1 Comparison in saturation crystallinity (X^{sat}) at U_p = 0.6 induced from microphase separated melt without annealing and with annealing.

x_B	A-Block		B-block	
	Without	With	Without	With
0.125	0.72	0.72	0.60	0.61
0.25	0.71	0.70	0.64	0.63
0.375	0.71	0.71	0.66	0.65
0.50	0.70	0.71	0.67	0.65
0.625	0.70	0.71	0.67	0.67
0.75	0.70	0.71	0.68	0.69
0.875	0.72	0.70	0.70	0.70

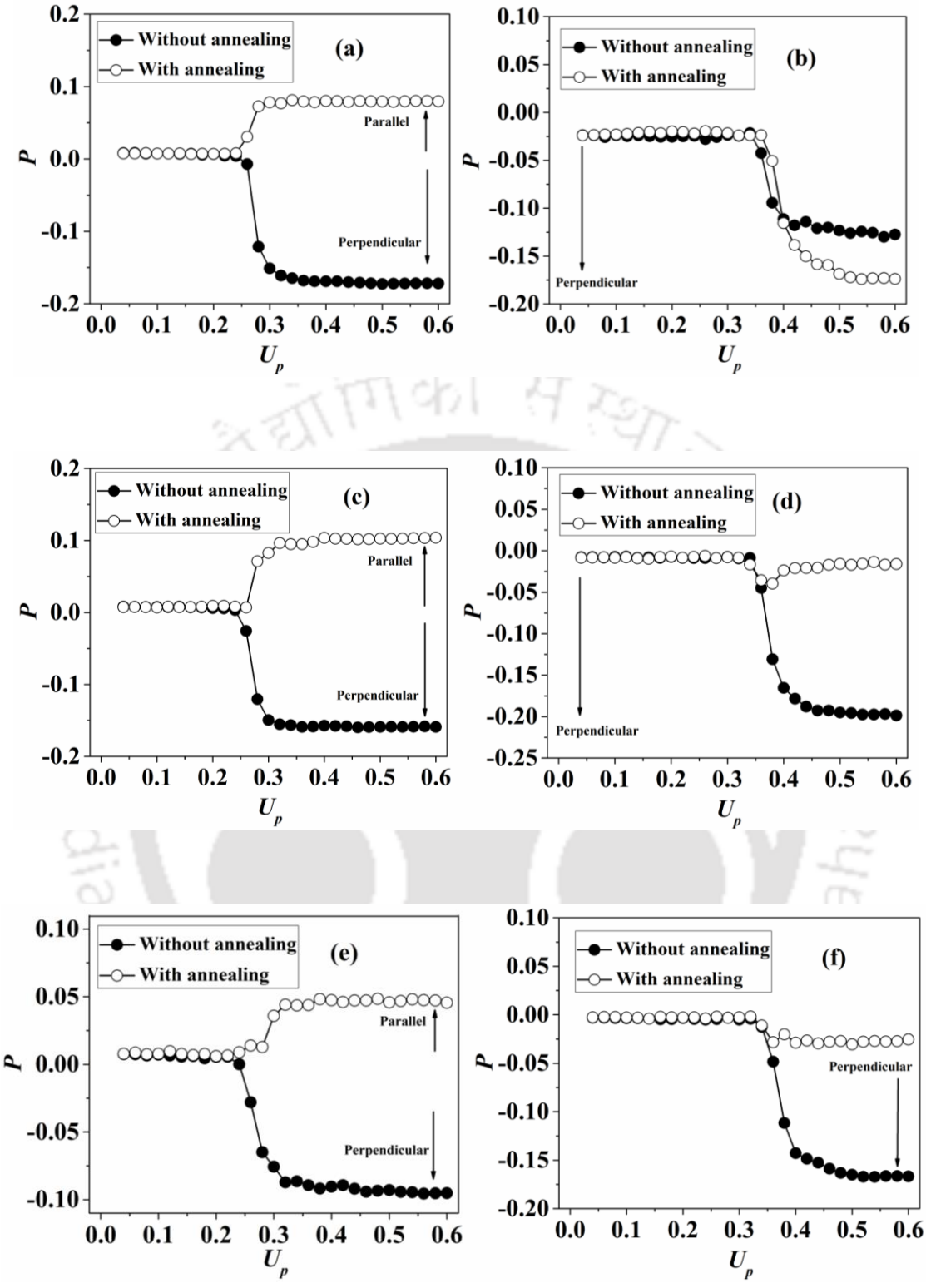

Figure 6.7 Change in bond orientation parameter (P) with U_P for (a) A-block of x_B = 0.25, (b) B-block of x_B = 0.25, (c) A-block of x_B = 0.50, (d) B-block of x_B = 0.50, (e) A-block of x_B = 0.75 and (f) B-block of x_B = 0.75 crystallized from microphase separated melt without and with annealing.

6.2.2.2 Morphological Evolution

We calculate the average lamellar thickness $\langle l \rangle$ separately for both the blocks as a function of U_p for all compositions (x_B). Figure 6.8 and 6.9 represent the variation of $\langle l \rangle$ as a function of U_p induced from microphase separated melt without annealing and with annealing, respectively. The trend of $\langle l \rangle$ vs. U_p is similar to the crystallinity behaviour (Figure 6.6). With the increase of U_p, the lamellar thickness increases to saturation value and after that there is no substantial change. We compare the saturation value of lamellar thickness $\langle l \rangle$ for both the blocks at U_p = 0.6 induced from microphase separated melt without annealing and with annealing in Table 6.2. There is no remarkable difference in the value of lamellar thickness between the two different melt systems (viz., with and without annealing) as we have seen in crystallinity trends. However, the lamellar thickness, $\langle l \rangle$ of both the blocks shows an unusual behavior with block composition (x_B). Lamellar thickness of A-block $\langle l_A \rangle$ remains almost similar (~3.1) up to block x_B = 0.5, due to the confinement effect induced by microphase separated melt microdomains ensuing thinner crystals within the system. The magnitude of $\langle l_A \rangle$ shows a steep increase with increasing x_B beyond 0.50. This increase in value of $\langle l_A \rangle$ at higher value of x_B (viz., lower value of x_A) is attributed to the dilution effect exhibited by B block. At higher value of x_B, B-block acts like a solvent, diminishing topological restriction, for the crystallization of A-block, producing thicker crystals [45]. On the other hand, the lamellar thickness of B-block, $\langle l_B \rangle$ does not change effectively with block composition (x_B) due to confinement created by phase separated melt.

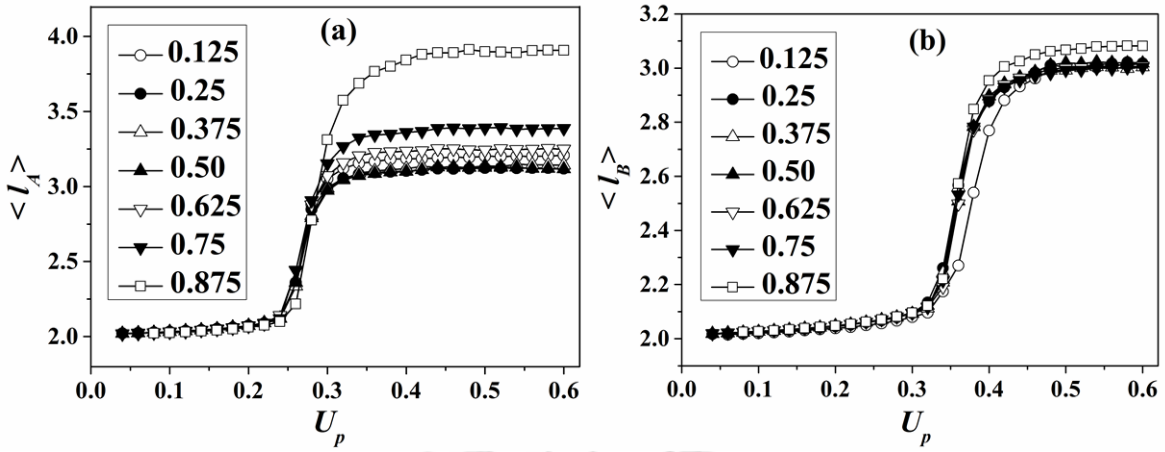

Figure 6.8 Change in average lamellar thickness of (a) A-block $\langle l_A \rangle$ and (b) B-block $\langle l_B \rangle$ with U_p for different x_B induced from microphase separated melt without annealing.

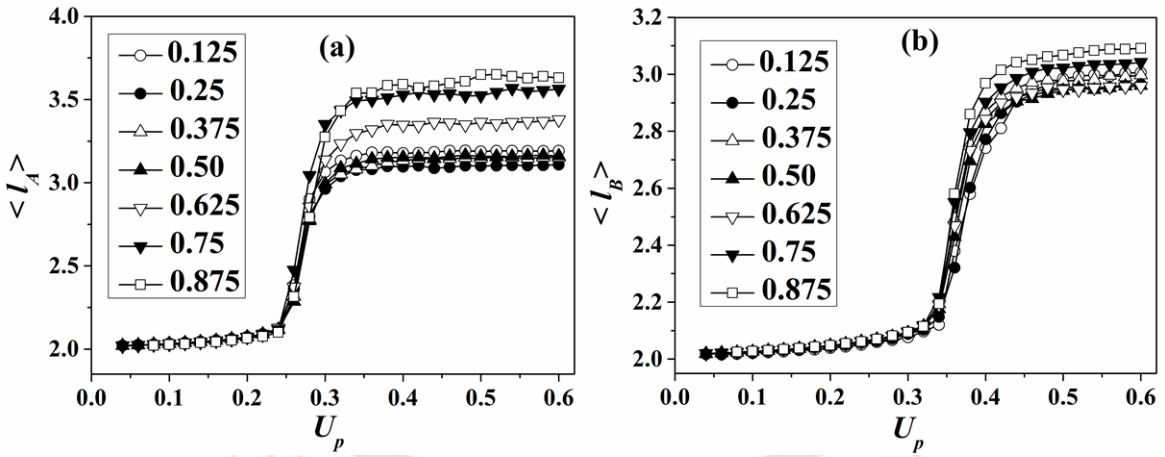

Figure 6.9 Change in average lamellar thickness of (a) A-block $\langle l_A \rangle$ and (b) B-block $\langle l_B \rangle$ with U_p for different x_B induced from microphase separated annealed melt.

Table 6.2 Comparison in lamellar thickness $\langle l \rangle$ at U_p = 0.6 induced from microphase separated melt without annealing and with annealing.

x_B	A-Block		B-block	
	Without	With	Without	With
0.125	3.20	3.19	3.01	3.00
0.25	3.11	3.10	3.01	2.96
0.375	3.14	3.15	3.00	2.99
0.50	3.11	3.16	3.01	2.96
0.625	3.24	3.37	3.00	2.96
0.75	3.38	3.56	3.00	3.04
0.875	3.90	3.62	3.08	3.09

6.2.2.3 Calculation of Radius of Gyration

We calculate the change in mean square radius of gyration $\langle R_g^2 \rangle$ with U_p for all the block compositions investigated in both the systems (viz., without and with annealing). Figure 6.10 shows the change in $\langle R_g^2 \rangle$ with U_p for all the block compositions. It is clearly visible from the figures that the system induced from phase separated melt without annealing gives appreciable change in $\langle R_g^2 \rangle$ value compared to the system induced from an annealed melt. When we anneal our microphase separated system for long enough time ($1\text{x}10^6$ *MCS*), it yields a more relaxed structure with relatively larger microdomains. Therefore, the change in $\langle R_g^2 \rangle$ is negligible in crystals introduced by annealed melt compared to that of without annealing. By definition, the square radius of gyration is the average squared distance of any point from its center of mass. This is an important parameter to understand morphological evolution. Therefore, we found a significant change in the value of the radius of gyration from microphase separated melt without annealing during crystallization which triggers morphological perturbation (Figure 6.12). On the other side, for the annealed melt there is no

significant change in the value of radius of gyration which leads to unperturbed morphology (Figure 6.13). We also calculate the ratio of $\left\langle R_g^2 \right\rangle$ without annealing and with annealing, $\left\langle R_g^2 \right\rangle_{without} / \left\langle R_g^2 \right\rangle_{with}$ for all the block compositions (x_B) in Figure 6.11. Figure 6.11 clearly demonstrates that the change in $\left\langle R_g^2 \right\rangle_{without} / \left\langle R_g^2 \right\rangle_{with}$ is relatively less in highly asymmetric diblock copolymer (viz., x_B = 0.125 and 0.875) compared to the rest of the compositions. Figure 6.12 displays the snapshots of semi-crystalline structure (at U_p = 0.6) for x_B = 0.125, 0.25, 0.375, 0.50, 0.625, 0.75 and 0.875, crystallized from microphase melt without annealing, where blue lines represent crystalline bonds of A-block, orange lines represent crystalline bonds of B-block and yellow lines represent non-crystalline bonds of both the blocks. We observe a morphological perturbation of phase separated melt during crystallization over all the compositions except highly asymmetric diblock copolymer (x_B = 0.125 and 0.875). This happens because microphase separated melt without annealing is associated with more intra- and inter-chain entanglement, and relatively less relaxed structure, which produces melt microdomain that can be modified during non-isothermal crystallization. Due to the above reason, we also observe a significant increase in the value of radius of gyration which triggers morphological perturbation. On the other hand, the morphology of microphase separated melt with annealing remains almost unperturbed during crystallization. Annealing of microphase separated melt develops microdomains within melt morphology, which are less facile to be modified upon crystallization, irrespective of the block compositions. There is no appreciable change in the radius of gyration which triggers unperturbed morphology upon crystallization. The snapshots of semi-crystalline structure crystallized from annealed melt for x_B = 0.125, 0.25, 0.375, 0.50, 0.625, 0.75 and 0.875 are shown in Figure 6.13 where blue lines represent crystalline bonds of A-block, orange lines represent crystalline bonds of B-block and yellow lines represent non-crystalline bonds of both the blocks.

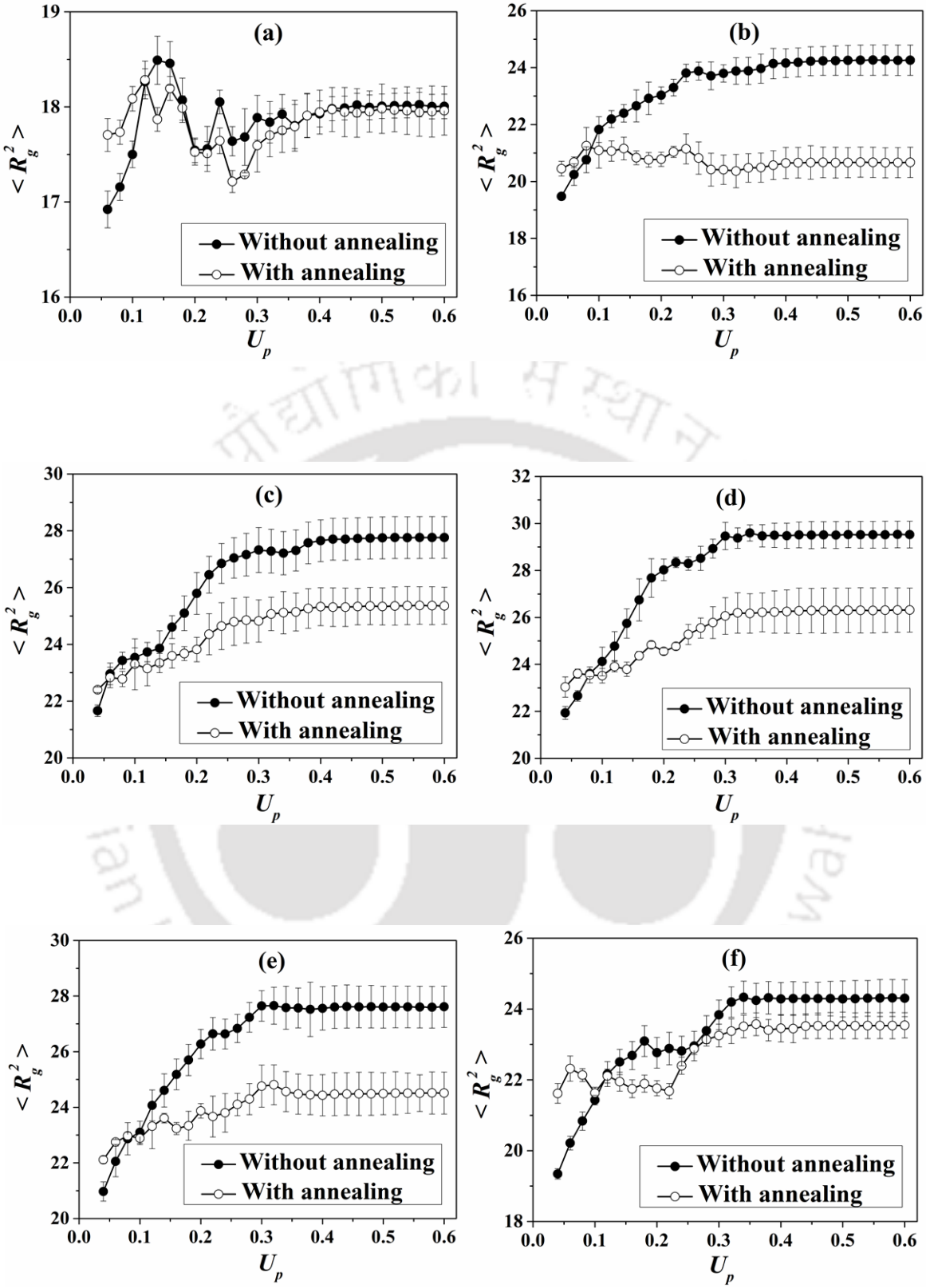

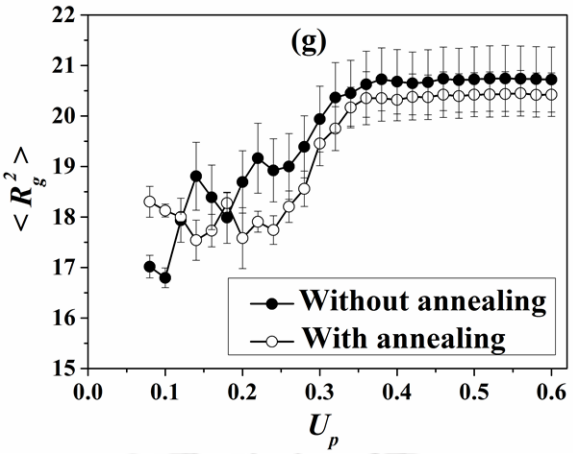

Figure 6.10 Change in mean square radius of gyration $\langle R_g^2 \rangle$ with U_p of (a) x_B = 0.125, (b) x_B = 0.25, (c) x_B = 0.375, (d) x_B = 0.50, (e) x_B = 0.625, (f) x_B = 0.75 and (g) x_B = 0.875 induced from microphase separated melt.

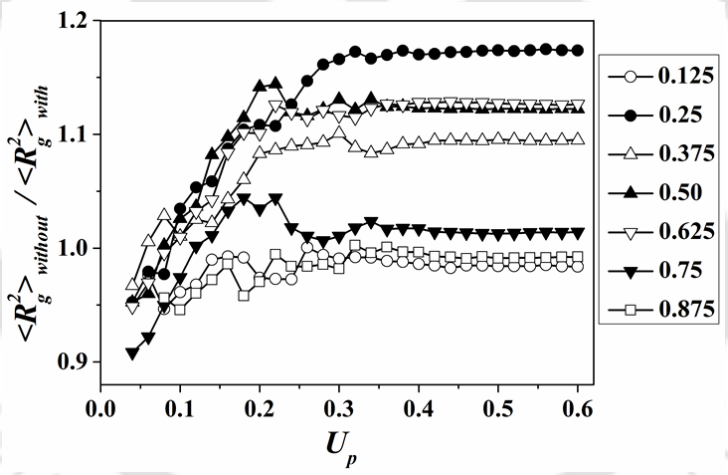

Figure 6.11 Change in $\langle R_g^2 \rangle_{without} / \langle R_g^2 \rangle_{with}$ in respect to U_p of diblock copolymer induced from microphase separated melt without annealing and with annealing.

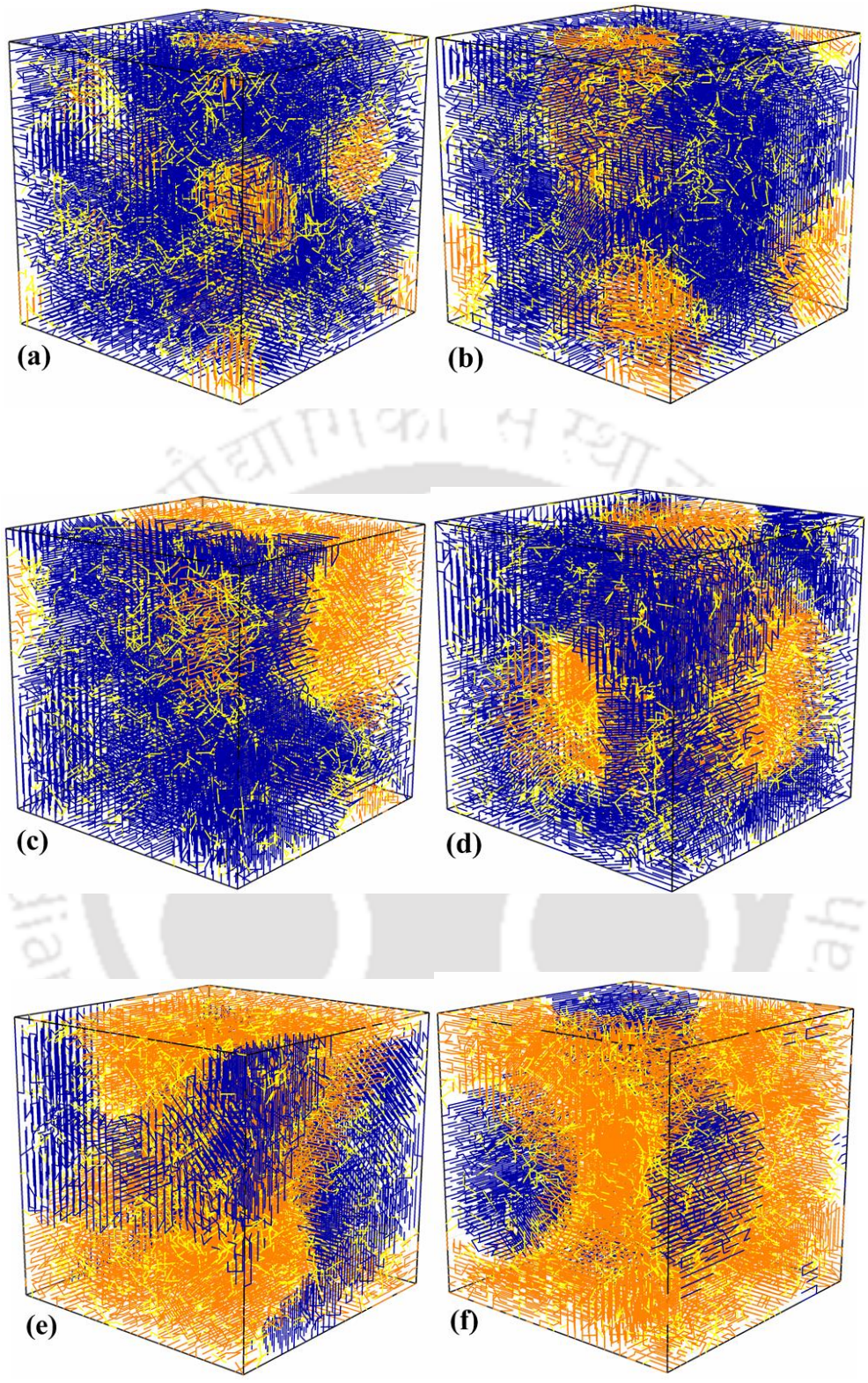

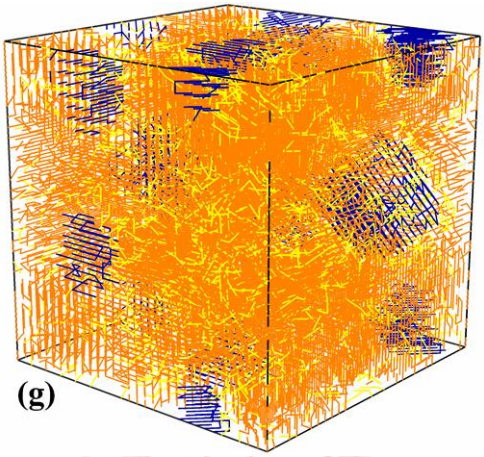

Figure 6.12 Snapshots of semi crystalline structures of diblock copolymer at U_p = 0.6 for (a) x_B = 0.125, (b) x_B = 0.25, (c) x_B = 0.375, (d) x_B = 0.50, (e) x_B = 0.625, (f) x_B = 0.75 and (g) x_B = 0.875 induced from microphase separated melt without annealing.

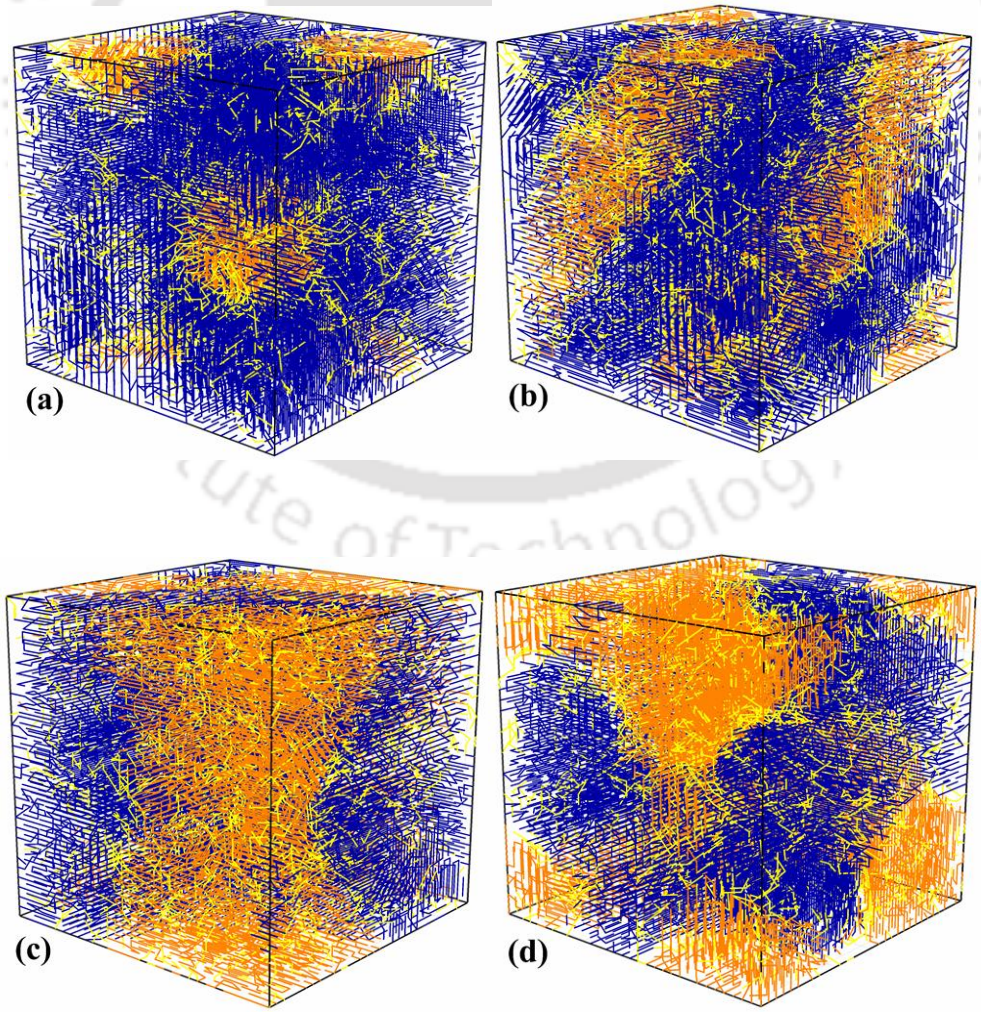

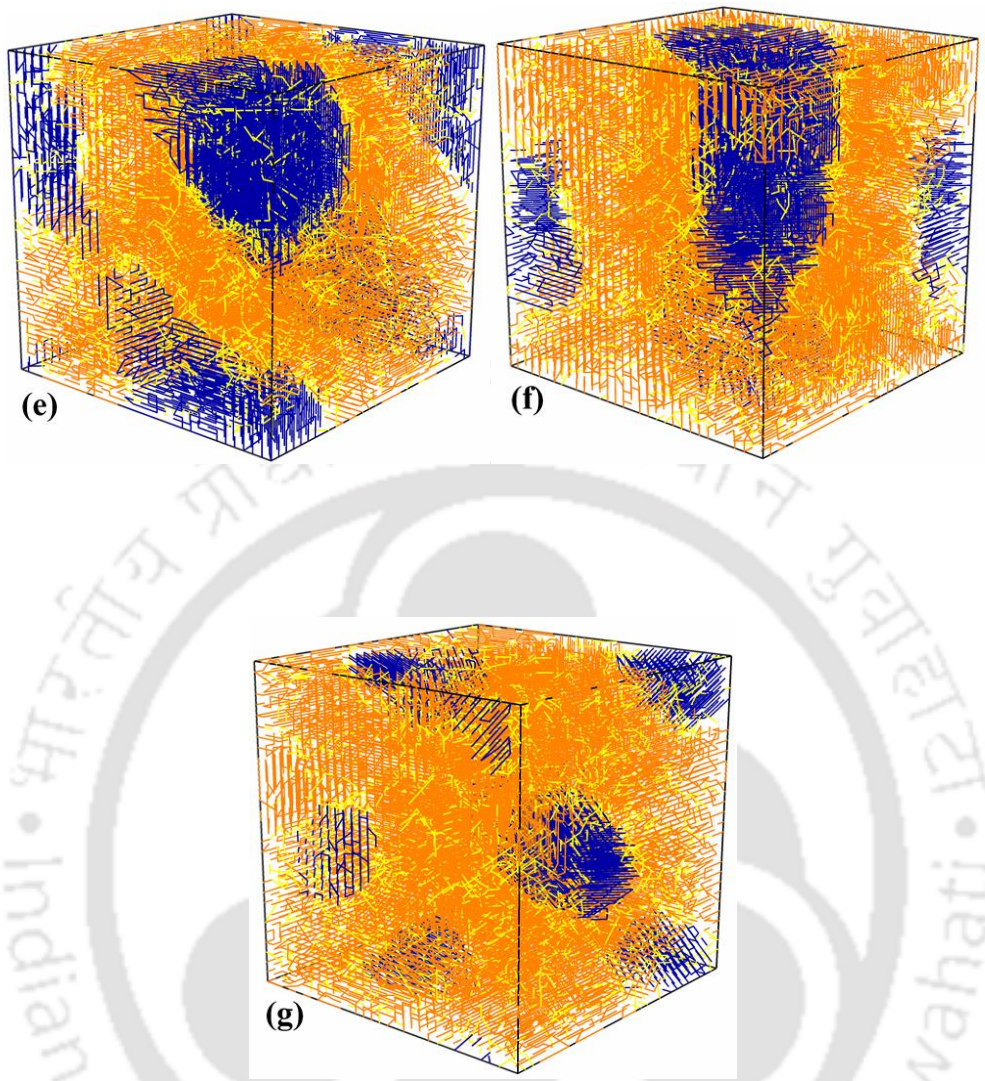

Figure 6.13 Snapshots of semi crystalline structures of diblock copolymer at U_p = 0.6 for (a) x_B = 0.125, (b) x_B = 0.25, (c) x_B = 0.375, (d) x_B = 0.50, (e) x_B = 0.625, (f) x_B = 0.75 and (c) x_B = 0.875 induced from microphase separated annealed melt.

6.2.3 Isothermal Crystallization

6.2.3.1 One-step Cooling

To implement isothermal crystallization, we quench our sample from the respective microphase separation point, $U_p^{\#}$ (see Figure 6.2) to U_p = 0.6 directly and annealed for 10^5 *MCS*. We observe the development of overall crystallinity (Figure 6.14) with *MCS* crystallized from microphase separated melt without annealing and with annealing, for all the compositions. We also calculate scaled crystallinity, $X_c^* = (X_c - X_{ci})/(X_{cf} - X_{ci})$, ranges from 0 to 1 for individual blocks with *MCS*. Figure 6.15 and 6.16 represent the scaled crystallinity (X_c^*) of individual blocks of diblock copolymer crystallized from microphase separated melt without annealing and with annealing, respectively. Isothermal crystallization reveals that the transition kinetics follows different pathways for different block compositions in the diblock copolymer. As the crystallization driving force for isothermal crystallization (viz., U_p = 0.6) is sufficient to introduce crystallinity for both the blocks, the mode of crystallization is coincident crystallization where both the blocks crystallize simultaneously. The above observation is in accord with the isothermal crystallization of poly(ρ-dioxanone)-*block*-poly(ε-caprolactone) diblock copolymer, where the crystallization kinetics of both the blocks are overlapping [3].

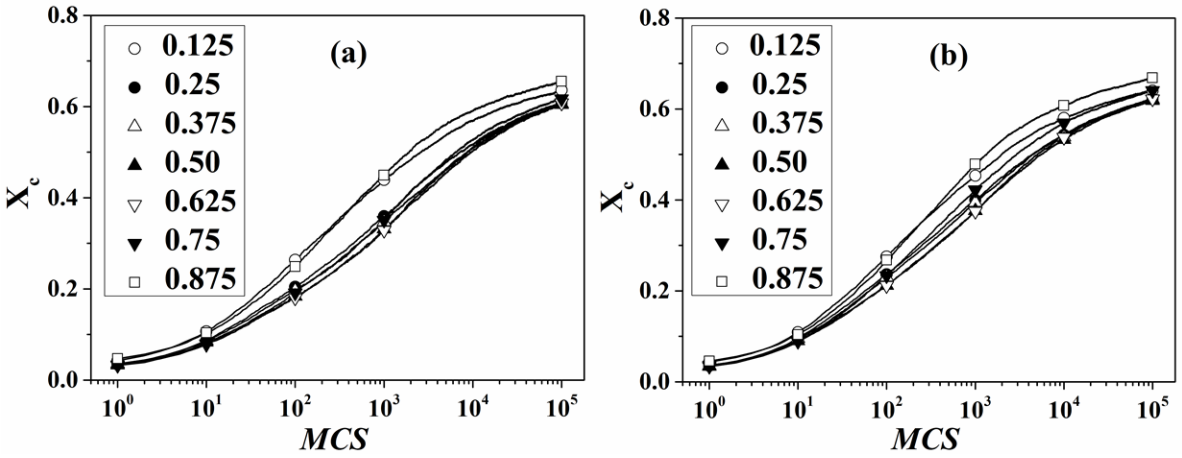

Figure 6.14 Change in overall crystallinity (X_c) with Monte Carlo Steps (*MCS*) at U_p = 0.6 for diblock copolymer introduced by microphase separate melt (a) without annealing and (b) with annealing during one-step isothermal crystallization.

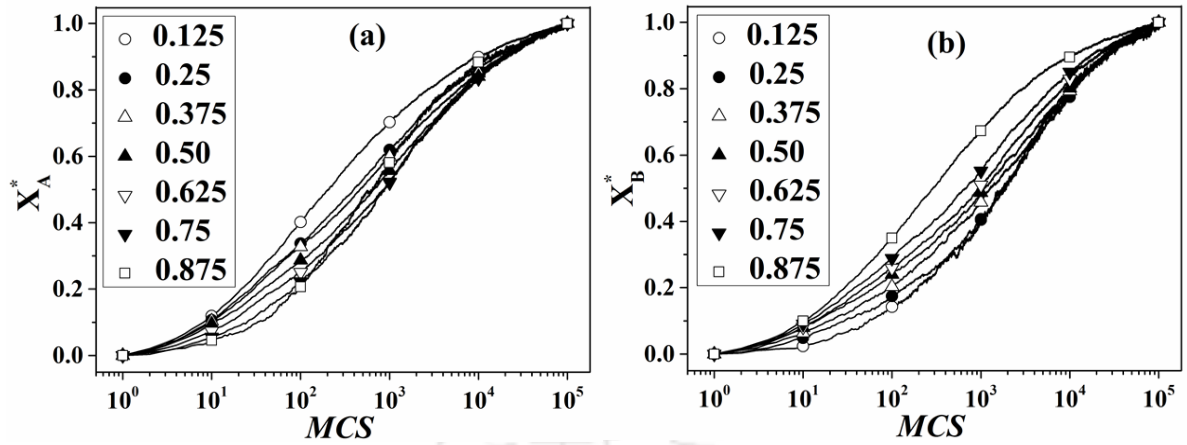

Figure 6.15 Change in scaled crystallinity (X_c^*) with Monte Carlo Steps (MCS) at U_p = 0.6 for (a) A-block and (b) B-block introduced by microphase separate melt without annealing during one-step isothermal crystallization.

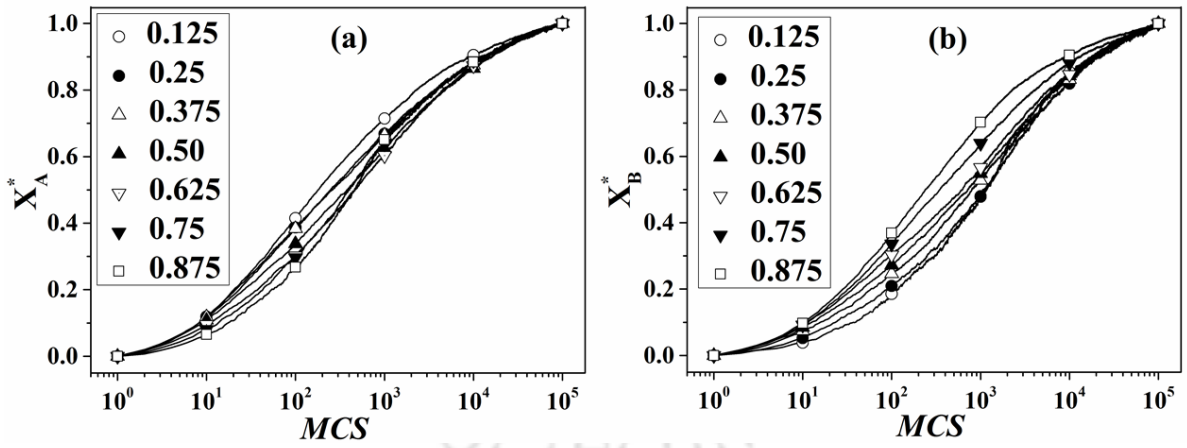

Figure 6.16 Change in scaled crystallinity (X_c^*) with Monte Carlo Steps (MCS) at U_p = 0.6 for (a) A-block and (b) B-block introduced by microphase separate annealed melt during one-step isothermal crystallization.

We compare the change in mean square radius of gyration, $\langle R_g^2 \rangle$ with MCS for diblock copolymer introduced by microphase separated melt without annealing and with annealing in Figure 6.17. There is no substantial change in the value of $\langle R_g^2 \rangle$ with *MCS* in both the melt systems, but the magnitude of $\langle R_g^2 \rangle$ of microphase separated annealed melt is higher than microphase separated melt without annealing. The morphology set during the microphase separation and subsequent annealing remains unperturbed upon isothermal crystallization. In non-isothermal crystallization, which follows a step-wise cooling method, allow the chain segments to change conformational pattern, and we have observed a gradual increase in $\langle R_g^2 \rangle$ upon cooling of the sample without annealing (Figure 6.10). However, in isothermal crystallization, wherein the sample is directly quenched to U_p = 0.6 from U_p = 0, the conformational change is restricted due to the onset of crystallization. We plot the saturation value of radius gyration at U_p = 0.6 for all the block compositions in Figure 6.18. The value of $\langle R_g^2 \rangle$ of microphase separated annealed melt is higher compared to microphase melt without annealing for most of the block compositions except highly asymmetric block. The non-monotonic trend in $\langle R_g^2 \rangle$ with composition is attributed to the block asymmetry present in the system. Figure 6.19 exhibits the snapshots of final crystal structure (viz., at U_p = 0.6) of diblock copolymer, isothermally crystallized from microphase melt without annealing. Similarly, Figure 6.20 displays the snapshots of the semi crystalline structure of diblock copolymers developed during isothermal crystallization from microphase separated annealed melt. The snapshots clearly indicate that the molecular arrangement of phase separated melt morphology is almost unperturbed during isothermal crystallization, wherein the development of crystallinity is fast enough to restrict a morphological rearrangement (viz., perturbation). Finally, isothermal crystallization preserves microphase separated melt morphology intact. The above observation in accord with the semi crystalline diblock copolymer of polyethylene-*block*-atactic polypropylene where rapid quenching preserves melt morphology introduced by the microphase separated block copolymer [33].

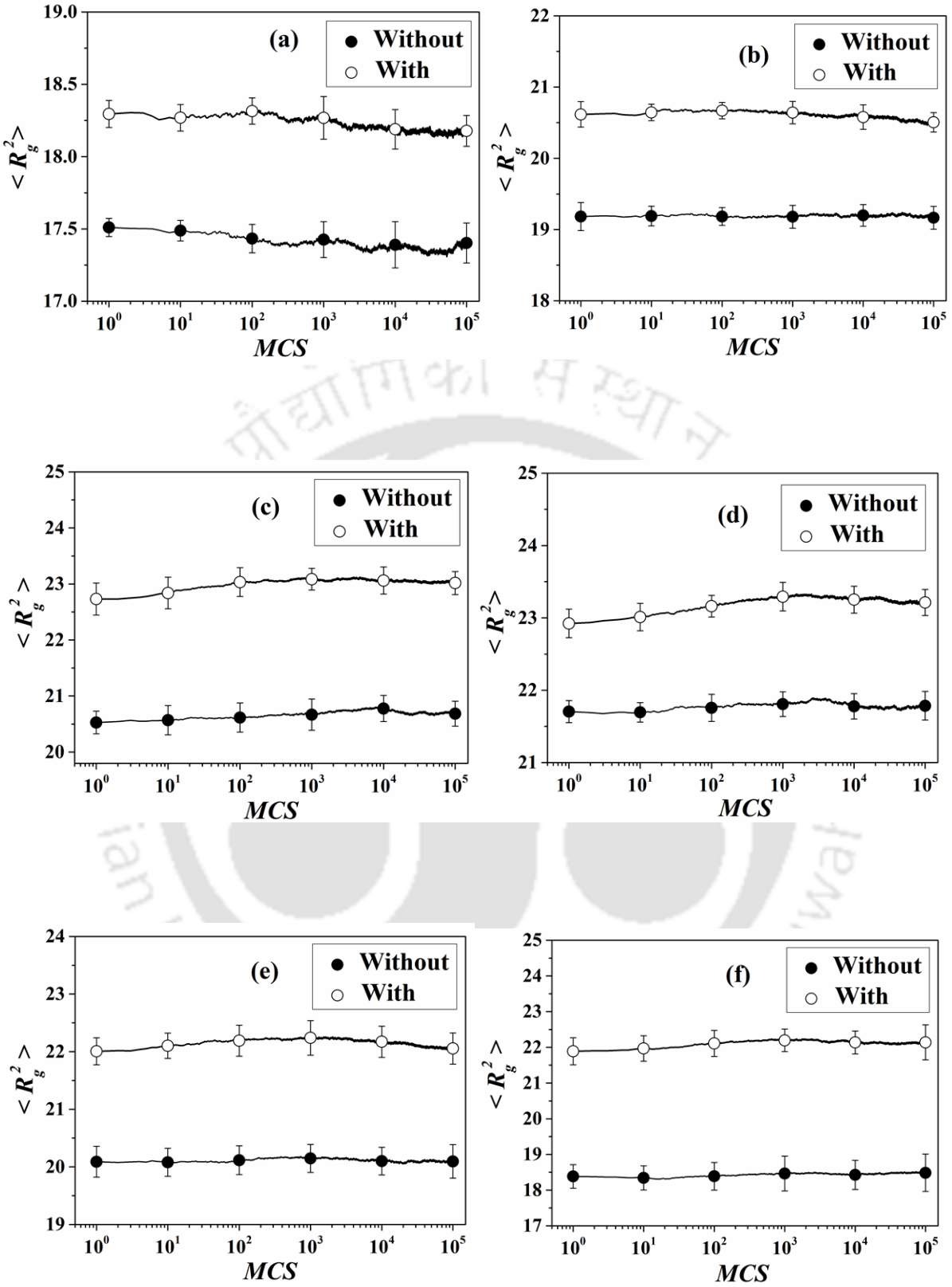

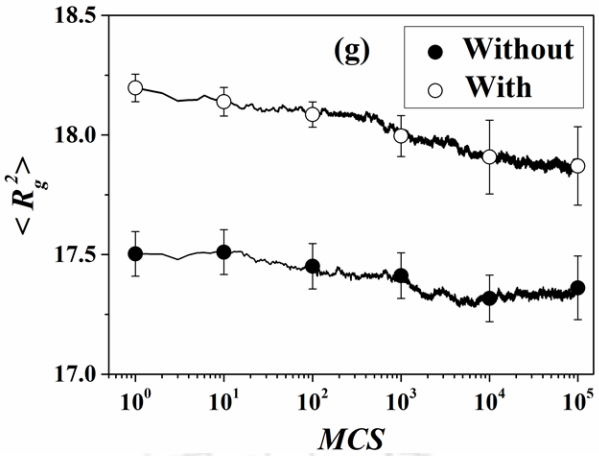

Figure 6.17 Change in mean square radius of gyration $\langle R_g^2 \rangle$ with MCS at U_p = 0.6 for (a) x_B = 0.125, (b) x_B = 0.25, (c) x_B = 0.375, (d) x_B = 0.50, (e) x_B = 0.625, (f) x_B = 0.75 and (g) x_B = 0.875 from microphase separated melt without and with annealing.

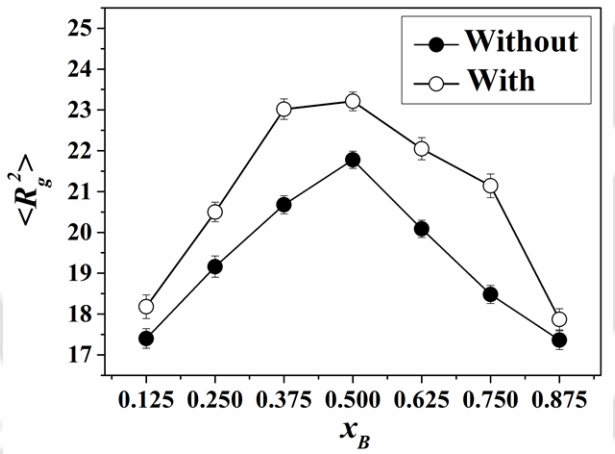

Figure 6.18 Change in mean square displacement $\langle R_g^2 \rangle$ with x_B at U_p = 0.6 of diblock copolymer induced from microphase separated melt without and with annealing.

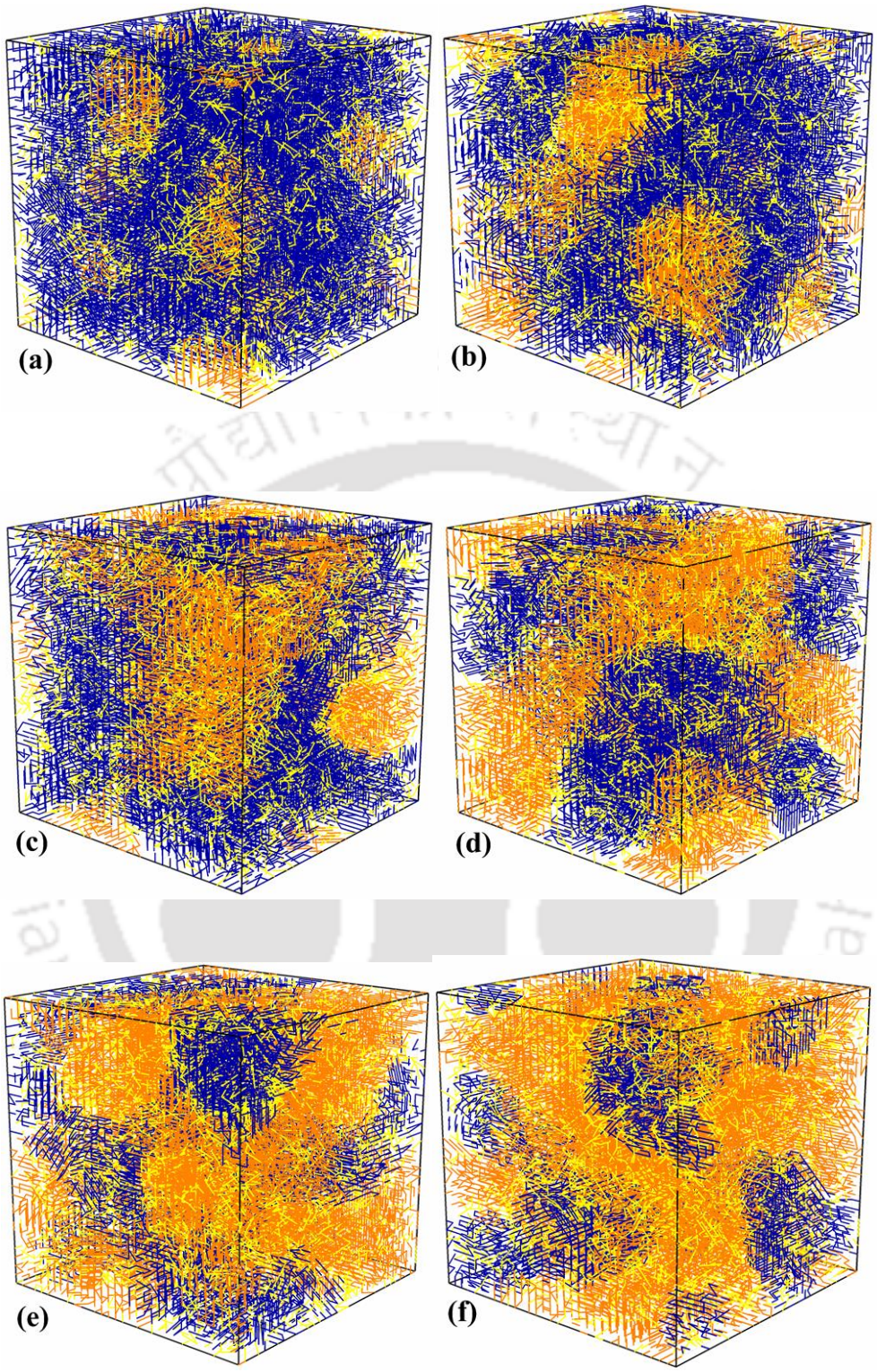

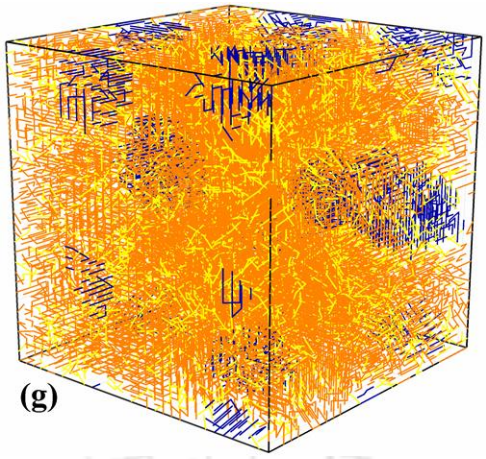

Figure 6.19 Snapshots of semi-crystalline structure of diblock copolymer induced from microphase separated melt without annealing at U_p = 0.6 for (a) x_B = 0.125, (b) x_B = 0.25, (c) x_B = 0.375, (d) x_B = 0.50, (e) x_B = 0.625, (f) x_B = 0.75 and (g) x_B = 0.875. Blue and orange lines represent crystalline bonds of A-block and B-block respectively, and yellow lines represent non-crystalline bonds of both the blocks.

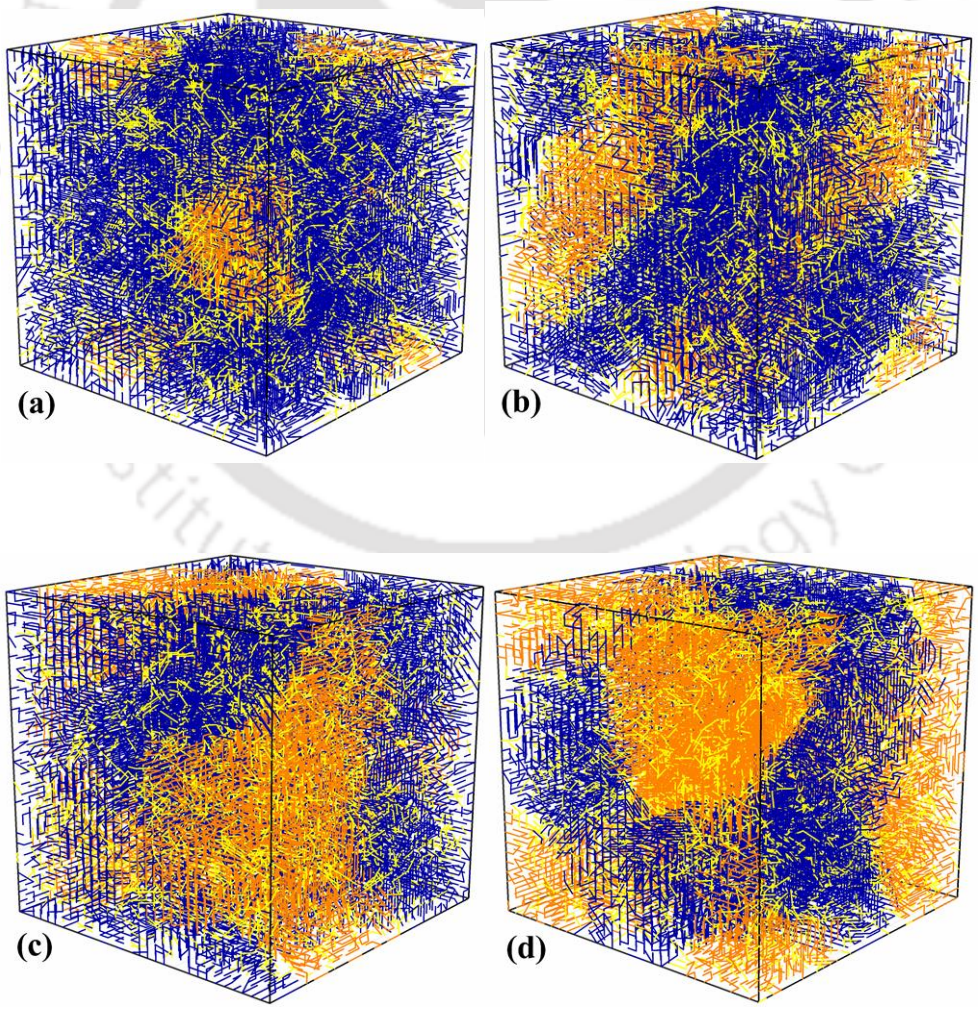

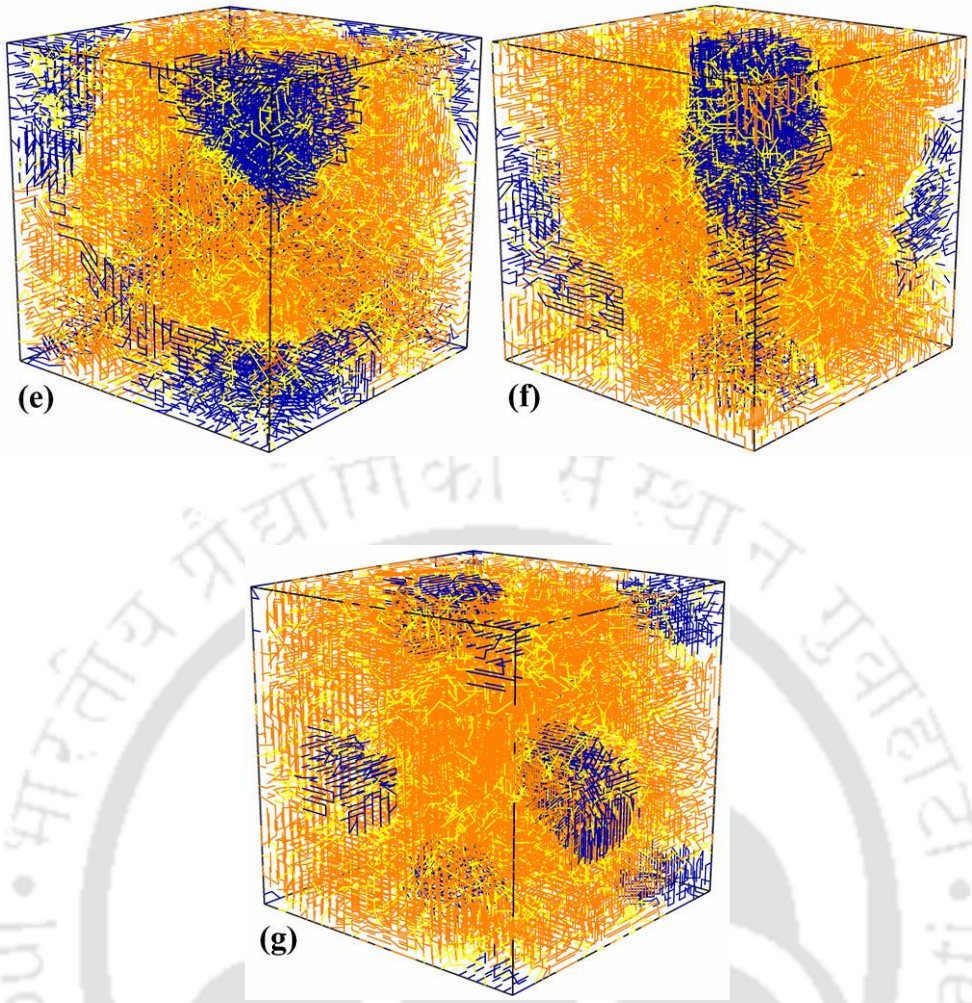

Figure 6.20 Snapshots of semi-crystalline structure of diblock copolymer induced from microphase separated annealed melt at U_p = 0.6 for (a) x_B = 0.125, (b) x_B = 0.25, (c) x_B = 0.375, (d) x_B = 0.50, (e) x_B = 0.625, (f) x_B = 0.75 and (g) x_B = 0.875. Blue and orange lines represent crystalline bonds of A-block and B-block respectively, and yellow lines represent non-crystalline bonds of both the blocks.

Time evolution of crystallinity can be described by Avrami equation [48]:

$$(1 - X_c^*) = \exp(-kt^n)$$

Where X_c^* represents the scaled crystallinity ranges from 0 to 1. We estimate the value of Avrami index (n) for individual blocks based on primary crystallization [49] with block composition (Figure 6.21) which is suggestive about the type of crystal geometry. The value

of Avrami index (n) for both the blocks ranges from 0.5 to 1.1 which indicates the presence of homogeneous nucleation with two dimensional crystal growths. Lower value of Avrami index (n) attributes to the restricted growth under confinement due to microphase separated melt morphology. This result is in line with the partially miscible highly asymmetric poly(L-lactide)-*block*-poly(ε-caprolactone) diblock copolymer, which follows a homogeneous nucleation pathway with Avrami index ~ 1.0 [50]. During isothermal crystallization of PCL block in asymmetric PLLA-*b*-PCL diblock copolymer, PCL block exhibits first order transition kinetics with Avrami Index close to 1.0 [51, 52]. Similarly the crystallization of crystalline-amorphous diblock copolymers where the crystalline block is confined within the microdomain of amorphous block also follows homogeneous nucleation [2, 31, 53] with Avrami index ~ 1.0 [31, 52, 53]. For example, crystallization of polyethylene oxide, confined within the large number of microdomain of polystyrene exhibits homogeneous nucleation [2]. Similarly PLLA block in PLLA-*b*-PS diblock copolymer also follows homogeneous nucleation with Avrami index close to 1.0 [31]. However, the value of Avrami Index (n) is smaller for both the blocks crystallized from microphase melt without annealing compared to that of annealed melt. The system with more relaxed microdomain structure gives a relatively higher value of Avrami Index (n) due to less entanglement effect in the polymer matrix.

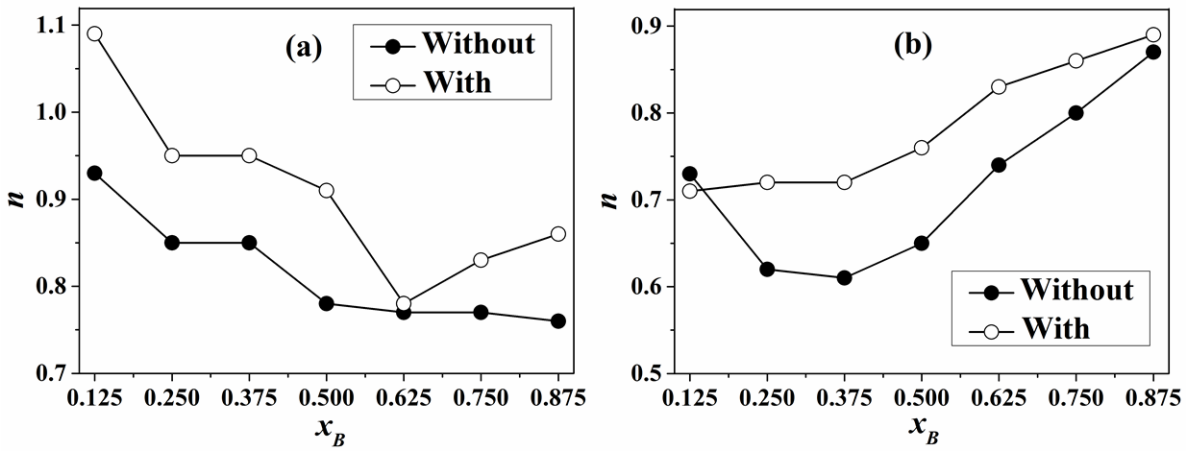

Figure 6.21 Change in Avrami Index (n) of (a) A-block and (b) B-block with x_B induced from microphase separated melt without annealing and with annealing.

We calculate crystallization half-time ($t_{1/2}$) [3] in terms of number of Monte Carlo Steps, to get an approximate idea of the rate of crystallization. We locate the number of *MCS* required to produce a crystallinity, which is 50% of the saturated value (viz., at the end of isothermal crystallization). Table 6.3 displays the value of $t_{1/2}$ for both the blocks, in terms of *MCS* for all compositions of diblock copolymer crystallized from microphase separated melt with and without annealing. From the above table, we observe that annealed melt crystallizes at a relatively faster rate in comparison with the microphase separated melt without annealing. This change in rate with annealing happens due to the presence less entanglement and more relaxed structure of the annealed melt which generates more stable micro domains. On the other hand, microphase separated melt without annealing would need to relax the melt structure over a few more *MCS* before the crystallization. Thus, the rate of crystallization is much faster for annealed melt than melt without annealing.

Table 6.3 Comparison in crystallization half-time ($t_{1/2}$) of A and B-block separately for diblock copolymer induced from microphase separated melt without annealing and with annealing.

x_B	A-Block		B-block	
	Without	With	Without	With
0.125	210	180	1870	1100
0.25	400	250	1770	1165
0.375	470	280	1275	800
0.50	650	380	1100	720
0.625	855	465	935	630
0.75	875	400	550	350
0.875	650	460	290	240

6.2.3.2 Two-step Cooling

We perform two-step isothermal crystallization to examine the effect of quench depth on the crystallization of microphase separated melt. In the first step, we cool the equilibrated system from the respective microphase separation point ($U_p^{\#}$) to U_p = 0.3 and annealed for 10^5 Monte Carlo Steps. In this process, only A-block is crystallized while B-block remains in a molten state. Following this, we quench the system from U_p = 0.3 to U_p = 0.6 and annealed for $10^5 MCS$ to initiate crystallization of B-block. We compare the saturation crystallinity (X^{sat}) of individual blocks during two step and one-step isothermal crystallization crystallized from microphase separated melt. Table 6.4 and 6.5 compare the saturation crystallinity (X^{sat}) of diblock copolymer, crystallized from microphase separated melt without annealing and with annealing respectively. We observe a comparable increase of crystallinity of A-block in two-step crystallization than one-step crystallization, whereas the crystallinity of B-block remains almost same for both the process. The changing mode of crystallization is responsible for this significant difference in crystallinity. Two-step cooling follows a sequential crystallization mechanism, where the development of crystallinity of A-block is unaffected by the crystallization of B-block. One-step cooling follows a coincident crystallization mechanism, where both the blocks experience a competition for crystallization. As a result, crystallization (also crystallinity) of A-block is hindered.

Table 6.4 Comparison in saturation crystallinity (X^{sat}) of diblock copolymer induced from microphase separated melt without annealing at U_p = 0.6 during two-step and one-step isothermal crystallization.

x_B	A-Block		B-block	
	Two-step	One-step	Two-step	One-step
0.125	0.73	0.65	0.54	0.56
0.25	0.72	0.62	0.57	0.58
0.375	0.71	0.61	0.59	0.59
0.50	0.71	0.60	0.59	0.60
0.625	0.72	0.60	0.60	0.61
0.75	0.73	0.60	0.63	0.62
0.875	0.76	0.62	0.65	0.66

Table 6.5 Comparison in saturation crystallinity (X^{sat}) of diblock copolymer induced from microphase separated annealed melt at U_p = 0.6 during two-step and one-step isothermal crystallization.

x_B	A-Block		B-block	
	Two-step	One-step	Two-step	One-step
0.125	0.73	0.65	0.58	0.56
0.25	0.72	0.63	0.58	0.60
0.375	0.71	0.62	0.60	0.61
0.50	0.72	0.61	0.60	0.62
0.625	0.72	0.61	0.62	0.63
0.75	0.73	0.62	0.64	0.64
0.875	0.75	0.64	0.66	0.67

Similarly, we compare the lamellar thickness of both the blocks in Table 6.6 and 6.7 for microphase separated melt without annealing and with annealing, respectively. The lamellar thickness of A-block is larger in two-step compared to one-step isothermal crystallization. The above observation is in accord with Hoffman-Weeks formula which describes the development of crystallinity governed by the degree of cooling [54]. When we implement two-step cooling at U_p = 0.3, the crystallization driving force induces crystallization of A-block; at U_p = 0.6, the crystallization driving force induces crystallization of B-block. Due to difference in degree of cooling, A-block produces different lamellar thickness in two-step compared to one step isothermal crystallization. However, in both the processes, the degree of cooling for B-block is similar as it is implemented at U_p = 0.6. So, the crystallinity and lamellar thickness is the same for B-block irrespective of two-step and one-step isothermal crystallization.

Table 6.6 Comparison in lamellar thickness $\langle l \rangle$ of diblock copolymer induced from microphase separated melt without annealing at U_p = 0.6 during two-step and one-step isothermal crystallization.

x_B	A-Block		B-block	
	Two-step	One-step	Two-step	One-step
0.125	3.27	2.52	2.59	2.67
0.25	3.21	2.46	2.54	2.60
0.375	3.23	2.46	2.54	2.55
0.50	3.25	2.46	2.50	2.52
0.625	3.46	2.50	2.51	2.52
0.75	3.69	2.59	2.55	2.55
0.875	3.38	2.79	2.60	2.62

Table 6.7 Comparison in lamellar thickness $\langle l \rangle$ of diblock copolymer induced from microphase separated annealed melt at U_p = 0.6 during two-step and one-step isothermal crystallization.

x_B	A-Block		B-block	
	Two-step	One-step	Two-step	One-step
0.125	3.26	2.53	2.66	2.70
0.25	3.23	2.48	2.57	2.61
0.375	3.25	2.48	2.55	2.58
0.50	3.25	2.48	2.53	2.55
0.625	3.42	2.53	2.53	2.55
0.75	3.60	2.63	2.60	2.59
0.875	4.20	2.83	2.65	2.66

6.3 Summary

The simulation study of diblock copolymer crystallization, crystallized from microphase separated melt is reported with two different patterns of melt morphology (viz., annealed and without annealed). We observed a morphological perturbation during non-isothermal crystallization for diblock copolymer crystallized from microphase separated melt without annealing, whereas melt morphology remains unperturbed for diblock copolymer crystallized from microphase separated annealed melt, as evidenced from the trend of $\langle R_g^2 \rangle$. Annealing induces re-orientation of chain segments and coalescence of microdomains created during microphase separation. The morphology set during the annealing remains unaffected during crystallization (isothermal and non-isothermal). Highly asymmetric diblock copolymer (viz., high enough composition of B-block) shows an enhancement of lamellar thickness of A-block, which is attributed to the dilution effect shown by B-block. This dilution effect is observed in both the melts (with and without annealing).

We study isothermal crystallization with two different modes of cooling (viz., one- and two-step) to understand the effect of quench depth on crystallization. We implement one-step isothermal crystallization by quenching microphase phase separated melt directly from the respective microphase separation point ($U_p^{\#}$) to U_p = 0.6, which results in denial of morphological perturbation irrespective of melt morphology (viz., annealed and without annealed microphase separated melt). Simultaneously, we execute two–step isothermal crystallization by cooling microphase separated melt from the respective microphase separation point to U_p = 0.3, followed by cooling from U_p = 0.3 to U_p = 0.6. Two-step crystallization yields better crystallinity of A-block compared to one-step isothermal crystallization, but crystallinity of B-block remains identical for both the melts without morphological change. Crystallization of B-block happens in the presence of the confinement created during the crystallization of A-block. As a result, no morphological change is observed for B-block during crystallization. Our findings suggest that understanding on the morphological development with annealing (viz., varying the annealing temperature) would enable to tune the semi-crystalline morphology of diblock copolymers.

References

1. Loo Y-L, Register RA, Ryan AJ, and Dee GT. Macromolecules 2001;34(26):8968-8977.
2. Muller AJ, Balsamo V, Arnal ML, Jakob T, Schmalz H, and Abetz V. Macromolecules 2002;35(8):3048-3058.
3. Albuerne J, Marquez L, Muller AJ, Raquez JM, Degee P, Dubois P, Castelletto V, and Hamley IW. Macromolecules 2003;36(5):1633-1644.
4. Shin D, Shin K, Aamer KA, Tew GN, Russel TP, Lee JH, and Jho JY. Macromolecules 2005;38(1):104-109.
5. Castillo RV, Muller AJ, Lin M-C, Chen H, Jeng U-S, and Hillmyer MA. Macromolecules 2008;41(16):6154-6164.
6. Loo Y-L and Register RA. Phys. Rev. Lett. 2000;84(18):4120-4123.
7. Nojima S, Akutsu Y, Washino A, and Tanimoto S. Polymer 2004;45:7317-7324.
8. Sakurai T, Ohguma Y, and Nojima S. Polym. J. 2008;40(10):971-978.
9. Lin M-C, Chen H-L, Lin W-F, Huang P-S, and Tsai J-C. J. Phys. Chem. B 2012;116:12357 - 12371.
10. Lin M-C, Chen H-L, Su W-B, Su C-J, Jeng U-S, Tzeng F-Y, Wu J-Y, Tsai J-C, and Hashimoto T. Macromolecules 2012;45:5114−5127.
11. Lohwasser RH, Gupta G, Kohn P, Sommer M, Lang AS, Thurn-Albrecht T, and Thelakkat M. Macromolecules 2013;46:4403 - 4410.
12. Chen L, Jiang J, Wei L, Wang X, Xue G, and Zhou D. Macromolecules 2015;48:1804 - 1812.
13. Darling SB. Prog. Polym. Sci. 2007;32:1152-1204.
14. Bates FS and Fredrickson GH. Annu. Rev. Phys. Chem. 1990; 41:525-557.
15. Bates FS and Fredrickson GH. Phys. Today 1999; 52(2):32-38.
16. Bates CM, Maher MJ, Janes DW, Ellison CJ, and Willson CG. Macromolecules 2014;47:2-12.
17. Yao D, Zhang K, and Chen Y. Polymer 2016;94:1-7.
18. Schacher FH, Rupar PA, and Manners I. Angew. Chem. Int. Ed. 2012;51(32):7898-7921.
19. Botiz I and Darling SB. Mater. Today 2010;13(5):42-51.
20. Zhu L and Wang Q. Macromolecules 2012;45(7):2937-2954.

21. Zhu L, Cheng SZD, Calhoun BH, Q.Ge, Quirk RP, Thomas EL, Hsiao BS, Yeh F, and Lotz B. Polymer 2001;42:5829 - 5839.
22. Ueda M, Sakurai K, Okamoto S, Lohse DJ, MacKnight WJ, Shinkai S, Sakurai S, and Nomura S. Polymer 2003;44:6995 - 7005.
23. Shiomi T, Tsukada H, Takeshita H, Takenaka K, and Tezuka Y. Polymer 2001;42:4997-5004.
24. Shiomi T, Takeshita H, Kawaguchi H, Nagai M, Takenaka K, and Miya M. Macromolecules 2002;35:8056 - 8065.
25. Ryan kJ, Hamley IW, Bras W, and Bates FS. Macromolecules 1995;28(11):3860-3868.
26. Quiram DJ, Register RA, and Marchand GR. Macromolecules 1997;30(16):4551-4558.
27. Nojima S, Kato K, Yamamoto S, and Ashida T. Macromolecules 1992;25(8):2237-2242.
28. Nojima S, Nakano H, and Ashida T. Polymer 1993;34(19):4168-4170.
29. Hamley IW, Fairclough JPA, Terrill NJ, Ryan AJ, Lipic PM, and Bates FS. Macromolecules 1996;29(27):8835-8843.
30. Loo Y-L, Register RA, and Ryan AJ. Macromolecules 2002;35(6):2365-2374.
31. Ho R-M, Lin F-H, Tsai C-C, Lin C-C, Ko B-T, Hsiao BS, and Sics I. Macromolecules 2004;37(16):5985-5994.
32. Fu J, Luan B, Pan C, Li B, and Han Y. Macromolecules 2005;38:5118 - 5127.
33. Hong S, Bushelman AA, MacKnight WJ, Gido SP, Lohse DJ, and Fetters LJ. Polymer 2001;42(13):5909-5914.
34. Huang Y-Y, Yang CH, Chen H-L, Chiu F-C, Lin T-L, and Liou W. Macromolecules 2004;37(2):486-493.
35. Zha L and Hu W. Prog. Polym. Sci. 2016;54–55:232-258.
36. Nakagawa S, Marubayashi H, and Nojima S. Eur. Polym. J. 2015;70:262-275.
37. Hamley lW, Fairclough JPA, Ryan AJ, Bates FS, and Towns-Andrews E. Polymer 1996;37(19):4425-4429.
38. Nojima S, Fujimoto M, Kakihira H, and Sasaki S. Polym. J. 1998;30(12):968-975.
39. Nojima S, Toei M, Hara S, Tanimoto S, and Sasaki S. Polymer 2002;43:4087-4090.
40. Nojima S, Nakano H, Takahashi Y, and Ashida T. Polymer 1994;35(16):3479-3486.
41. Nojima S, Ito K, and Ikeda H. Polymer 2007;48:3607-3611.
42. Nojima S, Akutsu Y, Akaba M, and Tanimoto S. Polymer 2005; 46 4060–4067.

43. Yu X, Yang H, Wu S, Geng Y, and Han Y. Macromolecules 2012;45:266-274.
44. Kundu C and Dasmahapatra AK. Polymer 2014;55(3):958-969.
45. Kundu C and Dasmahapatra AK. J. Chem. Phys. 2014;141:044902-1 - 044902-12.
46. Kim JK, Park D-J, Lee M-S, and Ihn KJ. Polymer 2001;42:7429-7441.
47. Castillo RV and Müller AJ. Prog. Polym. Sci. 2009;34(6):516-560.
48. Avrami M. J. Chem. Phys. 1939;7:1103-1112.
49. Lorenzo AT, Arnal ML, Albuerne J, and Müller AJ. Polym. Test. 2007;26(2):222-231.
50. Castillo RV, Muller AJ, Raquez J-M, and Dubois P. Macromolecules 2010;43(9):4149–4160.
51. Hamley IW, Parras P, Castelletto V, Castillo RV, Müller AJ, Pollet E, Dubois P, and Martin CM. Macromol. Chem. Phy. 2006;207(11):941-953.
52. Michell RM and Müller AJ. Prog. Polym. Sci. 2016;54–55:183-213.
53. Müller AJ, Balsamo V, and Arnal ML. Nucleation and Crystallization in Diblock and Triblock Copolymers. In: Abetz V, editor. Block Copolymers II. Berlin, Heidelberg: Springer Berlin Heidelberg, 2005. pp. 1-63.
54. Marand H, Xu J, and Srinivas S. Macromolecules 1998;31(23):8219-8229.

Chapter 7

Crystallization on Thin Films

In this chapter, we present the crystallization behaviour of a diblock copolymer on thin films. The magnitude of film thickness and the role of substrate are the prime factors that dictate the crystallization mechanism and the final morphology. In a diblock copolymer, the interplay between crystallization and microphase separation plays an important role to determine final crystal morphology. By introducing thin film, we have added an extra confinement, where the molecular mobility of polymer chains is restricted within two dimensions. The crystallization under 1-D confinement affects nucleation, crystal growth and final orientation of crystal morphology. In our model system, substrate is considered inert and hence does not provide any effective interaction with diblock copolymer.

7.1 Literature Review

Polymer crystallization under spatial confinement, especially in thin films (typical thickness less than 1000 nm) and ultrathin films (typical thickness less than 100 nm) is an interesting topic due to its unique structural property [1, 2]. Block copolymer thin films offer many prospective applications in the field of lithography, electronics, nonporous membranes and solar cells [2-5]. For example, poly (styrene-*block*-methyl methacrylate) diblock copolymer is widely used for nano patterning or creating periodic structure in nanoscale. At 225˚C, PS-*b*-PMMA produces the perpendicular orientation of micro domains after annealed on a neutral substrate [3, 4]. There is a new feasibility to reshape the molecular properties of block polymers for the use of cost effective electronic devices [2, 6-8]. Several thiophene based all conjugated block copolymers (i.e, PPP-*b*-P3HT) have been fabricated due to their excellent charge transporting mobility and highly ordered structure [7]. Diblock copolymer consisting of polystyrene and poly(perylene acrylate) exhibits an outstanding n-type performance with high electron transport mobility, low threshold voltages, and good electron injection from gold electrodes [8]. Moreover, as thin polymer films are considered as one-dimensional (1D) confinement system, it provides great opportunity to study the effects of

confinement and interface (viz., substrate-specific properties) on polymer crystallization [2, 9, 10]. The chain orientation, segmental mobility, transport properties, and surface free energy at the interface, which are usually less significant in bulk, become important factors in thin films. Therefore, a set of new mechanisms other than bulk crystallization of polymers may be evolved [2, 11].

The crystallization behaviour of diblock copolymer thin films unfolds a new avenue as it offers diverse orientation of the crystalline lamellar morphology [2, 10, 12-14]. The microphase separated morphology on thin films largely varies in respect to bulk behaviour. For example, the final crystal morphologies of poly(butadiene-*block*-caprolactone) diblock copolymer are compared in bulk (0.5 – 1mm) and thin films (~ 5μm) [15]. Bulk films of diblock copolymer ($PB_{0.2}PCL_{0.8,}$ where subscripts denote the mass fraction of individual block) exhibit cylindrical microstructures. During crystallization, PCL block crystallizes within microphase separated structure without producing large scale spherulites. However, thermally treated thin films generate large and well defined spherulites upon crystallization [15]. Another pivotal point in thin film crystallization is whether the process of crystallization disrupts the previous melt morphology, or melt morphology keeps intact during the crystallization process. The crystallization behaviour of poly (butadiene-*block*-ethylene oxide) diblock copolymer in thin films (approximately 100nm) has been examined from microphase separated melt with the parallel lamellar orientation to the substrate [16, 17]. The process of crystallization under high cooling rate with short PEO block provides perpendicular lamellar orientation [16, 17], whereas annealing close to melting point or preserving the sample at room temperature for several months allows the development of lamellar structure with parallel orientation [17]. Again, the crystallization of polyethylene oxide (PEO) in 12nm spheres of PB-*b*-PEO diblock copolymer reveals that all the spheres crystallize individually and independently, which establishes new dimension to manipulate material properties in nanometer scale [18]. The transition of lamellar crystal from flat-on to edge-on in ultrathin films of polystyrene-*block*-polyethylene oxide has been investigated via solvent vapour treatment [19]. When PS-*b*-PEO films are annealed under toluene vapour for long enough time, break-out crystals develop quickly, and their orientation transforms from flat-on to edge-on [19]. The morphological evolution of poly (ethylene oxide-*block*-1,4 butadiene) has been studied during crystallization from thin films with an average thickness of 40nm [20]. In melt system, PEO-*b*-PB diblock copolymer exhibits lamellar morphology oriented parallel to the substrate. Crystallization at high temperature preserves the phase

separated melt morphology with the formation of thicker lamella. The final crystal morphology consists of alternating layers of PEO and PBD, where PEO crystalline chains results in perpendicular orientation to the lamellar layers of the microphase-separated structure [20]. On the other hand, the melt structure of PE spheres in SEB matrix of polyethylene-*block*-poly(styrene-r-ethylene-r-butene) diblock copolymer is completely disrupted upon crystallization of thin films (film thickness ≤ 33nm),where the primary island and hole structures transform to layered crystal structure [21]. The thin film morphology of symmetric oxyethylene-*block*-oxybutylene diblock copolymer has been also followed minutely for $E_{76}B_{38}$, $E_{114}B_{56}$, $E_{155}B_{76}$ and $E_{224}B_{113}$, where E and B denote oxyethylene and oxybutylene and subscripts refer to the average degree of polymerization [22]. The thin films with lower molar mass ($E_{76}B_{38}$, $E_{114}B_{56}$ and $E_{155}B_{76}$) give lamellar structure parallel to the substrate, whereas the thin film with high molar mass ($E_{224}B_{113}$) exhibits the lamellar orientation perpendicular to substrate [22]. Annealing at 35˚C for 30 hour in a vacuum system leads to the development of spherulite morphology with perpendicular lamellar structure to the surface [22].

7.2 Results and Discussion

To simulate the crystallization from a thin film, first we generate a set of homogeneous melts by varying the length of z-axis, and we implement non-isothermal crystallization as well as isothermal crystallization to study the effect of film thickness on crystallization. Film thickness is measured in terms of lattice units along the z-axis. The simulation has been carried out at weakly segregated system, $\lambda = 1$.

7.2.1 Preparation of Thin Films

To implement thin film crystallization, we restrict molecular mobility of polymer chains along z-axis. Periodic boundary condition is not implemented along z-axis. All attempted Monte Carlo moves along the z-axis are denied. We vary the length of z-axis from z = 4 to z = 20 to study the effect of film thickness on crystallization. The length along other axis remains same for the entire simulation. The occupation density of all system is taken as 0.85. Therefore, the number of chains is variable for different film thickness (z). For z = 4,

we take 55 polymer chains with 64 repeat units. Similarly, we consider 110, 165, 220 and 275 polymer chains for film thickness of 8, 12, 16, and 20 respectively. We start our simulation from a homogeneous melt at $U_p = 0$ where, A-type and B-type monomers are evenly dispersed for symmetric block composition (Figure 7.1).

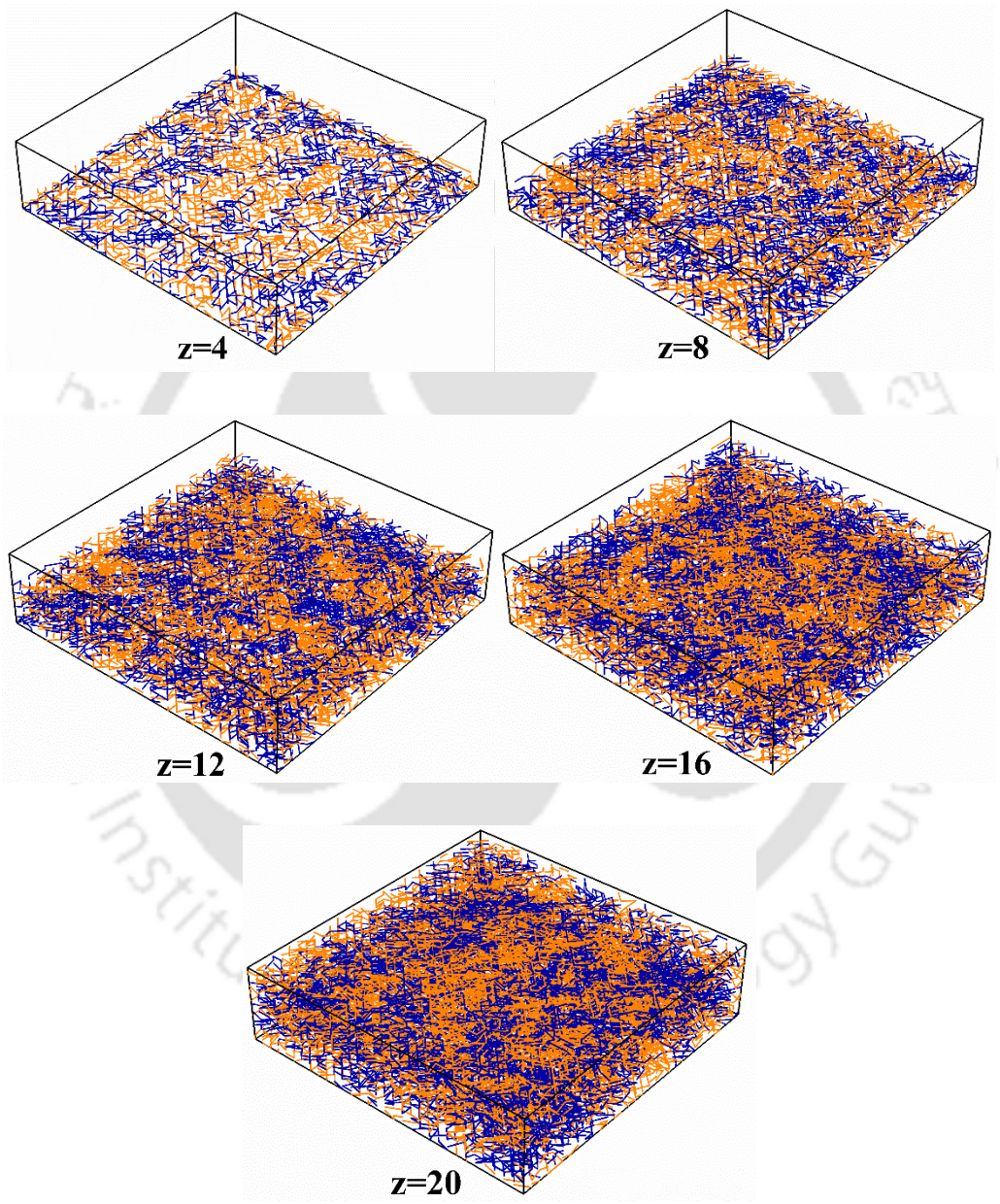

Figure 7.1 Snapshots of simulation box at $U_p = 0$ representing homogeneous melt of symmetric block composition ($x_B = 0.5$) where blue lines represent A-block and orange lines represent B-block.

7.2.2 Effect of Non-Isothermal Crystallization

7.2.2.1 Locating Transition Point

We monitor crystallization of the diblock copolymer by following the change in equilibrium specific heat (C_v), calculated from energy fluctuations as a function of U_p. At the transition point, C_v gives a peak as fluctuations in energy and the U_p value at which peak appears on cooling is considered as crystallization U_p^* in tune with experimental observation [23]. We plot C_v vs. U_p (Figure 7.2a) for a series of film thicknesses (viz., z = 4 to z = 20) to locate the transition points for symmetric diblock copolymer. As the diblock copolymer consists of two crystallizable blocks, Figure 7.2a gives two different peaks of U_p representing the phase transition of A- and B-block at different values of U_p, respectively. A-block crystallizes first due to its higher driving force towards crystallization, followed by B-block. The transition points of both the blocks get affected by the confinement introduced by thin films. Figure 7.2b displays the change of U_p^* with film thickness (z). With the decrease in film thickness, the transition points of both the blocks move towards lower value of U_p (viz., higher temperature). As the confinement is increased (viz., z is decreased), the mobility of polymer chains is drastically reduced. As a result, the diffusion of the crystalline segments towards the growth front is reduced, resulting increase in crystallization temperature. We calculate chain mobility by measuring the mean square displacement of centre of mass of polymer chains in Figure 7.3, which clearly signifies the reduced chain mobility with reducing film thickness. We also consider the effect of block asymmetry (x_B) on transition points of both the blocks. Figure 7.4 displays the change in transition points in terms of U_p with block composition (x_B) for a specific film thickness (z = 8). From Figure 7.4, we can conclude that, crystallization temperature remains similar for most of the block compositions except at higher block asymmetry. At x_B = 0.875, there is a small depression in crystallization temperature of A-block which is reflected by the increase of U_p value. As the process of crystallization is primarily dominated by the degree of cooling (ΔT), the transition points of both blocks remain unaffected with most of the compositions. However, at x_B = 0.875, due to the dilution effect (see Chapter 05, page: 57) imposed by B-block, the depression in crystallization temperature of A-block is observed. At higher x_B, B-block acts

like a "solvent" which gives higher mobility to polymer chains, while A-block crystallizes. Therefore, polymer chains of A-block are less facile to crystallize, leading to a depression in crystallization temperature. On the other hand, crystallization temperature of B-block reduces to a lower value of U_p resulting higher crystallization temperature for x_B = 0.125. At x_B = 0.125, the confinement effect introduced by A-block reduces the molecular mobility of polymer chains which affects the transition point of B-block.

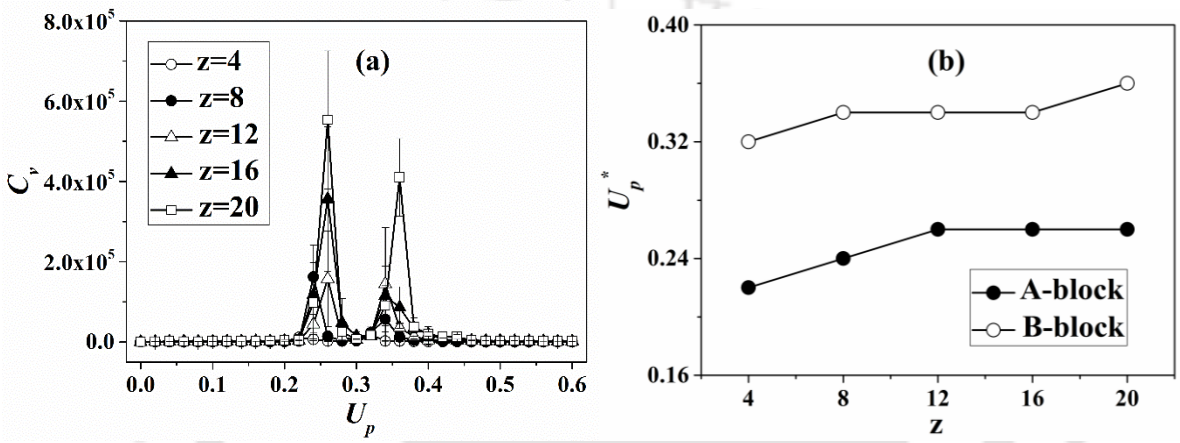

Figure 7.2 (a) Change in specific heat, C_v with U_p for z = 4, 8, 12, 16 and 20. (b) Change in U_p^* with film thickness (z).

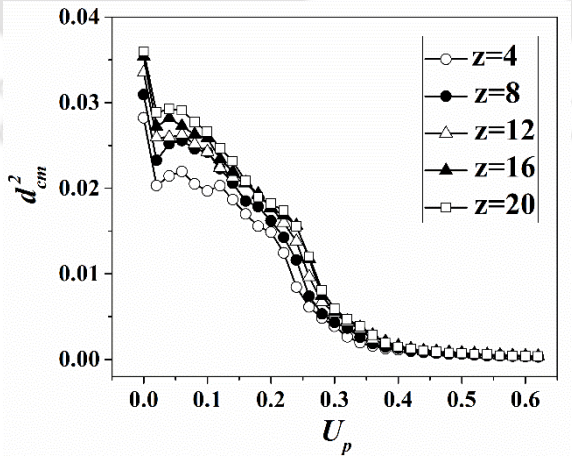

Figure 7.3 Change in mean square displacement of centre of mass (d_{cm}^2) with U_p for z = 4, 8, 12, 16 and 20.

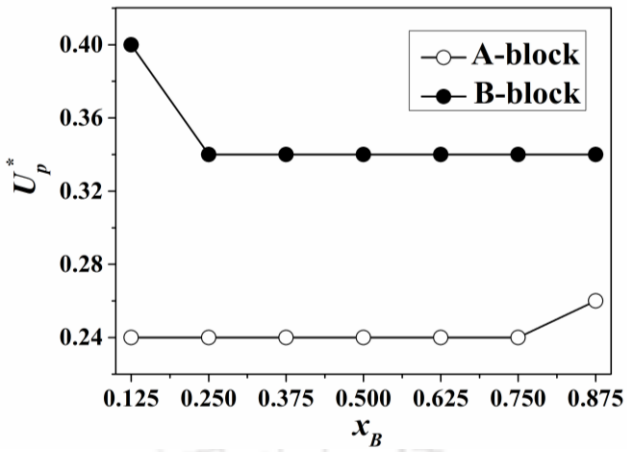

Figure 7.4 Change in transition points, U_p^* with x_B for film thickness (z) of 8.

7.2.2.2 Development of Crystallinity

We monitor the crystallization by calculating crystallinity of individual blocks. Overall crystallinity (X_c) is calculated as the weighted average of the summation of A-block (X_A) and B-block (X_B). The change in overall crystallinity (X_c) with U_p introduced by diblock copolymer thin film is available in Figure 7.5a for symmetric diblock copolymer. In Figure 7.5a, there is an abrupt increment of crystallinity at a certain value of U_p and after that there is no appreciable change in crystallinity (cf., saturation crystallinity, X^{sat}). The comparison in saturation crystallinity (X^{sat}) of both the blocks induced from thin films is given in Figure7.5b. There is no significant difference in saturation crystallinity of A- and B-block (X_A^{sat} and X_B^{sat}) across different film thicknesses. This happens because the development of crystallinity is primarily driven by the degree of cooling (ΔT). For all the film thickness, we use the same degree of cooling to implement non-isothermal crystallization. As we crystallize each film thickness within the same of degree of cooling, the crystallization driving force is equal, resulting development of comparable crystallinity for all the thin films. Figure 7.6 shows the change in saturation crystallinity (X^{sat}) with block composition (x_B) for a film thickness, z = 8. As the value of block composition (x_B) increases, the saturation crystallinity of B- block increases due to enhanced number of B-units in the diblock copolymer. However, for A-block, the saturation crystallinity remains almost similar.

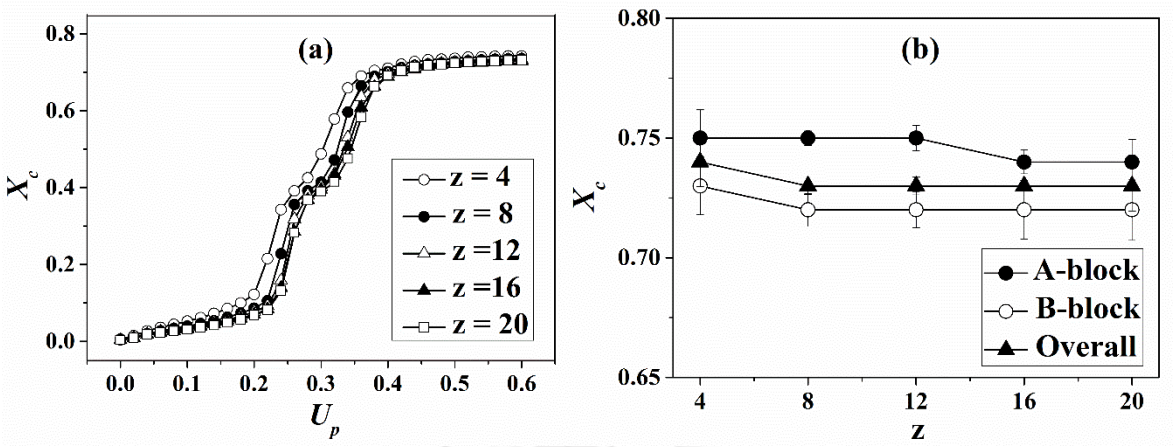

Figure 7.5 (a) Change in overall crystallinity, X_c with U_p for z = 4, 8, 12, 16 and 20. (b) Change in saturation crystallinity, X^{sat} with film thickness (z).

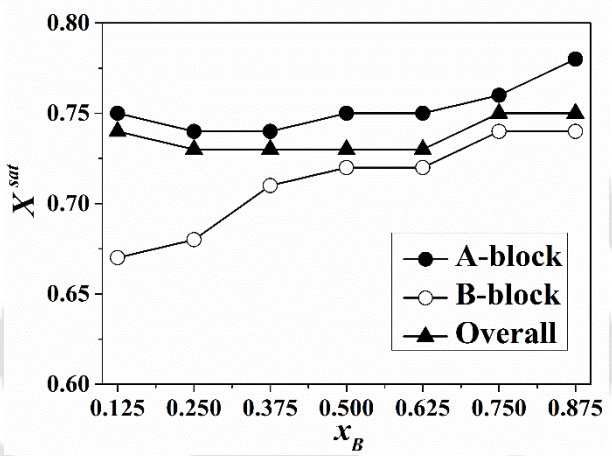

Figure 7.6 Change in saturation crystallinity, X^{sat} with block composition (x_B) at film thickness of z = 8.

7.2.2.3 Structural Analysis

To understand the structural evolution during crystallization, we estimate the average crystallite size $\langle S \rangle$ and the lamellar thickness $\langle l \rangle$ as a function of U_p for a series of film thicknesses. We observe a wider distribution of crystallites size compared to that of lamellar thickness. The magnitude of crystallite size is much higher than lamellar thickness of crystallites, indicating the formation of two dimensional crystals. Figure 7.7 presents the change in $\langle S \rangle$ and $\langle l \rangle$ of A- and B-block with film thickness (z) for symmetric diblock

copolymer, at U_p = 0.6. With the decrease in film thickness, the crystallites size is decreased, whereas the lamellar thickness is increased for both the blocks. When we decrease the film thickness, due to confinement effect, the mobility of polymer chains is reduced, resulting in the lowering of entropy. Hence to make the crystallization process feasible (viz., lowering the free energy), the change in enthalpy becomes highly negative, by increasing the number of contacts between similar units, which is reflected in the enhanced value the lamellar thickness at lower film thickness. We also calculate the average lamellar thickness $\langle l \rangle$ for asymmetric diblock copolymers. Figure 7.8 shows the change in $\langle l \rangle$ at U_p = 0.6 with block composition (x_B) for z = 8. With increasing the block composition of B (x_B), the lamellar thickness of A-block remains almost same upto x_B = 0.50. After that, $\langle l_A \rangle$ increases appreciably in the presence of large proportion of B-block, which is attributed to the dilution effect imposed by B-block. When x_B less than 0.5, the crystallization of A-block is typically affected by chain entanglements resulting in "melt crystallization". However, when the block composition increases further, A-block crystallizes within a matrix of B-block which acts like a "solvent", dictating "solution crystallization". Therefore, the molten B-block provides marginal hindrance towards the crystallization of A-block, facilitating the formation of thicker crystals. The lamellar thickness of B-block does not change appreciably with block composition (x_B). The final snapshots of thin films after crystallization are available in Figure 7.9.

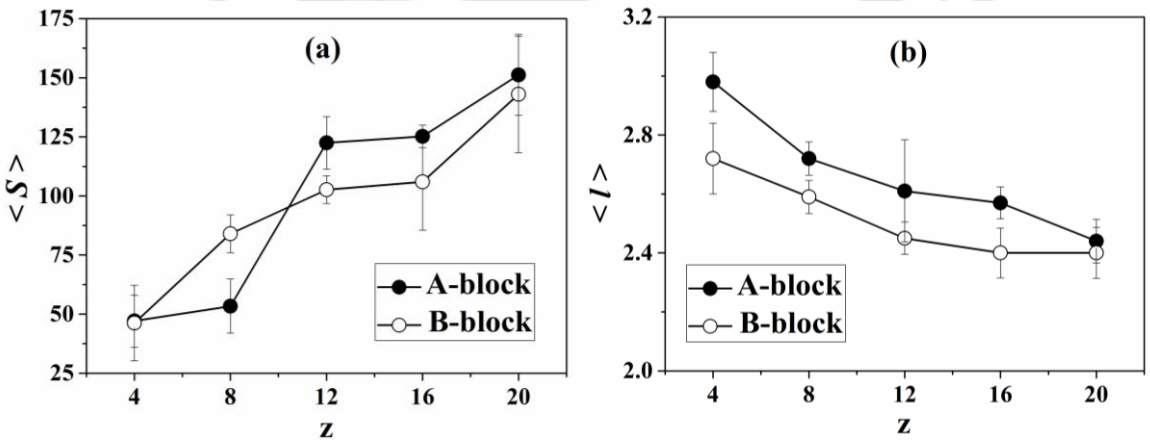

Figure 7.7 (a) Change in average crystallites size, $\langle S \rangle$ with film thickness (z). (b) Change in average lamellar thickness, $\langle l \rangle$ with film thickness (z) for a symmetric diblock copolymer at U_p = 0.6.

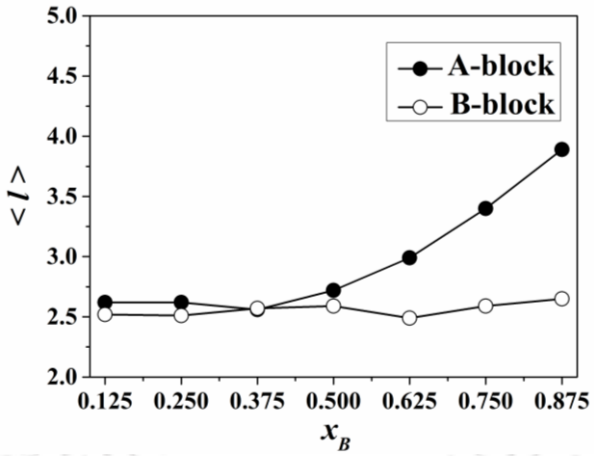

Figure 7.8 Change in average lamellar thickness, $\langle l \rangle$ with block composition (x_B) at film thickness of z = 8.

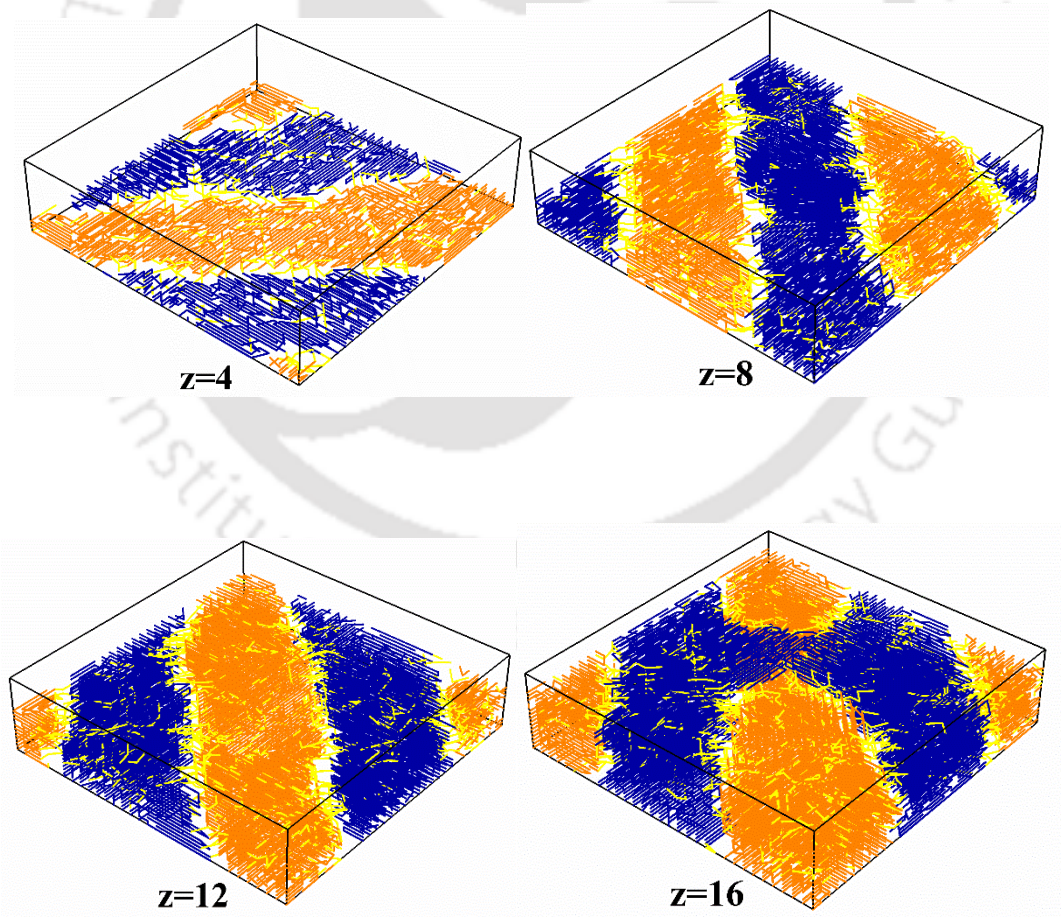

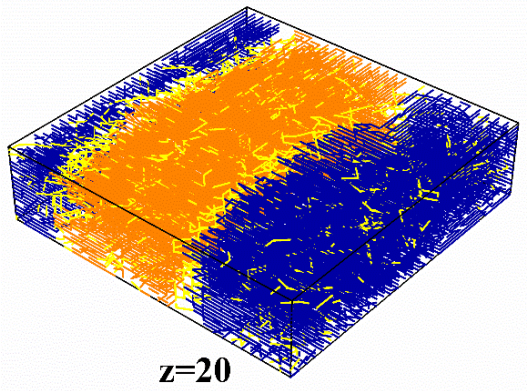

Figure 7.9 Snapshots of semi crystalline structures of symmetric diblock copolymer on thin films at U_p = 0.6 for (a) z = 4, (b) z = 8, (c) z = 12, (d) z = 16 and (e) z = 20. Blue lines represent crystalline bonds of A-block, orange lines represent crystalline bonds of B-block and yellow lines represent non-crystalline bonds of both the blocks.

7.2.3 Effect of Isothermal Crystallization

To follow transition kinetics, we implement isothermal crystallization. In isothermal crystallization, we have not calculated any average quantity; rather we have followed the time evaluation of crystallinity. We observe the change in crystallinity as a function of time. In our simulation, one time step is expressed as one Monte Carlo Step (MCS). We cool our system from U_p = 0 to U_p = 0.6 directly and anneal for 10^5 MCS. Figure 7.10a represents the development of overall crystallinity with MCS for different film thickness (z). We observe that the transition kinetics follows different kinetic pathways for different z. To apprehend transition kinetics in more details, we analyze the Avrami index (n) for different film thickness (z), presented in Figure 7.10b. We estimate the value of Avrami index [24] based on primary crystallization, which is measured as the conversion of crystallinity up to 20% [25]. For all the film thicknesses, the value of Avrami index lies in between 1.0 to 1.7, which clearly indicates a first order transition kinetics with homogeneous nucleation. Figure 7.11 exhibits the change in Avrami index (n) with block composition (x_B) for z = 8.

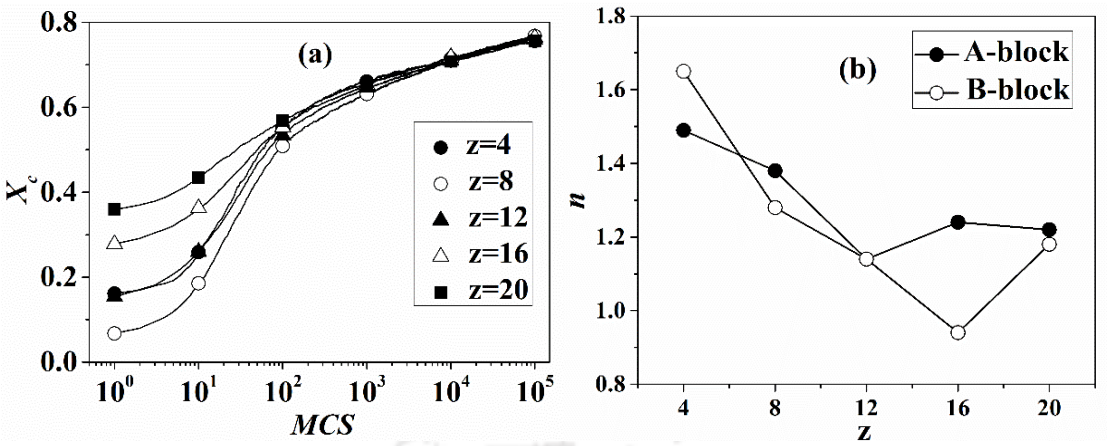

Figure 7.10 (a) Change in crystallinity, X_c with Monte Carlo Steps (MCS). (b) Change in Avrami index, (n) with film thickness (z).

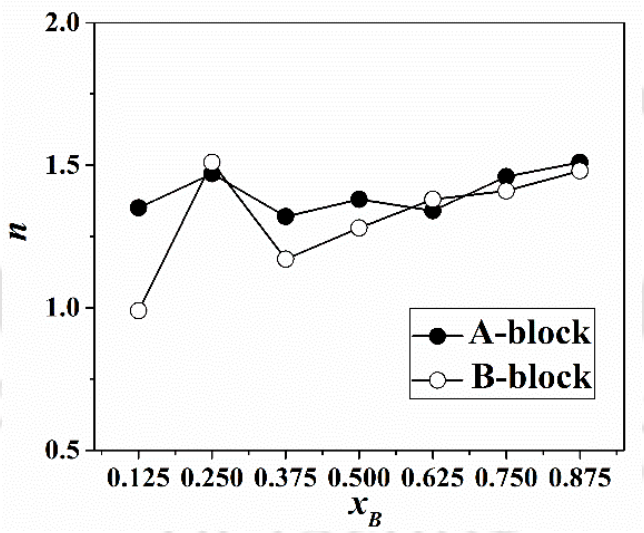

Figure 7.11 Change in Avrami index, (n) with block composition (x_B) at film thickness of z = 8.

7.3 Summary

The crystallization of diblock copolymer thin films is explored by Dynamic Monte Carlo Simulation. Film thickness is one of the most influential parameters for thin film crystallization, which governs the final crystal morphology. We study the non-isothermal crystallization of symmetric diblock copolymer for a series of film thickness (z) ranging from $z = 4$ to $z = 20$. The transition points of both the blocks are influenced by film thickness (z). The crystallization temperature of both blocks decreases with the increase in film thickness (z). With the increase in film thickness, the average crystallite size is increased. However, the average lamellar thickness reduces with increasing film thickness. Isothermal crystallization reveals that the transition kinetics follows different pathways with the variation of film thickness (z). The value of Avrami index confirms the presence of homogeneous nucleation with the formation of two-dimensional crystals. We have also investigated the effect of block asymmetry on thin film crystallization. At weak segregation (viz., $\lambda = 1$), we observe a small depression in crystallization temperature of A-block at $x_B = 0.875$, which is attributed to the dilution effect imposed by B-block. The lamellar thickness of A-block also significantly increases for $x_B = 0.75$ and 0.875 at $\lambda = 1$ which is attributed to the dilution effect enforced by B-block.

References

1. Frank CW, Rao VV, Despotopoulou MM, Pease RFW, Hinsberg WD, Miller RD, and Rabolt JF. Science 1996;273(5277):912-915.
2. Liu Y-X and Chen E-Q. Coord. Chem. Rev. 2010;254(9):1011-1037.
3. Bates CM, Maher MJ, Janes DW, Ellison CJ, and Willson CG. Macromolecules 2014;47(1):2-12.
4. Peters RD, Yang XM, Kim TK, Sohn BH, and Nealey PF. Langmuir 2000;16(10):4625-4631.
5. Albert JNL and Epps TH. Mater. Today 2010;13(6):24-33.
6. Bi W, Teguh JS, and Yeow EKL. Phys. Rev. Lett. 2009;102(4):048302.
7. Yu X, Yang H, Wu S, Geng Y, and Han Y. Macromolecules 2012;45:266-274.
8. Huttner S, Sommer M, and Thelakkat M. Appl. Phys. Lett. 2008;92(9):093302.
9. Prudhomme RE. Prog. Polym. Sci. 2016;54–55:214-231.
10. Hamley IW. Prog. Polym. Sci. 2009;34(11):1161-1210.
11. Li H and Yan S. Macromolecules 2011;44(3):417-428.
12. Darling SB. Prog. Polym. Sci. 2007;32:1152-1204.
13. Michell RM and Müller AJ. Prog. Polym. Sci. 2016;54–55:183-213.
14. Nandan B, Hsu JY, and Chen HL. J Macromol Sci. Part C 2006;46(2):143-172.
15. Kim G, Han CC, Libera M, and Jackson CL. Macromolecules 2001;34(21):7336-7342.
16. Reiter G, Castelein G, Hoerner P, Riess G, Blumen A, and Sommer J-U. Phys. Rev. Lett. 1999;83(19):3844-3847.
17. Reiter G, Castelein G, Hoerner P, Riess G, Sommer J-U, and Floudas G. Eur. Phys. J. E 2000;2:319-334.
18. Reiter G, Castelein G, Sommer J-U, Röttele A, and Thurn-Albrecht T. Phys. Rev. Lett. 2001;87(22):226101.
19. Yang P and Han Y. Langmuir 2009;25(17):9960-9968.
20. Hong S, MacKnight WJ, Russell TP, and Gido SP. Macromolecules 2001;34(9):2876-2883.
21. Li Y, Loo Y-L, Register RA, and Green PF. Macromolecules 2005;38(18):7745-7753.
22. Liang G-D, Xu J-T, Fan Z-Q, Mai S-M, and Ryan AJ. Macromolecules 2006;39(16):5471-5478.
23. Dasmahapatra AK, Nanavati H, and Kumaraswamy G. J. Chem. Phys. 2009;131:074905-074901-074905-074910.
24. Avrami M. J. Chem. Phys. 1939;7:1103-1112.
25. Lorenzo AT, Arnal ML, Albuerne J, and Müller AJ. Polym. Test. 2007;26(2):222-231.

Chapter 8

Conclusions and Future Studies

Crystallization of diblock copolymer is an active research topic due to its numerous applications in surface patterning and biomedical area. Continuous efforts have been executed to understand the process of crystallization under different modes of confinement. In the present thesis, crystallization mechanism has been explored from homogeneous melt and microphase separated melt. Subsequently, crystallization of diblock copolymer under thin film confinement has been investigated. In this chapter, we summarize our important findings and we explore future possibility of our study.

8.1 Conclusions

We first discuss the simulation results on crystallization behaviour of symmetric diblock copolymers from a homogeneous molten state to a phase separated crystalline state. The crystallization behaviour majorly driven by segregation strength, λ (viz., demixing energy between A- and B-block units). With increasing value of λ (from 0 to 5), we notice the gradual decrease in crystallinity of both the blocks associated with smaller and thinner crystals. In our model, A-block has larger driving force for crystallization than B-block. Therefore A-block crystallizes first with the development of lamellar morphology. The crystalline lamella of A-block generates confinement for the crystallization of B-block. As a result, crystallinity of B-block is reduced compared to A-block. There is a significant increase in the mean square radius of gyration of the chain during crystallization, which is attributed to the tension at the block junction promoted by the segregation strength. Higher the value of λ, higher is the influence of the chain stretching at the junction that leads to the formation of smaller size domains which restricts the development of crystal growth. Isothermal crystallization reveals that the crystallization pathway is strongly dictated by segregation strength. The value of Avrami index is ~ 1.0, which designates homogeneous nucleation with two dimensional crystals, where crystallization takes place within a spatial confinement. Two-steps, compared to one-step quenching produces higher crystallinity in A-block. In one-

step quenching (at U_p = 0.6), both the blocks compete with each other towards crystallization resulting formation of less crystalline materials in first crystallizable block. However, the crystallinity of B-block in one-step and two-step quenching is close to each other. The above observation suggests that the effective driving force for the crystallization of B-block is almost same irrespective of the mode of quenching. Lamellar thickness of A-block, $\langle l_A \rangle$ at U_p = 0.6 (one-step cooling) is less than that of at U_p = 0.3 (during two-step cooling), which is in accord with the Hoffman-Weeks relation. However, lamellar thickness of B-block is almost same irrespective of one-step or two-step cooling.

We report the effect of block asymmetry on crystallization of double crystalline diblock copolymer at two different levels of segregations. Non-isothermal cooling produces sequential crystallization mechanism regardless of composition. We notice a small depression in crystallization temperature of A-block at x_B = 0.875, which is attributed to the dilution effect of the B-block. We also observe a significant increase in chain mobility (in terms of mean square displacement of the centre of mass) of A-block at U_p = 0.3 compared to that of B-block at higher x_B. The crystallization temperature of the B-block monotonically increases with increasing block composition. At strong segregation, the transition points of both the blocks exhibit non-monotonic trend with block composition due to the confinement effects dominated by microphase separated melt. The crystallinity of A-block remains same over a wide range of block composition whereas the crystallinity of B-block increases with increasing block length of B at weak segregation. However the crystallinity of both the blocks produce non-monotonic trend with x_B at strong segregation. The lamellar thickness of A-block significantly increases for x_B = 0.75 and 0.875 at λ = 1 which is attributed to the dilution effect imposed by B-block. When the composition of A-block is very less in the system, B-block behaves as a “diluent”, which reduces topological restriction favouring crystal thickening. Isothermal crystallization confirms the dependence of the compositions on transition kinetics at both the levels of segregations. The Avrami indexes demonstrate the presence of homogeneous nucleation with the formation of two-dimensional crystals. The dilution effect is more prominent in two-stage isothermal crystallization compared to one-stage crystallization due to the change in mode of crystallization. Thus, manipulating block asymmetry with a proper choice of crystallization pathway, desired morphological pattern can be achieved.

Simulation study of diblock copolymer crystallization, crystallized from microphase separated melt is followed with two different pattern of melt morphology (viz., annealed and without annealed). We observed a morphological perturbation during non-isothermal crystallization for diblock copolymer crystallized from microphase separated melt without annealing, whereas melt morphology remains unperturbed for diblock copolymer crystallized from microphase separated annealed melt. We study isothermal crystallization simultaneously with two different mode of crystallization. We implement one-step isothermal crystallization by quenching phase separated melt from the respective microphase separation point ($U_p^{\#}$) to U_p = 0.6 directly which results in denial of morphological perturbation irrespective of melt morphology (viz., annealed and without annealed microphase separated melt). Simultaneously, we execute two–step isothermal crystallization by cooling microphase separated melt from the respective microphase separation point to U_p = 0.3, followed by cooling from U_p = 0.3 to U_p = 0.6. Two-step crystallization yields better crystallinity of A-block compared to one-step isothermal crystallization, but crystallinity of B-block remains similar for both types of crystallization. Two-step isothermal crystallization also preserves melt morphology intact.

We first implement non-isothermal cooling to study the crystallization of symmetric diblock copolymer for a series of film thickness (z) ranging from z = 4 to z = 20. The film thickness (z) determines the relative location of transition points. The crystallization temperature of both blocks decreases with the increase in film thickness (z). With the increase in film thickness, overall crystallinity remains identical with the formation of thinner crystals. Isothermal crystallization reveals that the transition kinetics follows different pathways with the variation of film thickness (z). The value of Avrami index confirms the presence of homogeneous nucleation with two-dimensional crystals. To investigate the effect of block asymmetry on thin film crystallization, we vary the composition of B-block (x_B). At weak segregation (viz., λ = 1), we observe a small depression in crystallization temperature of A-block at x_B = 0.875, which is attributed to the dilution effect imposed by B-block. The lamellar thickness of A-block also significantly increases for x_B = 0.75 and 0.875 at λ = 1 which also triggers the dilution effect enforced by B-block.

8.2 Future Studies

In this thesis, we have implemented Dynamic Monte Carlo simulation to study crystallization of diblock copolymer. There are numerous possibilities to extend this work in several dimensions.

- The phase behaviour and crystallization of diblock copolymer can be observed through Molecular Dynamics simulation by using Gromacs or LAMMPS.
- The current simulation methodology can be implemented to study surface induced crystallization of diblock copolymer. In thin film crystallization, film thickness as well as substrate plays a major role to determine the process of crystallization.
- With the help of different type of substrate, surface patterning can be possible in thin films of diblock copolymer.
- In our simulation process, additional confinement can be introduced. Polymer crystallization under droplet confinement can be examined. Similarly, polymer crystallization under nanotube confinement can also be followed.
- It is possible to study triblock copolymer crystallization using Dynamic Monte Carlo Simulation. For that purpose, an extension of energy functions of current simulation methodology is necessary.

Appendix

A Symbols and Abbreviations

T_m	Melting temperature
T_m^∞	Equilibrium melting temperature
G	Growth rate
ΔG_v	Gibb's free energy
γ	Surface energy
E_D	Activation energy
T_g	Glass transition temperature
l	Lamellar thickness
σ	Lateral surface energy
σ_e	Fold surface energy
$T_{g,PS}$	Glass transition temperature of Polystyrene
T_C	Crystallization temperature
T_{ODT}	Order-disorder transition temperature
N	Degree of polymerization
N_A	Number of A-type repeat units
N_B	Number of B-type repeat units
U_{AB}	Repulsive interactions between two blocks
U_P	Attractive interactions between parallel bonds
U_C	Attractive interactions between collinear bonds
U_{PA}	Parallel bond interaction energy of A-block
U_{PB}	Parallel bond interaction energy of B-block
U_{CA}	Collinear bond interaction energy of A-block
U_{CB}	Collinear bond interaction energy of B-block

ΔN_P	Net change in numbers of parallel bonds
ΔN_C	Net change in numbers of collinear bonds
ΔN_{AB}	Net change in contacts between A and B-units
χ	Flory-Huggins interaction parameter
λ	Segregation strength
q	Coordination number
k_β	Boltzmann constant
X_A	Fractional crystallinity of A-block
X_B	Fractional crystallinity of B-block
X_C	Overall crystallinity
C_v	Specific heat
U_P^*	Crystallization temperature in terms of U_P
U_{PA}^*	Crystallization temperature of A-block
U_{PB}^*	Crystallization temperature of B-block
x_A	Block composition of A-block
x_B	Block composition of B-block
d_{cm}^2	Mean square displacement of centre of mass
C_{v-AB}	Specific heat based on demixing energy
$U_P^\#$	Microphase separation point
$\langle R_g^2 \rangle$	Mean square radius of gyration
X_A^{sat}	Saturation crystallinity of A-block
X_B^{sat}	Saturation crystallinity of B-block
$\langle S_A \rangle$	Average crystallite size of A-block
$\langle S_B \rangle$	Average crystallite size of B-block

$\langle l_A \rangle$	Average lamellar thickness of A-block
$\langle l_B \rangle$	Average lamellar thickness of B-block
X_C^*	Scaled crystallinity
n	Avrami index
X	Crystallinity during single Monte Carlo step
X^{sat}	Saturation crystallinity
P	Bond order parameter
θ	Angle of crystalline bond with Z-axis
$E-b-EP$	Ethylene-*b*-Ethylene-alt-propylene
$PE-b-PEE$	Polyethylene-*b*-Polyethylethylene
$PCL-b-PS$	Poly(ε-caprolactone)-*b*-Polystyrene
$PE-b-PEO$	Polyethylene-*b*-Polyethylene oxide
$LPE-b-hPN$	Linear polyethylene-*b*-Polynorbornene
$PCL-b-PE$	Poly(ε-caprolactone)-*b*-Polyethylene
$PPL-b-PE$	Poly(β-propiolactone)-*b*-Polyethylene
$PLLA-b-PEO$	Poly(ι-lactide)-*b*-Polyethylene oxide
$PLLA-b-PCL$	Poly(ι-lactide)-*b*-Poly(ε-caprolactone)
$PLLA-b-PEG$	Poly(ι-lactide)-*b*-Poly(ethylene glycol)
$PLLA-b-PE$	Poly(ι-lactide)-*b*-Polyethylene
$PPDX-b-PCL$	Poly(p-dioxanone)-*b*-Poly(ε-caprolactone)
$PEG-b-PCL$	Poly(ethylene glycol)-*b*-Poly(ε-caprolactone)
$PEG-b-PBd$	Poly(ethylene glycol)-*b*-Poly(butadiene)
$PE-b-aPP$	Polyethylene-*b*-(atactic Polypropylene)
$PPP-b-P3HT$	Poly (2,5-dihexyloxy-p-phenylene)-*b*-(3-hexythiophene)
$sPP-b-PCL$	Syndiotactic Polypropylene-*b*-Poly(ε-caprolactone)

B Publications and Presentations

B1 Publications

1. Kundu, C., Dasmahapatra, A. K., **2014**, Crystallization of Double Crystalline Symmetric Diblock Copolymers, **Polymer** 55, 958-969.
2. Kundu, C., Dasmahapatra, A. K., **2014**, Effect of Block Asymmetry on the Crystallization of Double Crystalline Diblock Copolymers, **J. Chem. Phys.** 141, 044902.
3. Kundu, C., Dasmahapatra, A. K., **2015**, Crystallization of Double Crystalline Diblock Copolymer by Dynamic Monte Carlo Simulation, **Macromol. Symp.** 354, 314-323.
4. Kundu, C., Joshi, S. N., Dasmahapatra, A. K., **2016**, Crystallization of Diblock Copolymer from Microphase Separated Melt (Manuscript under review).
5. Kundu, C., Joshi, S. N., Dasmahapatra, A. K., **2017**, Crystallization of Diblock Copolymer on Thin Films (Manuscript under preparation).

B2 Presentations

1. Chitrita Kundu and Ashok Kumar Dasmahapatra, "Confinement Induced Crystallization of Double Crystalline Diblock Copolymer" presented on **CCP 2015** at Indian Institute of Technology Guwahati during December 2-5, 2015.
2. Chitrita Kundu and Ashok Kumar Dasmahapatra, "Crystallization of Double Crystalline Diblock Copolymer from Microphase Melt" presented on **4FAPS-IPC 2015** at Kualalumpur, Malaysia during Octobor 5-8, 2015.
3. Chitrita Kundu and Ashok Kumar Dasmahapatra, “Composition Dependent Crystallization behavior of Double crystalline Diblock Copolymer” presented on **MACRO 2015** at IACS, Kolkata during January 23-26, 2015.
4. Chitrita Kundu and Ashok Kumar Dasmahapatra, "Crystallization of Double Crystalline Diblock Copolymers Studied by Dynamic Monte Carlo Simulations", presented on **MACRO 2014** at Chiang Mai, Thailand during July 06 - 11, 2014.
5. Chitrita Kundu and Ashok Kumar Dasmahapatra, “Crystallization of Diblock Copolymer studied by Dynamic Monte Carlo simulation” presented on **MACRO 2013** at Indian Institute of Science Bangalore during May 15–18, 2013.

C Awards

1. Best Poster Presentation award in **CCP 2015**, XXVII IUPAP Conference on Computational Physics at IIT Guwahati during December 2-5, 2015.
2. International Travel Fellowship from **DST New Delhi**, to present research paper in **4FAPS-IPC 2015**, The 4th Federation of Asian Polymer Societies-International Polymer Congress at Kuala Lumpur, Malaysia during October 5-8, 2015.
3. International Travel Fellowship from **CICS Chennai**, to present research paper in **4FAPS-IPC 2015**, The 4th Federation of Asian Polymer Societies-International Polymer Congress at Kuala Lumpur, Malaysia during October 5-8, 2015.
4. Best Poster Presentation award in **MACRO 2015**, International Symposium on Polymer Science and Technology at IACS, Kolkata during January 23-26, 2015.
5. Best Paper Presentation award in **Reflux 2.0** at IIT Guwahati during March 29-30, 2014.
6. Best Poster Presentation award in **Reflux 2.0** at IIT Guwahati during March 29-30, 2014.